

2

NOTICE
PORTIONS OF THIS REPORT ARE ILLICIBLE.
It has been reproduced from the best
available copy to permit the broadest
possible availability.

UCRL--15629

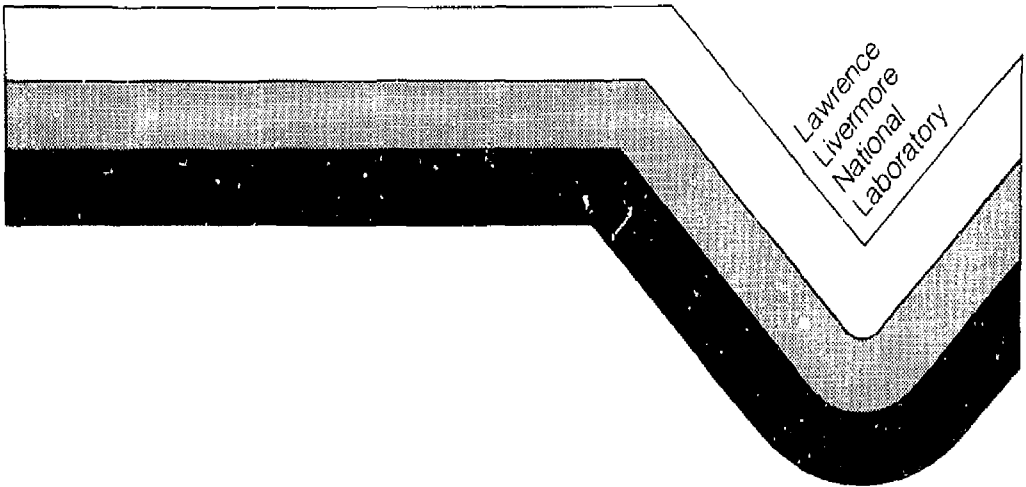
DE85 001013

IN SITU STRESS MEASUREMENTS
AT THE SPENT FUEL TEST --
CLIMAX FACILITY

John B. Creveling
Frank S. Shuri
Kevin M. Foster
Scott V. Mills

Foundation Sciences, Inc.
7630 S.W. Morrison Street
Portland, OR 97205
Under Contract 3106605

MAY 1984



DISTRIBUTION OF THIS DOCUMENT IS UNLIMITED

DISCLAIMER

This report was prepared as an account of work sponsored by an agency of the United States Government. Neither the United States Government nor any agency thereof, nor any of their employees, makes any warranty, express or implied, or assumes any legal liability or responsibility for the accuracy, completeness, or usefulness of any information, apparatus, product, or process disclosed, or represents that its use would not infringe privately owned rights. Reference herein to any specific commercial product, process, or service by trade name, trademark, manufacturer, or otherwise does not necessarily constitute or imply its endorsement, recommendation, or favoring by the United States Government or any agency thereof. The views and opinions of authors expressed herein do not necessarily state or reflect those of the United States Government or any agency thereof.

IN SITU STRESS MEASUREMENTS AT THE SPENT FUEL TEST -- CLIMAX FACILITY

by

John B. Creveling
Frank S. Shuri
Kevin M. Foster
Scott V. Mills

FOUNDATION SCIENCES, INC.
1630 S.W. Morrison St.
Portland, Oregon 97205

for

LAWRENCE LIVERMORE NATIONAL LABORATORY
Livermore, California

Under Contract 3106605

May 1984

MAY 1984

TABLE OF CONTENTS

	<u>Page</u>
1.0 INTRODUCTION	1
1.1 Background and Purpose	1
1.2 Scope of the Work	1
1.3 Acknowledgements	4
1.4 Applicability	4
2.0 SUMMARY	5
2.1 In Situ State of Stress	5
2.2 Stress Gradient into Rib from South Heater Drift	7
2.3 Pillar Stresses	7
2.4 Rock Deformational Properties	8
2.5 Quality of Test Results	8
3.0 SITE DESCRIPTION	10
3.1 Location and Topography	10
3.2 Geologic Setting	10
4.0 TEST PROCEDURES AND EQUIPMENT	13
4.1 General Concepts of Overcore Testing	13
4.2 Overcore Testing	18
4.2.1 General	18
4.2.2 Special Techniques	19
4.2.2.1 Borehole Deformation Gage Orientation	19
4.2.2.2 Temperature Monitoring and Control	21
4.2.2.3 Drill Water and Cuttings Removed from Downward Inclined Borehole ISS-11	24
4.2.3 Overcore Test Procedure	27
4.3 Biaxial Compression Testing	32
4.4 Approach to Field Work	34
4.5 Quality Assurance	36
5.0 ANALYSIS OF TEST DATA	37
5.1 General Approach to Data Reduction	37
5.2 USBM Gage Analysis	42

TABLE OF CONTENTS (continued)

	<u>Page</u>
5.2.1 Stress Tensor Calculation -- USBM Gage	42
5.2.2 Secondary Principal Stress Calculation -- USBM Gage	49
5.2.3 Biaxial Modulus Calculation -- USBM Gage	50
5.3 CSIRO Cell Analysis	52
5.3.1 Stress Tensor Calculation -- CSIRO Cell	52
5.3.2 Secondary Principal Stress Calculations -- CSIRO Cell	53
5.3.3 Biaxial Modulus and Poisson's Ratio Calcu- lation -- CSIRO Cell	55
6.0 BIAXIAL COMPRESSION TEST RESULTS	57
6.1 USBM Gage Tests	57
6.2 CSIRO Cell Tests	57
6.3 Comparison of Results	62
7.0 IN SITU STRESS MEASUREMENT RESULTS	63
7.1 General	63
7.2 Rib Stress Measurements -- Boreholes ISS-8, 9, 10, and 11	72
7.2.1 Secondary Principal Stress Solutions -- Rib Boreholes	72
7.2.2 Principal Stress Solutions -- Rib Boreholes	81
7.2.2.1 CSIRO Cell Solutions	81
7.2.2.2 USBM Gage Solutions	91
7.3 Pillar Stress Measurements -- Boreholes ISS-4, 5, 6 and 7	95
7.3.1 Secondary Principal Stress Solutions -- Pillar Boreholes	95
7.3.2 Principal Stress Solutions - Pillar Boreholes	95
7.4 Stress Measurements -- Discussion and Conclusions	95
7.4.1 Quality of Test Results	95
7.4.1.1 General	95
7.4.1.2 Quality of USBM Gage Data	100
7.4.1.3 Quality of CSIRO Cell Data	100
7.4.2 Stress Gradient Into Rib from South Heater Drift	103
7.4.3 In Situ State of Stress -- Rib Boreholes	104
7.4.4 Pillar Stresses	106

TABLE OF CONTENTS (continued)

	<u>Page</u>
8.0 REFERENCES	79
LIST OF TABLES	iv
LIST OF FIGURES	v
APPENDICES A, B AND C	

LIST OF TABLES

<u>Table No.</u>	<u>Title</u>	<u>Page</u>
4.1	Average Bearings and Inclinations from Collar to Total Depth for In Situ Stress Measurement Holes	35
5.1	USBM Gage -- Biaxial Modulus Test Results	44
5.2	CSIRO Cell -- Biaxial Modulus Test Results	46
6.1	USBM Gage Biaxial Compression Test Results	58
6.2	CSIRO Cell Biaxial Compression Test Results	60
6.3	Summary of Deformational Properties	62
7.1	Summary of USBM Gage Overcore Output Readings	64
7.2	Summary of USBM Gage Overcore Data	66
7.3	Summary of CSIRO Cell Overcore Data	68
7.4	Summary of Secondary Principal Stresses	74
7.5	Summary of CSIRO Cell Principal Stress Solutions	82
7.6	USBM Gage Principal Stress Solutions	93

LIST OF FIGURES

<u>Figure No.</u>	<u>Title</u>	<u>Page</u>
1.1	Spent Fuel Test Facility with In Situ Stress Measurement Borehole Locations	2
2.1	Summary of In Situ Principal Stresses	6
3.1	Spent Fuel Test Facility Vicinity Map	11
4.1	Overcore Test Schematic (Test with USBM Gage)	14
4.2	Biaxial Compression Test Schematic (Test with USBM Gage)	15
4.3	USBM Gage with Spare Parts	16
4.4	CSIRO Cell with Preparation Tools	17
4.5	Determining the Orientation of USBM Gage and CSIRO Cell	20
4.6	Typical CSIRO Cell Overcoring Data	25
4.7	Drilling Rig and Set Up for Inclined Borehole ISS-10	28
4.8	Installation of CSIRO Cell	29
4.9	Data Acquisition During Overcore Testing	30
4.10	Biaxial Modulus Test Equipment	33
5.1	USBM Gage Overcore Test, Strain Reading vs. Elapsed Time	38
5.2	USBM Gage Overcore Test, Strain Reading vs. Bit Penetration	39
5.3	CSIRO Cell Overcore Test, Strain Reading vs. Elapsed Time	40
5.4	CSIRO Cell Overcore Test, Strain Reading vs. Bit Penetration	41
5.5	USBM Gage - Biaxial Modulus Test, Pressure-Deformation Curve	43
5.6	CSIRO Cell - Biaxial Modulus Test, Pressure-Deformation Curve	45

LIST OF FIGURES (continued)

<u>Figure No.</u>	<u>Title</u>	<u>Page</u>
5.7	Definitions of Deformation Moduli	51
5.8	Orientation of Strain Gages in the CSIRO Cell	54
6.1	Phase II, CSIRO Cell Biaxial Modulus Test, Pressure-Deformation Curve	61
7.1	Axial Strains from CSIRO Cell Tests -- Boreholes ISS-8, 9, 10 and 11	73
7.2	Secondary Principal Stresses, Orientations and Magnitudes -- Borehole ISS-8	76
7.3	Secondary Principal Stresses, Orientations and Magnitudes -- Boreholes ISS-9 and ISS-10	77
7.4	Secondary Principal Stresses, Orientations and Magnitudes -- Borehole ISS-11	78
7.5	Secondary Principal Stresses, Profile -- Bore- hole ISS-8	79
7.6	Secondary Principal Stresses, Profiles -- Bore- holes ISS-9, 10, and 11	80
7.7	CSIRO Cell Principal Stresses -- Borehole ISS-8, All Tests	85
7.8	CSIRO Cell Principal Stresses -- Borehole ISS-8, Tests from 67 to 110 ft	86
7.9	CSIRO Cell Principal Stresses -- Borehole ISS-9	87
7.10	CSIRO Cell Principal Stresses -- Borehole ISS-10	88
7.11	CSIRO Cell Principal Stresses -- Borehole ISS-11	89
7.12	Combined CSIRO Cell Principal Stresses -- Bore- holes ISS-8, 9, 10, and 11	92
7.13	USBM Gage Principal Stresses -- Boreholes ISS-8, 9, 10, and 11	94
7.14	Secondary Principal Stresses, Orientations and Magnitudes -- Pillar Boreholes	96
7.15	Secondary Principal Stresses, Profiles -- Pillar Boreholes	97
7.16	CSIRO Cell Principal Stresses -- Pillar Bore- holes ISS-5 and 7	98

1.0 INTRODUCTION

1.1 Background and Purpose

The Spent Fuel Test-Climax is being conducted to demonstrate the feasibility of short-term storage and retrieval of spent fuel from a commercial nuclear power reactor in a deep geologic environment. A schematic of the Spent Fuel Test Facility is shown on Figure 1.1. One of the major activities of the program is site characterization, of which in situ stress measurement is an integral part (Ballou, et al., 1982).

Previous stress measurements were performed in 1979 by the U.S. Geological Survey (Ellis and Magner, 1982). The additional measurements reported in this study were undertaken for several reasons:

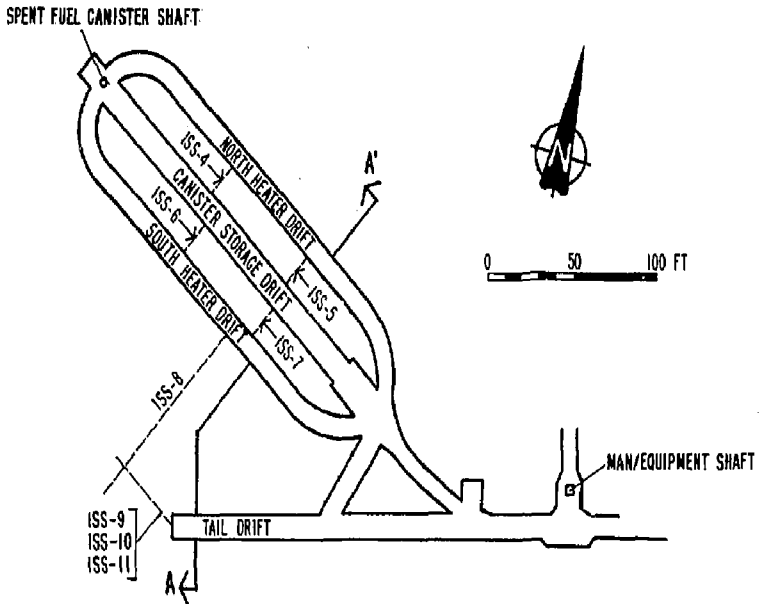
- a) The earlier work was done prior to excavation of the canister drift. The state of stress, especially near-field, could be changed both by this new opening and the thermal loading from the canisters and auxiliary heaters used during the Spent Fuel Test.
- b) The earlier measurements were made relatively close to the south heater drift, and may have been influenced by this opening.
- c) Anomalies in the earlier results, particularly a low vertical stress, could not be accounted for satisfactorily.

The stress measurement study presented in this report was intended to investigate these questions and provide a more complete picture of the stress at the test facility. The program had three major objectives:

- 1) To measure stresses in the pillars located between the canister drift and the north and south heater drifts.
- 2) To measure the stress gradient away from the test facility.
- 3) To measure the in situ stress outside the zone of influence of the test facility, as far as practical.

1.2 Scope of Work

To achieve the goals of the study, two phases of work were performed in which a total of eight boreholes were drilled and tested. The bore-




NOTE: ISS-10 IS INCLINED UPWARD ABOUT 45°.
 ISS-11 IS INCLINED DOWNWARD ABOUT 45°.
 BOTH ARE ON THE SAME BEARING AS ISS-9.
 OTHER BOREHOLES HORIZONTAL.

PLAN VIEW



SECTION A-A'

 ENGINEERS GEOLOGISTS	FOUNDATION SCIENCES, INC. PORTLAND, OREGON		
	LLNL SPENT FUEL TEST-CLIMAX SPENT FUEL TEST FACILITY WITH IN SITU STRESS MEASUREMENT BOREHOLE LOCATIONS		
DATE MAY 1984	JOB NO. 247-1	SCALE SHOWN	FIG. 1.1

hole locations are shown on Figure 1.1. The stress-measuring instruments used for this study included both the U.S. Bureau of Mines Borehole Deformation Gage (USBM gage) and the Australian CSIRO Hollow Inclusion Stress Cell (CSIRO cell).

The first phase of the study included drilling, testing, and data analysis for boreholes ISS-4 through 10. Boreholes ISS-4 through 7 were drilled through the pillars to measure pillar stress profiles. Borehole ISS-8 was drilled horizontally away from the south heater drift to measure the stress gradient near the test facility. To measure stresses outside the expected zone of influence of the test facility, borehole ISS-8 was extended into the rib, and boreholes ISS-9 and 10 were drilled from the tail drift toward borehole ISS-8. This would allow the determination of the three-dimensional undisturbed stress tensor using data from USBM gage tests made in relatively close proximity to one another. To minimize stress concentration effects of the test facility, tests were made at borehole depths of 40 to 110 ft to measure the undisturbed state of stress.

Field work for the first phase of testing began in June 1983 and was completed in September 1983. A report on the results of that phase of work was presented to LLNL in January 1984. Those results suggested that significant variations in stress conditions existed at depth in the rib between the south heater drift and the tail drift. No apparent physical mechanisms were identified that could reasonably account for the variation in measured stresses in a region of rock which should exhibit uniform stress conditions. For this reason, and because the results were not entirely conclusive, LLNL requested that a second phase of work be performed to further investigate the in situ stresses in the rib. The additional work consisted of drilling, testing, and data analysis for borehole ISS-11, which was also drilled from the tail drift toward borehole ISS-8. Field work for the second phase of work began in February 1984 and was completed in April 1984. Under Phase II, the Phase I data was re-evaluated in light of data

from borehole ISS-11. This report presents a complete description of the work performed for both Phases I and II, and supercedes the January 1984 report.

Additional information obtained during this study included modulus of deformation and Poisson's ratio of large-diameter rock core from the test facility, and geologic data from the core itself. Interpreting and reporting the geologic data are to be done by others.

1.3 Acknowledgements

The work described in this report was performed by Foundation Sciences, Inc. (FSI) for Lawrence Livermore National Laboratory (LLNL), under contract number 310665.

A number of people were responsible for the success of the study: Wesley Patrick was Project Manager for LLNL, with Dale Wilder, Jesse Yow Jr., Harold Ganow, Norman Rector, and John Scarafioti participating in the field operations; Frank Shuri served as Project Manager for FSI, with John Creveling, Kevin Foster, Scott Mills, and John Cooper performing the field work and assisting in data analysis and report preparation. Basil Baily of EG&G Corp. provided electrical services at the test facility, while Bill Smyth, Tom Clapp, Ron Murphy, Darrel Hansen, and Bob Johnson of REECO provided the drilling.

1.4 Applicability

The state of stress in a rock mass is complex and variable because of topographic, structural, material, and historical factors. All measurements of stress rely on indirect methods and analyses, necessarily, contain simplifying assumptions. While the work described in this report incorporates state-of-the-art techniques in rock stress measurements, there are still problems with technique and analysis which are far from resolved. For this reason, it is recommended that the results of this study be applied carefully, and with full appreciation for their uncertainties and limitations.

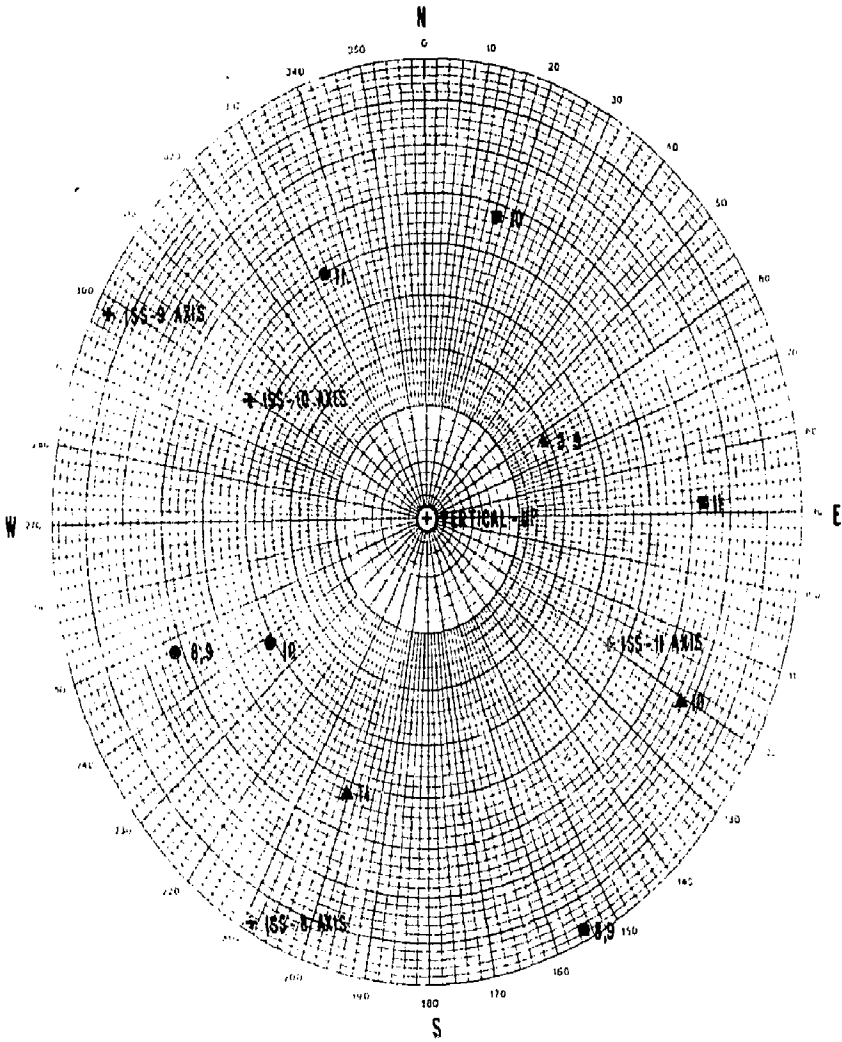
2.0 SUMMARY

2.1 In Situ State Of Stress

Four deep stress measurement boreholes were drilled from the south heater drift into the south rib of the test facility west of the tail drift. The logical assumption at the start of the study was that the in situ state of stress in this region would be uniform. However, based on the results of the stress measurements, the state of stress is not uniform and significant variations in stress exist at different locations within the rock mass.

Three general zones in the rib were tested during this study: two horizontal boreholes ISS-8 and 9, drilled perpendicular to one another, tested a zone near their intersection, which is at the same elevation as the test facility; upward-angled borehole ISS-10 tested a zone 50 to 70 ft above the intersection of boreholes ISS-8 and 9 and; downward-angled borehole ISS-11 tested a zone 50 to 70 ft below the intersection of boreholes ISS-8 and 9. As shown on Figure 2.1, the in situ state of stress is different in each zone. Stresses measured in the ISS-10 zone and the ISS-8 and 9 zone are relatively uniform within each zone. Also, the principal stress orientations in the ISS-10 zone are similar to those in the ISS-8 and 9 zone; however, the ISS-10 stress magnitudes are significantly higher. Principal stresses in the ISS-11 zone show a rotation of the major and intermediate principal stresses around the average axis of the minor principal stress, with increasing test depth. Average principal stress magnitudes in the ISS-11 zone, which are given on Figure 2.1, are similar to those in the ISS-10 zone, but the orientations are significantly different from either of the other zones.

Based on calculations of overburden pressures, a vertical stress component of about 1,600 psi is expected at the test facility. Test results indicate that only the ISS-11 stress zone has a similar average vertical stress. Vertical stresses for the ISS-8 and 9 zone and the ISS-10 zone are about 950 psi and 2,050 psi, respectively.



Principal stress, psi

Test Zone	σ_1	σ_2	σ_3
	●	■	▲
ISS-8,9	1,500	800	800
ISS-10	2,500	1,800	900
ISS-11	2,200	1,800	1,200

LLNL Spent Fuel Test-Climax
Summary of In Situ
Principal Stresses

Note: All stresses compressive

Figure 2.1

In addition to the large differences between average measured principal stresses in the three zones, smaller, but significant stress variations were measured within each zone.

The reason for the apparent changes in the average stress field over the relatively short distances between zones, the indicated regular rotation of stresses in borehole ISS-11, and the other smaller but significant variations in stress within a general zone are not obvious. Possible hypotheses include the effects of joints and shear zones in the rock mass, thermally induced stresses from the Spent Fuel Test, unrecognized effects of the test facility itself, cooling history of the quartz monzonite, influences from nearby nuclear detonations, and other geologic/tectonic mechanisms that may be recognized in the future, as work at the test facility progresses.

2.2 Stress Gradient into Rib from South Heater Drift

In borehole ISS-8, the major principal stress within 20 ft of the south heater drift is predominantly vertical and is on the order of about 1,500 psi. The minor principal stress is small (near zero) and is oriented in a near-horizontal direction, perpendicular to the axis of the south heater drift. Tests results indicate that there is no large concentration of vertical stress caused by the test facility. Beyond depth 20 ft, the minor principal stress increases, and the major principal stress rotates away from vertical and toward the orientation shown on Figure 2.1. A low stress zone of about 900 psi maximum was observed from depth 40 to 45 ft. The cause of the low stress is not clear, but it may be related to two open, weathered joints, that were seen in the core to intersect at a depth of about 40 ft. Beyond a depth of 60 ft, the principal stresses are relatively consistent in orientation and magnitude.

2.3 Pillar Stresses

Stress measurements in the four pillar boreholes present a relatively consistent profile of secondary principal stresses. The major secondary principal stresses are predominantly vertical and have a maximum value of about 2,000 psi near the heater drift face. These stresses decrease gradually but consistently toward the canister drift face, where the magnitude is about 700 psi.

The results of three CSIRO cell tests indicate that major principal stresses in the pillars are on the order of 2,300 to 3,000 psi, and are oriented at an angle of 20° to 50° from vertical. As would be expected, the minor principal stresses are low, averaging about 500 psi, and are oriented across the short dimension of the pillar. The intermediate principal stresses are nearly horizontal, oriented along the long axis of the pillars, and less than about 900 psi.

2.4 Rock Deformational Properties

Results of biaxial compression tests indicate that the Climax quartz monzonite tested during this study is generally homogeneous, isotropic, and elastic at the stress levels of interest.

Average material properties are:

$$\begin{aligned} \text{Biaxial Modulus of Deformation} &= 10 \times 10^6 \text{ psi} \\ \text{Poisson's Ratio} &= 0.29 \end{aligned}$$

2.5 Quality of Test Results

Great care was taken to standardize test procedures and to perform tests according to set procedures. Several specialized techniques were developed to minimize test errors associated with the relatively great depths of testing in the boreholes and the thermal effects associated with testing in artificially heated rock. We believe that the differences in measured stresses are greater than can be accounted for by the errors introduced by uncertainties in field measurements. Further, two fundamentally different stress measurement systems produce a consistent picture. Therefore, we conclude that the test results presented in this report are generally correct and that the in situ stress field around the Spent Fuel Test Facility is not simple or uniform.

Comparisons between CSIRO cell and USBM gage stress measurement results indicate good agreement between the two devices, except that USBM gage stress magnitudes average 30% higher. More confidence is placed in the USBM gage stress magnitudes due to its longer history of successful use, its less complex physical operation, and its

simpler theoretical basis, when compared to the CSIRO cell. The directions of the CSIRO principal stresses also appear to be systematically biased by the test borehole orientation. The test data indicate that the bias is probably in the range of 10° to 20°. The reasons for the suggested CSIRO deficiencies are not clear. Possible reasons include incomplete curing of the epoxy grout prior to overcoring, imperfectly balanced sensitivity of the nine strain gage orientations to the different components of the in situ stress tensor, and errors in the constants used in the stress tensor solution to correct for the mechanical properties and geometry of the device.

Because real variations exist in the stress field, the fundamental assumption of a uniform stress condition, inherent in calculating principal stresses from USBM gage tests in several boreholes, is not met. For this reason, USBM gage principal stress solutions do not result in an accurate assessment of in situ stresses, but instead tend to average the stress fields in which USBM gage tests are performed. The CSIRO cell principal stress solutions present a clearer picture of the in situ stress state in individual zones.

Despite the suggested CSIRO cell deficiencies, the errors associated with its use are considered minor for this study, and the ability to determine the complete stress state with one test significantly improves our understanding of the in situ stresses around the Spent Fuel Test Facility. We conclude that the CSIRO principal stress orientations are reasonably accurate, but that the calculated stress magnitudes, as given in section 7.0 of this report, should be increased 30%. This has been done for the summary principal stresses shown on Figure 2.1, which is based on combined solutions of CSIRO cell tests in each of the three stress zones.

3.0 SITE DESCRIPTION

3.1 Location and Topography

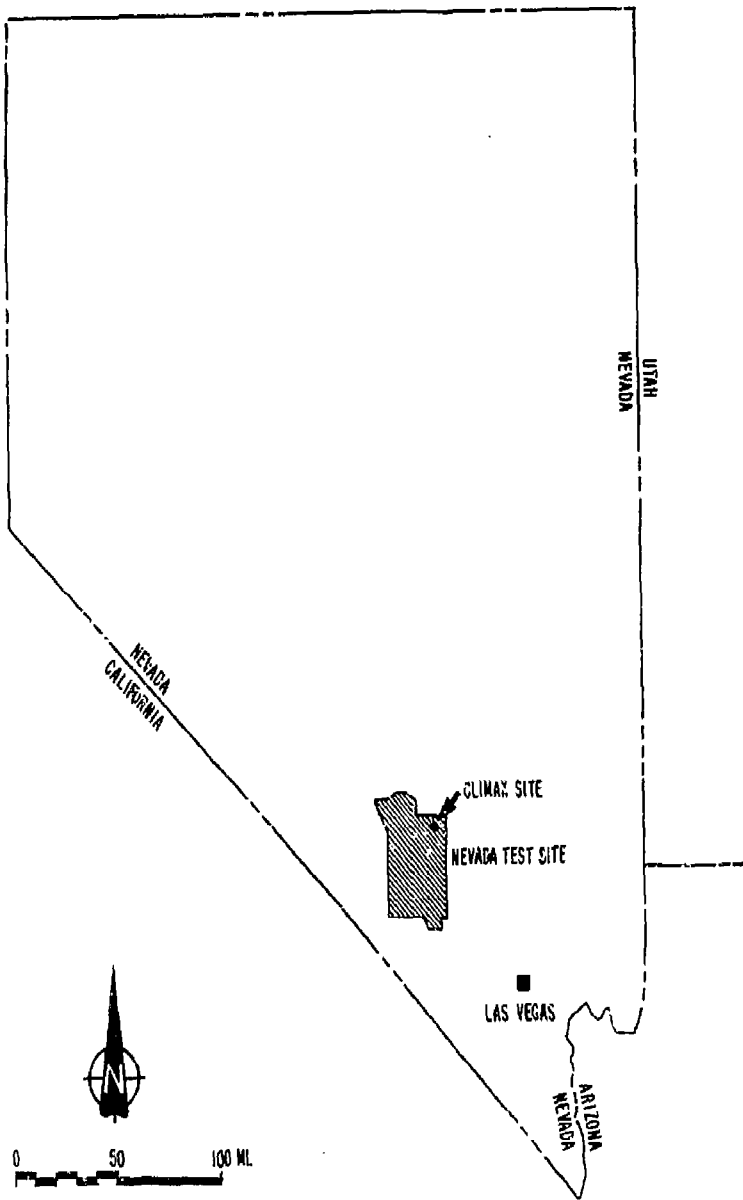
The Spent Fuel Test Facility is located at the north end of the Nevada Test Site about 100 miles northwest of Las Vegas, Nevada (see Figure 3.1). The test facility is approximately 1,375 ft below the ground surface within a granitic body. The general layout of the underground facility is shown on Figure 1.1.


The surface entrance to the test facility is located on a bench at an elevation approximately 500 ft above Yucca Flat to the south and 1,500 ft below Pahute Mesa to the west. The terrain falls gently to the southeast onto Yucca Flat and rises moderately to steeply to the north and west onto Pahute Mesa.

3.2 Geologic Setting

The strata of the Nevada Test Site region consist primarily of complexly folded and faulted sedimentary rocks of Paleozoic Age. These are overlain by Tertiary volcanic tuffs and lavas, with Tertiary and Quaternary alluvium in the valleys. The Spent Fuel Test site is located within the Climax stock, a composite granitic intrusive body of Cretaceous age. Geophysical evidence suggests that the stock, which outcrops over an area of about 1.6 km², expands conically to an area of about 100 km² at a depth of several kilometers. This stock is composed of two main units, a grandiorite and a quartz monzonite, which contain varying proportions of the same minerals. The test facility is located in the quartz monzonite unit. Grain sizes in both units range from 1 to 4 mm; however, the quartz monzonite contains scattered pink alkali feldspar crystals up to 50 mm in length (Wilder and Yow, 1981).

The quartz monzonite of the Climax stock is moderately to highly jointed with three prominent joint orientations (Heuze, et al., 1981):



 <p>ENGINEERS GEOLOGISTS</p>	<p>FOUNDATION SCIENCES, INC. PORTLAND, OREGON</p>		
	<p>LLNL SPENT FUEL TEST-CLIMAX SPENT FUEL TEST FACILITY VICINITY MAP</p>		
<p>DATE NOV. 1983</p>	<p>JOB NO. 247-1</p>	<p>SCALE SHOWN</p>	<p>FIG. 3.1</p>

	<u>Average Strike, degrees</u>	<u>Average Dip, degrees</u>
Set 1	N32W	22NE
Set 2	N64W	Near vertical
Set 3	N35E	Near vertical

There are also a number of shear zones intersecting the Spent Fuel Test site. In general, these shear zones have strikes of N30°W to N60°W and dips of 75° to 85° northeast.

Major faults in the vicinity of the Climax Stock include: the Yucca Fault, located south of the stock and trending northward; the Tippinip Fault, located west of the stock and trending north-northeast; and the Boundary Fault, which trends northeast and forms the southeast contact between the stock and the alluvium.

4.0 TEST PROCEDURES AND EQUIPMENT

4.1 General Concepts of Overcore Testing

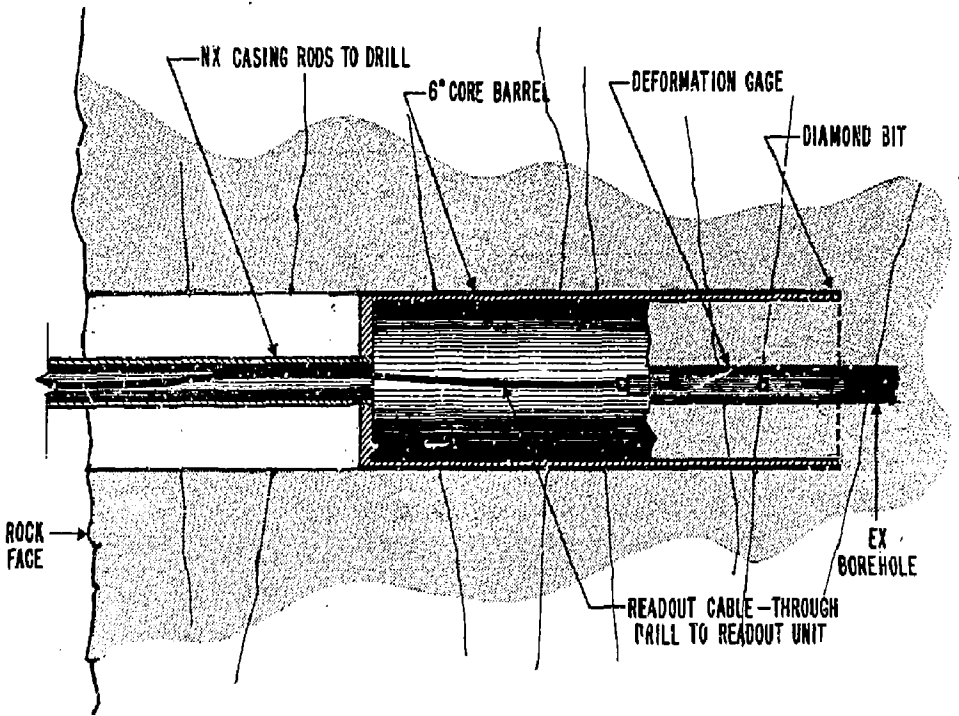
The overcore test is designed to measure the in situ state of stress in a rock mass. The test measures the deformation of a small-diameter borehole as it is isolated from the surrounding stress field. This is accomplished by advancing a 6-in.-diameter borehole to within about 1 ft of the test location. A concentric 1.5-in.-diameter borehole is then drilled about 2 ft beyond the end of the 6-in. borehole. A borehole deformation gage is placed in the smaller borehole and concentrically overcored with a 6-in.-diameter bit, thereby stress-relieving the core containing the gage, as shown on Figure 4.1.


With knowledge of the rock's deformational properties, the borehole deformations measured in the overcore test can be related to the change in stress in the rock core. This change in stress is assumed to be numerically equal, although opposite in sense, to the stresses existing in the parent rock mass.

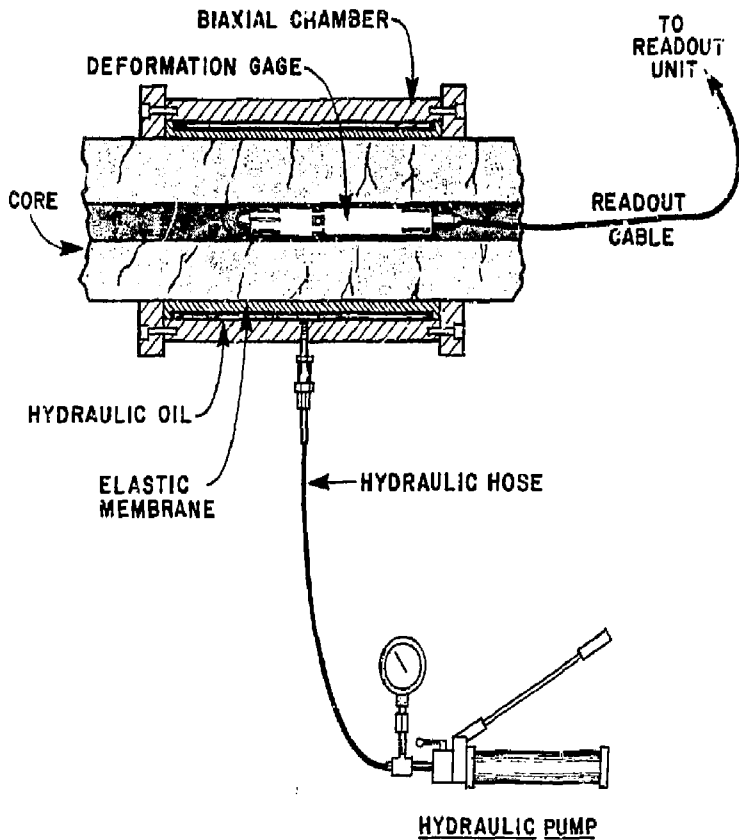
The deformational properties of the rock are determined by performing a biaxial compression test on the core recovered from an overcore test location. This test is accomplished by applying a known uniform radial pressure to the outside of the rock core and measuring the resulting deformations of the inner coaxial borehole with a borehole deformation gage, as shown on Figure 4.2.

For this study, two different instruments were used to measure deformations of the 1.5-in.-diameter borehole: the U.S. Bureau of Mines borehole deformation gage (USBM gage), shown on Figure 4.3, and the Australian Commonwealth Scientific and Industrial Research Organization triaxial hollow inclusion stress gage (CSIRO cell), shown on Figure 4.4.

The USBM gage measures the deformations of the 1.5-in.-diameter borehole across three diameters spaced 60° apart. This instrument's sensing system consists of three pairs of strain-gaged cantilevers, which are read electronically. Since stresses can only be measured



 ENGINEERS GEOLOGISTS	FOUNDATION SCIENCES, INC.		
	PORTLAND, OREGON		
LLNL SPENT FUEL TEST - CLIMAX OVERCORE TEST SCHEMATIC (TEST WITH USBM GAGE)			
DATE MAY 1984	JOB NO. 247-1	SCALE NONE	FIG. 4.1




 <p>ENGINEERS GEOLOGISTS</p>	<p>FOUNDATION SCIENCES, INC. PORTLAND, OREGON</p>		
	<p>LLNL SPENT FUEL TEST-CLIMAX BIAxIAL COMPRESSION TEST SCHEMATIC (TEST WITH USBM GAGE)</p>		
DATE NOV 1983	JOB NO. 247-1	SCALE NONE	FIG. 4.2



Figure 4.3 USBM Gage with spare parts.



Figure 4.4 CSIRO Cell with preparation tools.

in the plane perpendicular to the axis of the borehole, a minimum of three nonparallel holes are required to calculate the complete in situ stress tensor. This test assumes that the rock is homogeneous, isotropic, and elastic, and that the stress field is the same in all test locations. The principal advantages of the USBM gage are its re-usability and its relatively long history of successful use in other stress measurement programs. The construction and standard use of the USBM gage are well documented by Hooker, Aggson, and Bickel (1974); Hooker and Bickel (1974); and Panek (1966).

The CSIRO cell measures the deformation of the 1.5-in.-diameter borehole using nine independent strain gages in three 45°/90° rosettes which are read electronically. The strain gage rosettes are potted into the walls of a hollow epoxy cylinder, which in turn is epoxy glued to the walls of the borehole. The orientations of the strain gages are designed to result in relatively balanced sensitivity to the different components of the stress tensor and to allow for some redundancy in the measurements. The advantage of the CSIRO cell is the ability to determine the complete stress tensor at a single point in the rock mass with one test. The CSIRO cells and methods of analysis are described by Worotnicki and Walton (1976) and Duncan Fama and Pender (1980).

4.2 Overcore Testing

4.2.1 General

The overcoring test procedures used for this project were in substantial conformance with the procedures given by Hooker, Aggson, and Bickel (1974) and Hooker and Bickel (1974). However, special procedures and techniques were developed in response to conditions unique to this project. These include the relatively large depth in the boreholes at which the tests were performed (up to 110 ft), the high rock temperatures (up to 26°C) relative to the ambient temperature of the mine air and drill water (about 18°C), and the presence of standing water in a downward inclined borehole. The major technical problem associated with overcoring tests at depth is ac-

curately setting and determining the orientation of the borehole deformation gage. The problem with a large difference between rock and drill-water temperature is the thermally induced rock deformations and the offset/calibration factor changes in deformation gage electronics as the thermal regime changes during testing. Difficulties with placing and accurately orienting borehole deformation gages underwater, particularly with ensuring a successful epoxy bond between the CSIRO cell and the borehole wall, required that standing water be removed from the downward inclined borehole.

The following sections discuss the special techniques developed for this project and summarize the steps performed in conducting an overcore test. A detailed list of the drilling and test equipment used during the test is presented in Appendix A.

4.2.2 Special Techniques

4.2.2.1 Borehole Deformation Gage Orientation.

At test depths of more than 50 ft, it is difficult to obtain accurate angular orientation of the USBM gage, using either the standard level or a compass mounted in the handle of the setting tool. This is due to the torsional flex in the setting rods and the stick-slip rotation of the gage in the hole. A mercury orientation switch can be placed just behind the gage and monitored remotely, as is done with the CSIRO cell, which improves the orientation accuracy, but $\pm 10^\circ$ is still the best that can be expected at large depths.

For this project, the USBM gage was randomly oriented in the borehole. The CSIRO cell was set and initially oriented using a mercury switch located just behind the gage. Following removal of the setting tools for both gage types, the orientation of the gage was visually determined using a high-powered telescope, as shown in Figure 4.5. Adequate illumination of the back of the borehole and orientation pins on the gage was achieved by pushing a flashlight into the back of the hole. The crosshair in the eyepiece of the telescope was aligned with the orientation pins on the back of the borehole deformation gage, and the



Figure 4.5 Determining the orientation of USBM Gage and CISRO Cell.

orientation of the crosshair was then determined with the clinometer on a Brunton compass. The estimated error for this telescope orientation method was $\pm 2^\circ$ from 0 to 50 ft and $\pm 4^\circ$ from 50 to 110 ft. This method also allowed mapping of rock features exposed at the end of the 6-in. hole, which facilitated orientating the rock core following its recovery from the borehole.

Due to a slight curvature in borehole ISS-10, borehole deformation gages placed beyond 70 ft were not visible from the borehole collar. The orientations of such tests were determined by placing a mark at the bottom of the 6-in.-diameter core before overcoring. This was done by sliding a marking pen attached to the end of the setting rods along the bottom of the borehole. After carefully removing these cores from the borehole with the borehole deformation gages left in place and undisturbed, the orientation of the instrument was determined by measuring the angle between the orientation pins and the mark, which was assumed to be vertically down. The estimated error in this method, which was used for tests ISS-10-6-C, ISS-10-7-B, ISS-10-8-B and ISS-10-9-C, is $\pm 10^\circ$.

4.2.2.2 Temperature Monitoring and Control.

During the Spent Fuel Test, the rock surrounding the test facility was heated by the spent fuel canisters and electrical auxiliary heaters to temperatures above previously existing levels. The resulting rock temperatures at the time of this project were on the order of 24° to 26°C . The air and water temperatures in the mine, however, were at about 18°C . Usually, drill water is circulated both before and after overcore drilling to stabilize the borehole deformation gage temperatures. However, this procedure would have reduced the rock temperature. Therefore, using mine-temperature water for drill circulation could have induced local stress changes which would have been superimposed on the pre-existing stress field. Also, the effects of thermal contraction of the test core and the 1.5-in.-diameter hole would be superimposed on the measured deformations resulting from stress relief. In addition

to these rock stress changes, changes in gage temperature during testing will significantly offset USBM gage and CSIRO cell outputs. These thermal effects would be difficult, if not impossible, to evaluate analytically.

For these reasons, an effort was made to minimize the impact of thermal effects by controlling the temperature of the drill circulation water. To accomplish this, a closed water circulation system was used for drilling. Water was pumped from a tank of approximately 250 gallons capacity to the drill bit. The return water was collected at the borehole collar through an 8-in.-diameter pipe grouted into the rock face, and was returned to the supply tank. Rock temperature was monitored with a thermistor installed in the borehole instrument. Drill-water temperature was monitored with a thermistor submerged in the recirculation tank, and was manually controlled by energizing submerged electric heater elements to increase the temperature or by adding cooler mine water to decrease the temperature.

The goal at the start of the testing program was to maintain a constant rock temperature at the test location by drilling with water heated to the initial rock temperature. It soon became apparent, however, that this was not feasible because of heat produced by the cutting friction of the drill bit, the thermal inertia of the drill rod string, and the limited flow of water that could be circulated without dulling the drill bit. The goal of temperature control then evolved to minimizing the changes from initial rock temperature during drilling, and subsequently stabilizing the rock at its initial temperature.

The techniques used to efficiently minimize temperature deviations during drilling were arrived at through a process of trial and error. While the specific mixtures of warm and cool water, the volumes pumped, and the rates of delivery varied with each test, a general procedure was successfully established:

1. Initial rock temperatures were determined by allowing the deformation gage and the thermistor to fully equilibrate with the rock temperature prior to the start of water circulation.

To do this, gage output on all channels and gage temperature were read and recorded at 2-minute intervals. The gage was considered equilibrated when three consecutive sets of output readings did not differ by more than 5 strain units and gage temperature did not vary by more than 0.01°C, with no increasing or decreasing trends.

2. The initial drill-water temperature was adjusted so that it was 1° to 6°C cooler than the initial rock temperature. The actual temperature chosen was determined by temperature behavior observed during the previous test in a particular hole.
3. As drilling progressed, the gage temperature was monitored and the drill-water temperature and flow rate were adjusted as required to correct temperature excursions. Efficient temperature control required some experience because the heat generated at the bit varied, depending on bit sharpness, rock conditions and drill rig performance. Also complicating the procedure was the thermal inertia of the drill string. This resulted in a 5- to 20-min. lag between the time when the tank temperature was altered and the resulting effects were observed at the deformation gage. As test depths increased, the lag time increased.
4. When drilling was completed, the rock core was returned to the initial rock temperature by continuing circulation of drill water and adjusting water temperature as required. Final gage readings were taken after stabilizing the rock temperature and stopping water circulation. The time required to accomplish this was typically 20 min. to 1 hour.

With experience, temperature deviations during drilling could usually be maintained within $\pm 3^\circ\text{C}$ of the initial rock temperature and final temperatures within $\pm 0.1^\circ\text{C}$ could be achieved.

The effect of temperature change on strain gage readings is shown on Figure 4.6, which shows strain and temperature versus time for a typical CSIRO cell overcore test. Because stresses are calculated from the difference between readings recorded at the same temperatures at the beginning and end of the overcore test, temperature fluctuations that occur during the test do not affect the final stress calculations.

4.2.2.3 Drill Water and Cuttings Removal from Downward Inclined Borehole ISS-11.

Drill water and cuttings remaining after drilling in the downward inclined borehole ISS-11 would have presented difficulties in placing and accurately orienting the borehole deformation gages. A clean borehole without standing water or cuttings ensured a clean bonding surface for the CSIRO cell epoxy cement, firm contact between the USBM gage sensing buttons and the borehole wall, and a clear view of deformation gage orientation pins for telescopic orientation.

The techniques used to remove drill cuttings and water from borehole ISS-11 were arrived at through a process of trial and error. The following sequence of procedures, developed during the first half of the testing program and used routinely thereafter, proved to be the most effective.

1. After advancing the 6-in.-diameter borehole and removing the core, the water remaining in the borehole was removed by airlifting with compressed air discharged through the open end of an NX drill rod lowered to the bottom of the borehole. The borehole itself acted as the return line. The borehole was subsequently refilled with clean water and airlifted two more times. This process effectively removed the large volume of suspended fine drill cuttings generated during drilling of the 6-in.-diameter borehole, which otherwise would later have settled into and filled the 1.5-in.-diameter borehole.

Gage Reading in Strain units
Contraction ← → Extension

CSIRO Test No. ISS-8-7-C
Depth: 21.3 ft.

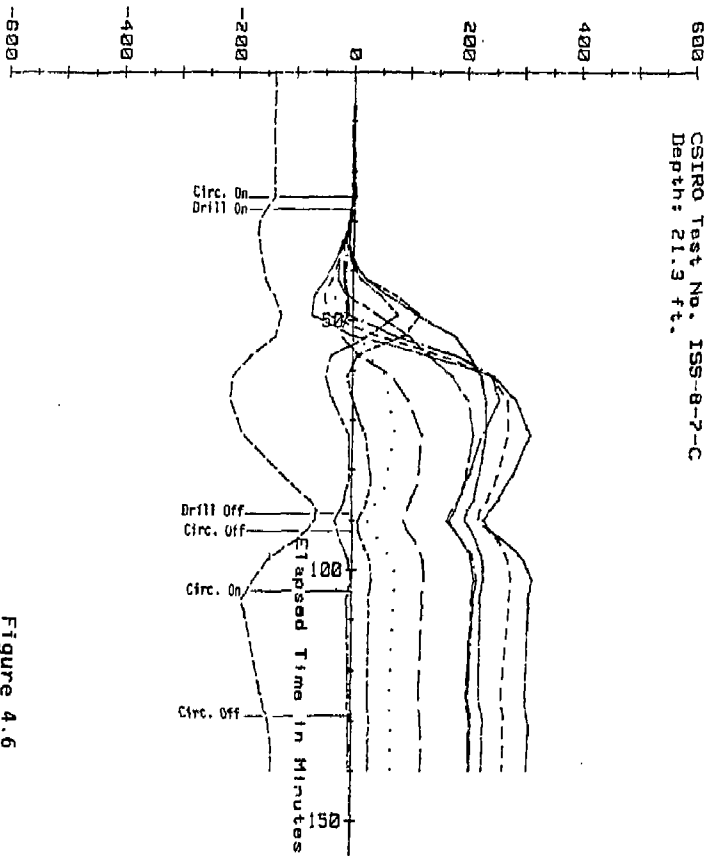
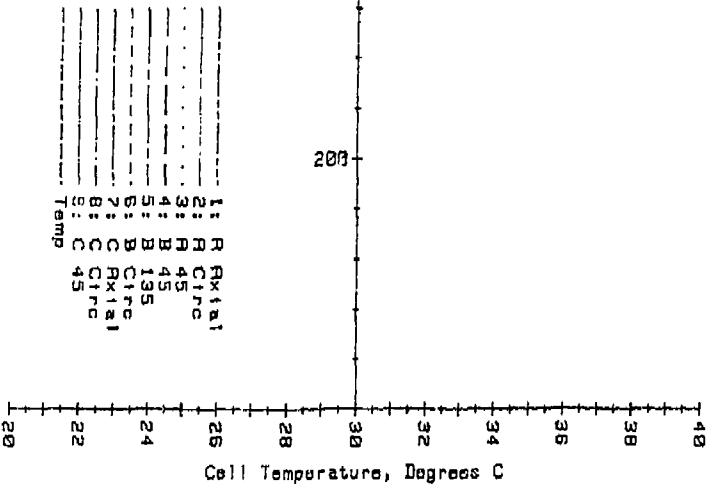


Figure 4.6
Typical CSIRO Cell Overcoming Data



2. After the EWT borehole (1.5-in.-diameter borehole) was drilled in the bottom of the 6-in.-diameter borehole, the water and cuttings from this operation were removed in preparation for placement of the borehole deformation gage as follows:

- a) After removal of the EWT core, a 1-in.-diameter PVC pipe was lowered to the bottom of the 1.5-in.-diameter borehole. Water and air were discharged through the PVC pipe to blow drill cuttings up and out of the 1.5-in.-diameter borehole and into the bottom of the sloping 6-in.-diameter borehole.
- b) The 6-in.-diameter borehole was then airlifted three times using the method described in step 1. This effectively removed all of the cuttings from the borehole and all of the water except that in the 1.5-in.-diameter borehole and the bottom 6 in. of the 6-in.-diameter borehole.
- c) A wicking tool, lowered by means of the deformation gage setting rods, was used to remove the remaining water. The wicking tool consisted of a used EWT core barrel, fitted at its forward end with a screw-on, pointed nose cone and at its rearward end with rolls of absorbant tissue paper.

As the wicking tool was lowered to the bottom of the 1.5-in.-diameter borehole, the closed EWT core barrel displaced most of the water in the smaller borehole up into the 6-in.-diameter borehole, where it was absorbed by the tissue paper. After allowing a 10 to 15 minute period for the paper to absorb the water, the tool was removed from the hole, and saturated rolls were replaced with dry rolls. This procedure was repeated two or three times until the paper rolls returned relatively dry from the bottom of the borehole, indicating that the water in the 6-in.-diameter borehole had been absorbed. This procedure left only about

4 in. of water in the bottom of the 1.5-in.-diameter borehole, which was below the deformation gage location.

- d) For CSIRO cell tests, the remainder of the water in the 1.5-in.-diameter hole was removed by refitting the wicking tool's EWT core barrel with a drilled-out nose cone and filling the hollow center of the barrel with absorbent paper towels. After the tool was relowered to the bottom of the borehole, less than 1 in. of water remained in the bottom of the small borehole.

4.2.3 Overcore Test Procedure

The steps performed to conduct an overcore test are presented sequentially below. Figures 4.7, 4.8, and 4.9 illustrate some of the test equipment and procedures used in performing the overcore test.

1. Advance 6-in.-diameter borehole to within 1 ft of proposed test location. For downward sloping borehole, flush cuttings and water out of hole.
2. Advance EWT borehole (1.5-in.-diameter borehole) at least 1.5 ft beyond the bottom of the 6-in.-diameter borehole. For downward sloping boreholes, flush cuttings and water out of hole and wick remaining water out of 1.5-in.-diameter hole.
3. Select test location. Inspect EWT core to avoid joints and large phenocrysts.
4. Prepare borehole deformation gage for installation at test location.
 - a) USBM gage: Check for proper fit of gage in 1.5-in.-diameter borehole and shim contact buttons as required for initial deflection in instrument mid-range.
 - b) CSIRO cell: Swab 1.5-in.-diameter borehole with organic solvents (ethanol and 1,1,1-trichloroethane) until clean;



Figure 4.7 Drilling rig and set up for inclined borehole ISS-10. Note 6-inch diameter core barrel against wall at right.



Figure 4.8 Installation of CSIRO Cell, note borehole cleaning tool against wall.



Figure 4.9 Data acquisition during overcore testing. Foreground: strain indicator unit with switch and balance. Background: temperature monitoring and control instruments including voltmeter, heater controller and power supply.

check operation of all nine strain gages, file spacer lugs to fit borehole; cut reaction rod to appropriate length; roughen cell surface with sand paper; mix epoxy cement and pour into cell body; and assemble cell with plunger and reaction rod.

5. Insert gage in 1.5-in.-diameter borehole. Let CSIRO cell set at least 16 hrs, in accordance with manufacturer's instructions, to allow adequate curing of the epoxy cement before overcoring.
6. Measure orientation of gages and sketch features at end of 6-in.-diameter borehole. Use telescope at depths greater than about 10 ft.
7. String signal cable through drill rods and connect signal leads to switch and balance unit and strain indicator readout unit. Connect thermistor leads to thermistor readout system.
8. Record initial gage readings and measure initial rock temperature until stable readings are obtained. Fill downward sloping hole with water heated to rock temperature, and again record gage readings and temperature until stable readings are obtained.
9. Start drill water circulation and wait for water return.
10. Overcore rock containing gage. Record deformation and temperature readings at each inch of drill bit penetration. Adjust drill water temperature to minimize excursions in gage temperature from initial rock temperature.
11. Stop drilling when all stress is relieved (generally 6 to 12 inches beyond measurement location).
12. Continue circulation while adjusting drill water temperature to achieve a final gage temperature at the initial gage temperature.

13. Turn off circulation.
14. Take final deformation and temperature readings.
15. Remove signal cable from drill rods.
16. Remove gage and 6-in.-diameter core from borehole, mark with depths, orientation, test number, and test locations.

4.3 Biaxial Compression Testing

The biaxial compression tests were performed using commercially available equipment and standard techniques. A list of the test equipment is contained in Appendix A. The steps performed to conduct a biaxial compression test are presented below in sequential order. Figure 4.10 shows the equipment used in performing the test.

1. Place the 5.5-in.-diameter core recovered from the overcore test in the biaxial compression chamber so that the overcore test location is centered in the chamber.
2. For cores recovered from USBM gage overcore tests, place the USBM gage in the core at the same location and orientation as it was during the overcore test. CSIRO cells are permanently bonded in the 1.5-in.-diameter hole and are therefore properly located and oriented when the core is centered in the biaxial chamber.
3. Connect the deformation gage signal leads to the switch and balance unit and strain indicator readout unit.
4. Incrementally pressurize the hydraulic fluid in the biaxial chamber to load the sample. At each pressure level, record the resulting deformations of the coaxial 1.5-in.-diameter borehole as measured by the borehole deformation gage. The load is applied in two cycles to maximum pressures of 1,500 and 3,000 psi, respectively. Each cycle has seven ascending and seven descending pressure levels. A typical test is shown in Table 5.1.
5. Remove the sample from the biaxial chamber. For USBM gage tests, remove the gage from the core.



Figure 4.10 Biaxial Modulus Test Equipment including strain indicator unit with switch and balance, biaxial chamber, and hydraulic pump with pressure gage.

6. Measure and record the diameters of the rock core and 1.5-in.-diameter borehole to the nearest 0.001 in. Sketch and describe rock features, such as joints and phenocrysts observed on the outside surface of the core. For CSIRO cell tests, the core is also cut to produce a rock disc about 1 in. thick at the strain gage location. The disc and mating surfaces are inspected to determine the quality of the epoxy cement bond, and the disc is sketched showing strain gage rosette orientations and selected rock features.

4.4 Approach to Field Work

To achieve the goals outlined in Section 1.0, eight test boreholes were drilled: two holes in each of the canister drift pillars and four deep holes into the rib generally between the taildrift and south heater drift, as shown on Figure 1.1. Table 4.1 gives the final orientation and length of each borehole. Test depths, recorded for each hole, were measured from a steel collar, which was set into the surface of the pillar or rib and protruded from the rock face to facilitate drill water circulation. Table 4.1 also gives the distance from the end of the steel collar to the rock face.

Individual overcore and biaxial compression tests for this project were identified as follows:

ISS-X-Y-Z

where:

ISS-X = borehole number

Y = test number in borehole X

Z = B for USBM gage test, or C for CSIRO cell test

Phase I field work was performed utilizing three drill rigs, two two-man drill crews, and two two-man instrument crews. This arrangement allowed the drill crews to remain productive while instruments were

Table 4.1
 AVERAGE BEARINGS AND INCLINATIONS FROM COLLAR TO TOTAL
 DEPTH FOR IN SITU STRESS MEASUREMENT HOLES

<u>Hole No.</u>	<u>Description</u>	<u>Average Bearing</u>	<u>Average Inclination</u>	<u>Distance from Collar Flange to Rock Face, ft</u>	<u>Final Depth of Borehole, ft</u>
ISS-4	North drift pillar, station 334.61 ft	S28° 57' 24.9"W	+1° 3' 34.9"	0.5	18.0
ISS-5	North drift pillar, station 265.77 ft	S28° 56' 47.0"W	+1° 22' 28.8"	0.7	16.9
ISS-6	South drift pillar, station 311.47 ft	N27° 51' 42.9"E	+1° 14' 38.0"	0.7	19.9
ISS-7	South drift pillar, station 258.19 ft	N29° 55' 13.1"E	+0° 55' 47.7"	0.6	18.4
ISS-8	South drift abutment, station 260 ft	S28° 38' 19"W	+2° 55' 29"	0.6	110.2
ISS-9	Tail drift horizontal, station 258 ft	N61° 51' 16"W	+3° 39' 12.0"	0.6	60.4
ISS-10	Tail drift inclined up, station 258 ft	N59° 54' 23"W	+46° 11' 41"	0.0	81.1
ISS-11	Tail Drift inclined down, station 258 ft.	N59° 42' 10.6"W	-43° 11' 24"	2.0	95.9

being installed or stabilized in another borehole by the instrument crews. Phase II field work was performed utilizing one drill rig, one three-man drill crew, and one two-man instrument crew. Biaxial compression tests and USBM gage calibrations were performed by instrument crews when drill crews were advancing boreholes between test locations, moving drill rigs from one borehole location to another, or upon the completion of all drilling.

To evaluate the quality of the data being collected and to determine when the project goals had been met, preliminary analyses of USBM gage and CSIRO cell tests (e.g. data plots, secondary principal stress calculations and CSIRO cell principal stress calculations) were performed as field testing progressed.

4.5 Quality Assurance

Quality assurance for this testing program consisted of personnel prequalification, equipment inspection and calibration, and performance verification. All supervisory personnel were prequalified for this testing program by virtue of previous experience and the understanding of the theoretical derivation and application of test results. All test equipment was periodically inspected, and documented calibrations were performed at regular intervals. All calibration equipment and reference standards are traceable to the National Bureau of Standards. A complete record of all calibration documents is contained in Appendix B.

5.0 ANALYSIS OF TEST DATA

5.1 General Approach to Data Reduction

The overcoring test data and biaxial compression test data are analyzed systematically so that each test can be evaluated at several points in the data reduction process. Erroneous and questionable data are eliminated to the greatest extent possible. A summary of the steps involved in the data reduction is presented in this section. A more detailed discussion and the mathematics of the analyses are presented in the following sections.

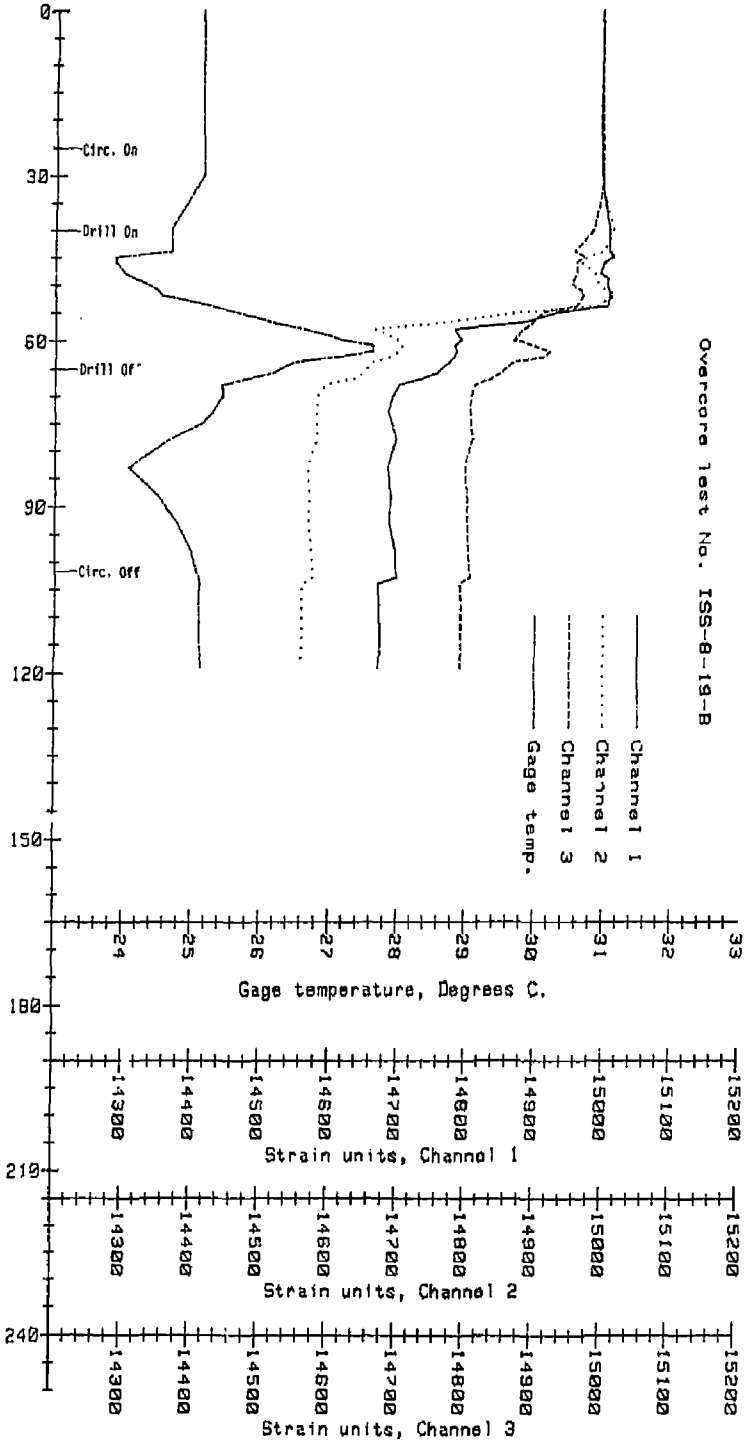
Initially, the field data for each test is reviewed, and potential problems are evaluated. Test data which is obviously bad as a result of equipment malfunction or error in procedure are eliminated, and questionable test data are flagged for further evaluation.

Next, preliminary results are calculated. For the overcore tests, the strain reading changes used to calculate the borehole deformations are chosen as the difference between stable readings before and after the test at similar gage temperatures. These preliminary data, together with assumed values for rock deformation modulus and Poisson's ratio, allow calculation of USBM gage secondary principal stresses and the CSIRO cell stress tensors as field testing progresses. For the biaxial compression tests, the differences between strain readings at 0 and 3,000 psi applied pressures are tabulated and compared.

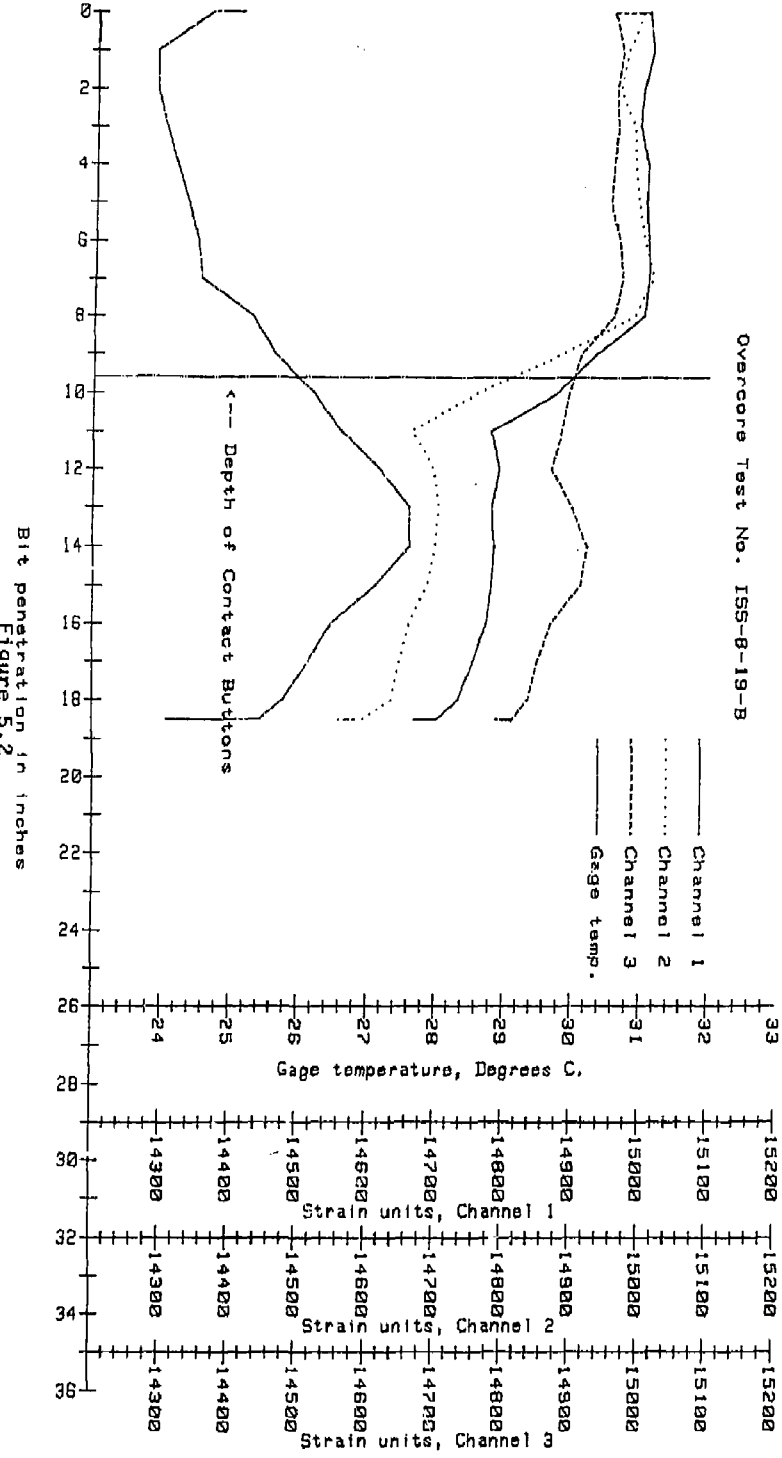
For the final stress analysis, the output from each channel of every overcoring test is plotted along with gage temperature against elapsed time and against drill bit penetration. These plots are inspected to confirm the preliminary strain changes and to detect any unusual deformation gage behavior during the test. Figures 5.1, 5.2, 5.3 and 5.4 show examples of these two graphs for USBM gage test ISS-8-19-B and CSIRO cell test ISS-8-7-C.

For the USBM gage data plots, the raw strain unit is a general unit and is equivalent within a few percent to a micro-inch, depending upon the exact calibration factor for each channel of the gage.

Overcore Test No. ISS-8-19-B



Overcore Test No. ISS-8-19-B



Bit penetration in inches
Figure 5.2

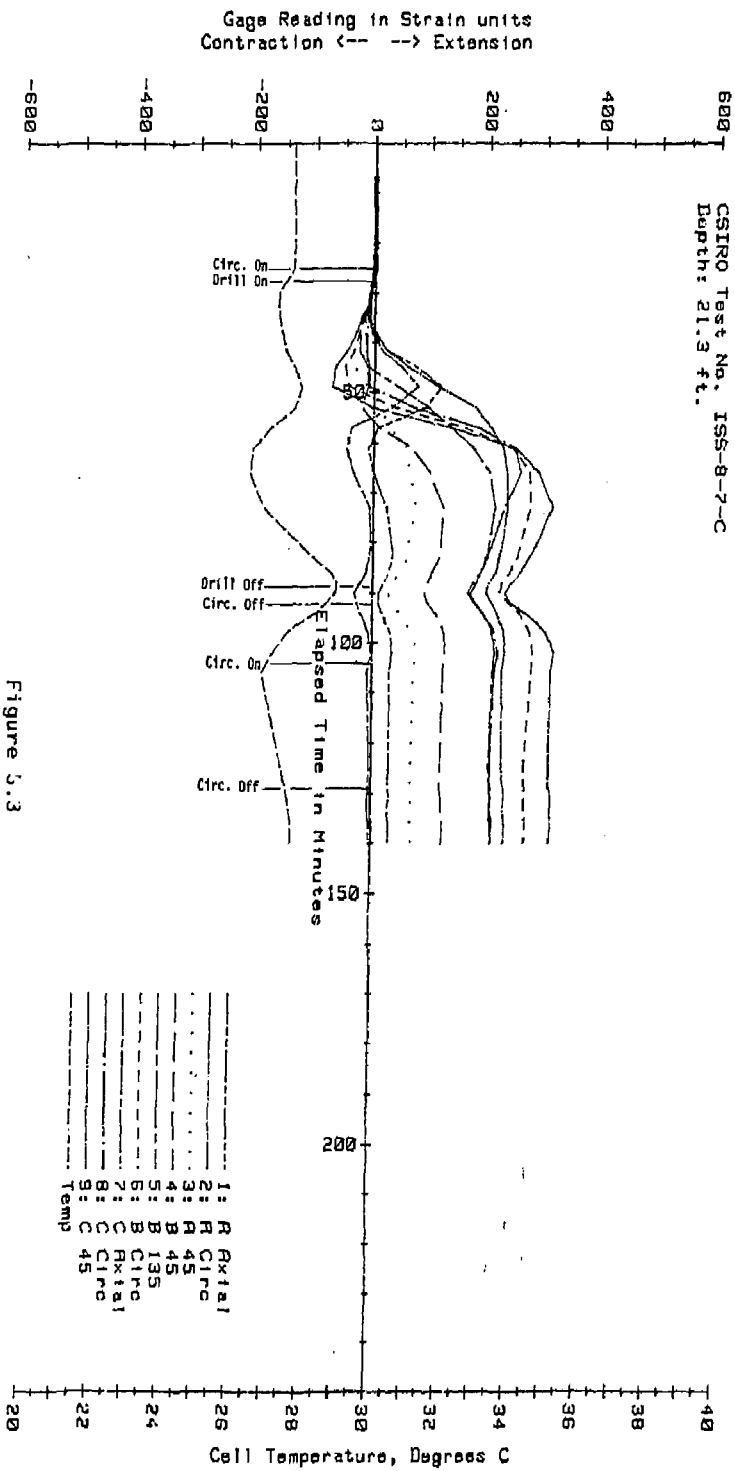


Figure 5.3

Gage Reading Change in Strain units
Contraction ← → Extension

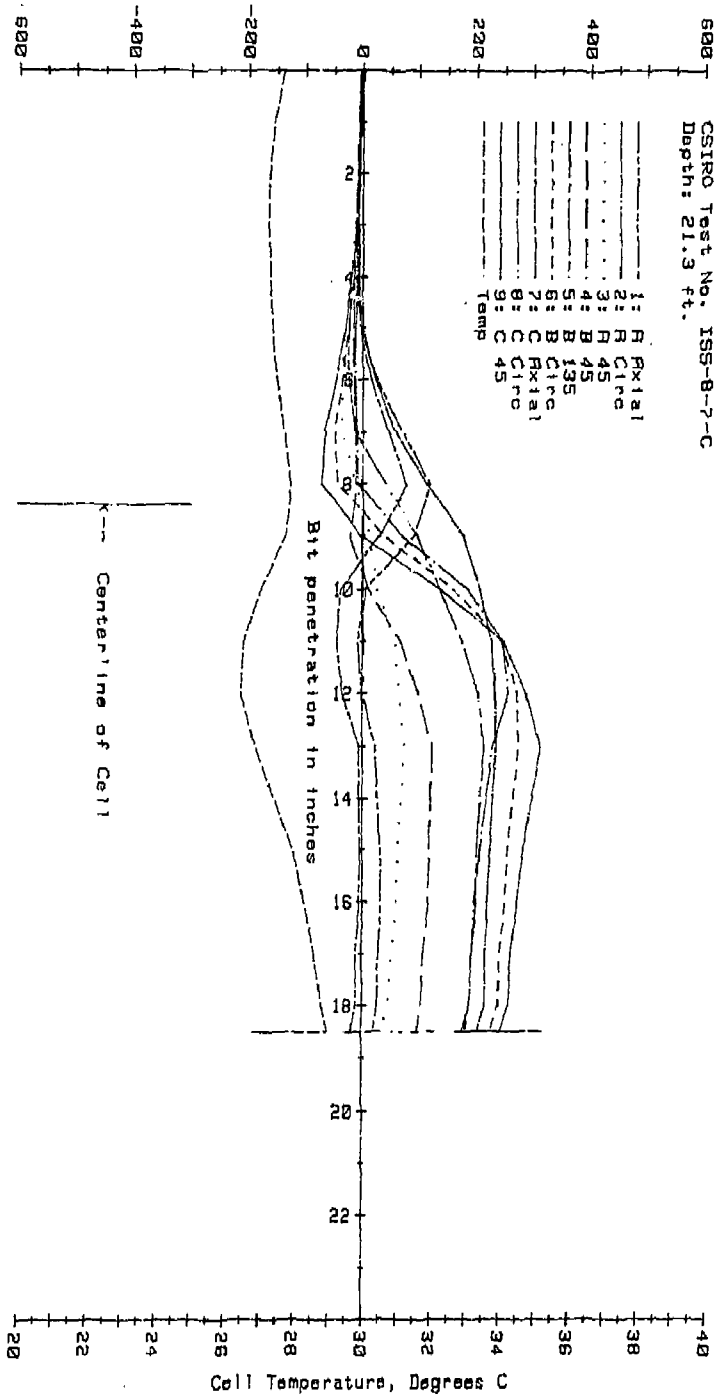


Figure 5.4

The actual diametral deformation equals the strain unit change multiplied by the calibration factor for the respective readout channel.

The biaxial compression test data are also plotted for review. Concurrently, the modulus of deformation (plus Poisson's ratio for CSIRO cell tests) is calculated for each pressure increment of the test. For the USBM gage, this is done for each of the three individual gage channels. For the CSIRO cell, the average circumferential and axial strains are used, and a single value is obtained. Figure 5.5 and Table 5.1 show the results for USBM gage test ISS-8-19-B, channel 1. Figure 5.6 and Table 5.2 show the results for CSIRO cell test ISS-8-7-C. These data are typical.

Once all of the required parameters for stress calculation have been determined, the secondary principal stresses are calculated for each overcore test. A plot of the secondary stress magnitudes and orientations is made for each borehole. This allows direct comparison of individual USBM gage and CSIRO cell test results. At this stage, trends in stress states along the borehole length are evaluated for stress concentration effects. Also, anomalous test results are re-evaluated for spurious data or unexpected stress regimes. For the three rib boreholes, the USBM gage tests which will be combined to calculate the undisturbed stress tensor are chosen.

Finally, the three-dimensional stress tensors and principal stresses are calculated for the individual CSIRO cell and combined USBM gage tests.

5.2 USBM Gage Analysis

5.2.1 Stress Tensor Calculation -- USBM Gage

At any point in the rock mass, the three-dimensional state of stress (stress tensor) is fully defined by a total of six independent stress components. These are the three mutually orthogonal components of normal stress σ_x , σ_y , and σ_z and the three components of shear stress

Figure 5.5

USBM GAGE - BIAXIAL MODULUS TEST

TEST NO.: ISS-8-19-B

9/25/83

Channel 1

Average tangent modulus: 10.4×10^6 psi
Average secant modulus: 10.7×10^6 psi
Average recovery modulus: 9.9×10^6 psi

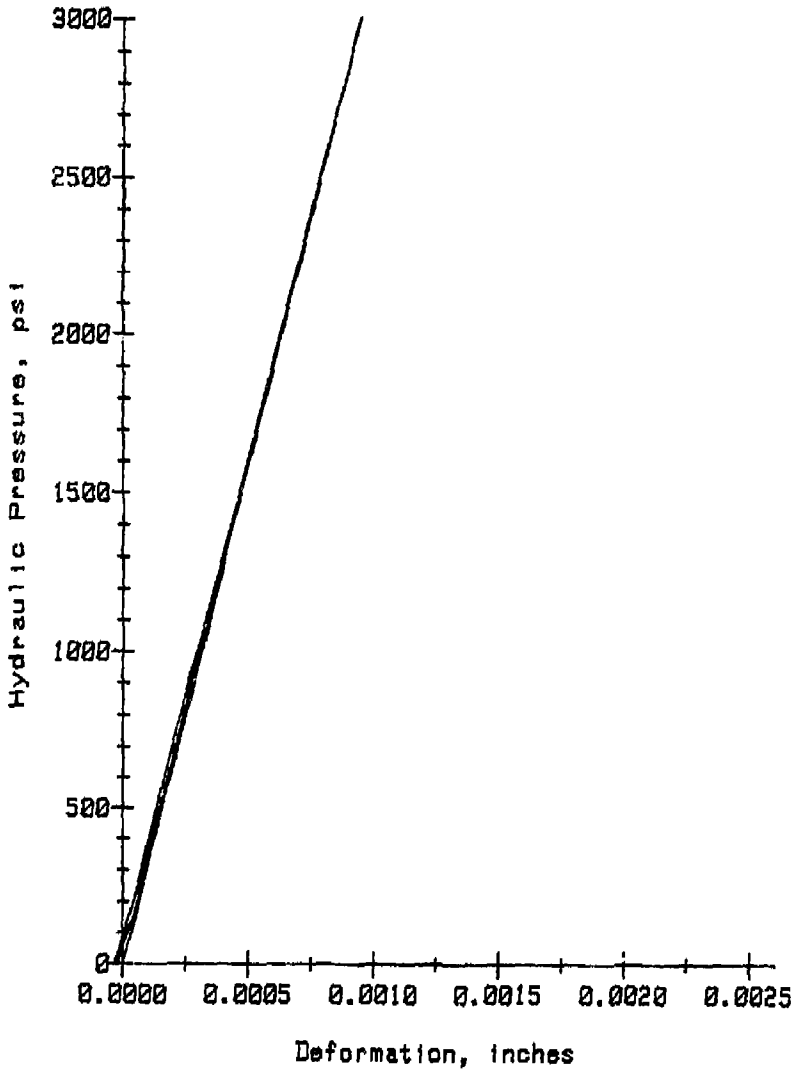


Table 5.1

USBM Gage - Biaxial Modulus Test Results

Test no.: ISS-8-19-B Channel 1
 Sample from depth: 86.1 ft
 Date: 9/25/83
 Gage no.: 60
 Storage file: B8-19

Pressure, psi	Deformation, $\times 10^{-6}$ in.	Modulus, $\times 10^6$ psi		
		Tangent	Secant	Recovery
150	53	9.2	9.2	----
300	93	12.0	10.4	----
450	143	9.7	10.2	----
600	181	13.1	10.8	----
900	279	9.8	10.4	----
1200	376	10.1	10.3	----
1500	465	10.9	10.5	----
1200	378	----	----	11.2
900	285	----	----	10.4
600	189	----	----	10.2
450	134	----	----	8.8
300	90	----	----	11.2
150	42	----	----	10.2
0	-21	----	----	7.6
300	74	10.2	13.1	----
600	165	10.8	11.8	----
900	261	10.1	11.2	----
1200	363	9.5	10.7	----
1800	561	9.8	10.4	----
2400	751	10.2	10.4	----
3000	943	10.1	10.3	----
2400	757	----	----	10.5
1800	569	----	----	10.3
1200	372	----	----	9.8
900	274	----	----	10.0
600	178	----	----	10.2
300	82	----	----	10.1
0	-32	----	----	8.6

Average tangent modulus: 10.4×10^6 psi
 Average secant modulus: 10.7×10^6 psi
 Average recovery modulus: 9.9×10^6 psi

Figure 5.6
 CSIRO Biaxial Modulus Test
 Test No.: ISS-B-7-C
 Depth: 21.3 ft.
 Date: 7/28/83

Average Tangent Modulus: 8.8×10^6 psi
 Average Secant Modulus: 8.4×10^6 psi
 Average Recovery Modulus: 8.8×10^6 psi
 Average Poisson's Ratio: .342

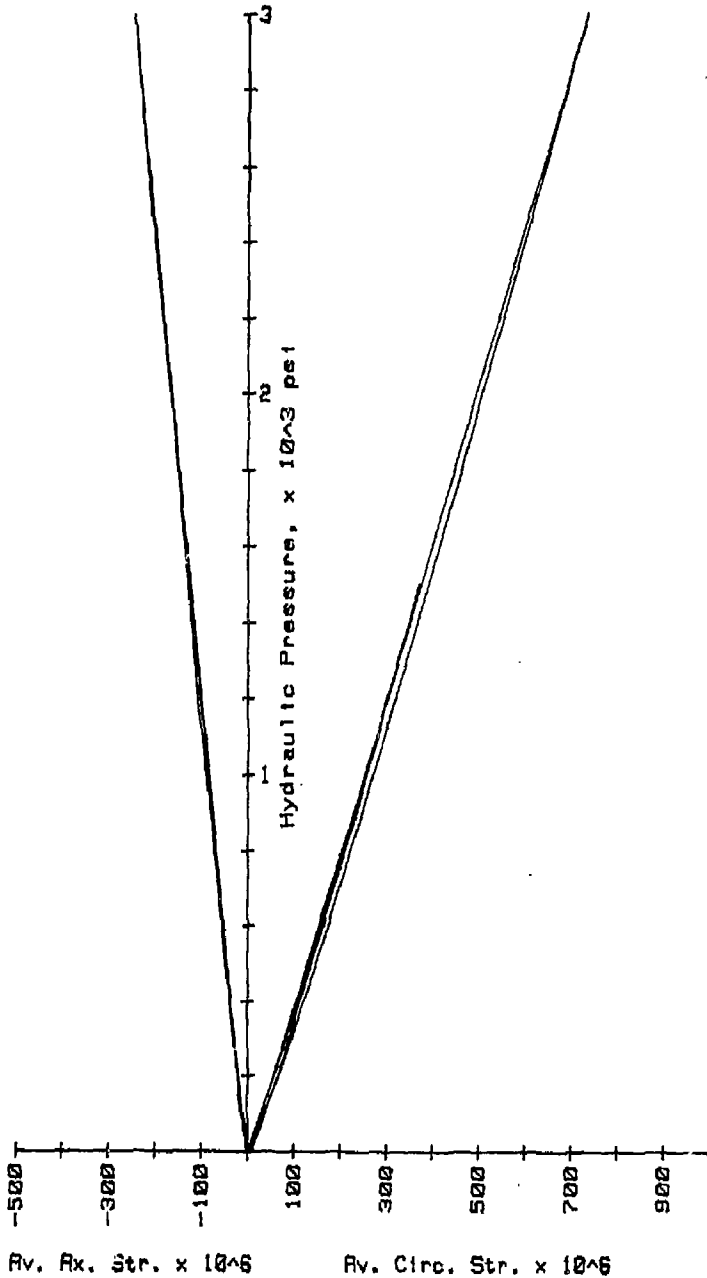


Table 5.2

CSIRO Cell - Biaxial Modulus Test Results

Test no.: ISS-8-7-C
 Sample from depth: 21.3 ft
 Date: 7/20/83
 Cell number: 149B
 Storage file: CB-7

Pressure, psi	Modulus, $\times 10^6$ psi			Poisson's Ratio
	Tangent	Secant	Recovery	
150	7.2	7.2	----	0.41
300	8.9	8.0	----	0.25
450	8.9	8.3	----	0.41
600	9.4	8.5	----	0.27
900	8.6	8.6	----	0.32
1200	8.9	8.6	----	0.34
1500	9.3	8.8	----	0.37
1200	----	----	9.6	0.39
900	----	----	9.3	0.37
600	----	----	9.1	0.30
450	----	----	8.7	0.35
300	----	----	9.7	0.36
150	----	----	8.4	0.31
0	----	----	6.8	0.34
300	8.2	7.7	----	0.35
600	9.0	8.3	----	0.33
900	9.0	8.5	----	0.32
1200	8.8	8.6	----	0.33
1800	9.1	8.8	----	0.34
2400	9.1	8.8	----	0.35
3000	9.0	8.9	----	0.33
2400	----	----	9.5	0.33
1800	----	----	9.7	0.38
1200	----	----	9.2	0.30
900	----	----	8.8	0.39
600	----	----	9.0	0.33
300	----	----	8.5	0.33
0	----	----	7.5	0.37

Average tangent modulus: 8.8×10^6 psi
 Average secant modulus: 8.4×10^6 psi
 Average recovery modulus: 8.8×10^6 psi
 Average Poisson's ratio: 0.34

τ_{xy} , τ_{yz} , τ_{zx} . If a local coordinate system is defined at an overcore test location such that σ_x acts along the axis of the borehole, then components τ_{xy} and τ_{zx} act parallel to the axis of the borehole and have negligible effect on the diametral deformation of the borehole. The change in borehole diameter is, therefore, a function of the three stress components σ_y , σ_z , and τ_{yz} acting perpendicular to the borehole axis, and the component σ_x acting parallel to the borehole axis.

Using the plane strain condition of the theory of elasticity (i.e., axial strain = 0), Panek (1966) solves for the borehole deformation caused by σ_y , σ_z and τ_{yz} . The effect of σ_x on the diametral deformation is then superimposed on this solution. The total change in borehole diameter may be expressed:

$$U = \sigma_x f_1 + \sigma_y f_2 + \sigma_z f_3 + \tau_{yz} f_5 \quad (5.2.1)$$

where:

$$f_1 = d(1+2\cos 2\theta)(1-\mu^2)/E + d\mu^2/E \quad (5.2.2a)$$

$$f_2 = -d\mu/E \quad (5.2.2b)$$

$$f_3 = d(1-2\cos 2\theta)(1-\mu^2)/E + d\mu^2/E \quad (5.2.2c)$$

$$f_5 = d(4\sin 2\theta)(1-\mu^2)/E \quad (5.2.2d)$$

and where:

U = change of borehole diameter

d = diameter of borehole

θ = angle of the diametral measurement axis from the horizontal of the local coordinate system

μ = Poisson's ratio of the rock

E = modulus of deformation of the rock

Each overcore test measures the borehole deformation, U , across three different diameters 60° apart. However, no information is obtained about either σ_x or ϵ_x (strain along borehole axis) acting per-

pendicular to the axis of measurement. Thus, equation (5.2.1) cannot be solved for the stress components unless additional information is obtained or assumed. Tests in differently oriented boreholes provide this information.

When determinations of U are made in more than one drill hole, all of the measurements must be related to a common coordinate system. Each stress component of the local (x, y, z) coordinate system may be expressed as a function of the stress tensor of the common (x', y', z') system according to the standard rules of transforming stresses from one rectangular coordinate system to another. Doing this allows equation (5.2.1) to be rewritten:

$$U = J_1\sigma_{x'} + J_2\sigma_{y'} + J_3\sigma_{z'} + J_4\tau_{x'y'} + J_5\tau_{y'z'} + J_6\tau_{z'x'} \quad (5.2.3)$$

where J_i is a function of the f_i defined in equations (5.2.2) and the direction cosines between the two coordinate systems.

With six independent measurements of U , the components of the stress tensor can be determined. Gray and Toews (1967) have shown that measurements in at least three non-parallel boreholes are required to fully define this tensor.

In practice, the precision of the stress components is increased by applying statistical methods to the data. The method used is a multiple regression least squares solution that can combine all the deformation measurements from any number of boreholes regardless of their orientation. The precision of the data may also be evaluated because of the statistics generated by the method.

Once the stress tensor is determined, the principal stresses in the rock mass are calculated using standard methods (Obert and Duvall, 1967). The statistical approach to the data reduction allows confidence levels to be assigned to the results.

The preceding derivations and methods are based upon several assumptions:

- the rock is linearly elastic
- the rock is homogeneous and isotropic
- the state of stress is the same at all measurement locations.

In practice, these assumptions are rarely completely correct.

5.2.2 Secondary Principal Stress Calculation -- USBM Gage

The secondary principal stresses are the two-dimensional principal stresses in the plane perpendicular to the axis of the overcoring borehole. Since the USBM gage overcoring technique does not measure rock deformation along the axis of the borehole, an exact solution of the secondary principal stresses is not possible unless some additional data is obtained regarding either axial deformation or axial stresses. For this project, axial strain measurements from nearby CSIRO cell overcore tests are used in the calculation. Secondary principal stresses are calculated for plane strain conditions with an assumed axial strain as given by Obert and Duvall (1967):

$$P, Q = \frac{E}{6d(1-\mu^2)} \left\{ (U_1^i + U_2^i + U_3^i) \pm \frac{\sqrt{2}}{2} [(U_1^i - U_3^i)^2 + (U_3^i - U_2^i)^2 + (U_2^i - U_1^i)^2]^{1/2} \right\} \quad (5.2.4)$$

$$\theta_{P, Q} = \frac{1}{2} \tan^{-1} \frac{\sqrt{3}(U_3^i - U_2^i)}{2U_1^i - U_3^i - U_2^i} \quad (5.2.5)$$

where:

- P = major secondary stress
- Q = minor secondary stress, perpendicular to P
- E = modulus of deformation of the rock
- μ = Poisson's ratio of the rock
- d = borehole diameter (1.5 inch)
- $\theta_{P, Q}$ = angle between U_1^i and P or Q
- U_i^i = diametral deformation, adjusted for axial strain:

$$U_i^i = U_i + \mu \epsilon_x d$$

where:

- U_i^i = measured diametral deformations, U_1 , U_2 , and U_3
- ϵ_x = assumed axial strain

5.2.3 Biaxial Modulus Calculation -- USBM Gage

The core used for the biaxial test is a thick cylinder; consequently, the modulus of deformation value is calculated using the equation (Obert and Duvall, 1967):

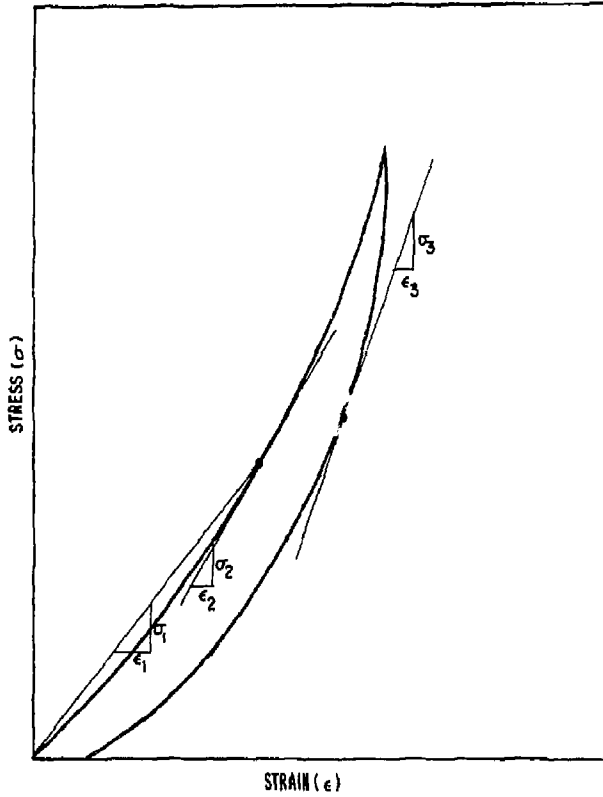
$$E = \frac{4Pb^2a}{U(b^2-a^2)} \quad (5.2.6)$$

where:


- E = modulus of deformation
- P = biaxial stress
- b = outer radius of rock cylinder
- a = inner radius of rock cylinder
- U = diametral deformation (as indicated by the appropriate channel of the borehole deformation gage)

Modulus of deformation values are calculated for each of the three diameters using the pressure change and the resulting deformation. For each pressure increment, a secant modulus and a tangent modulus are calculated. For pressure decrements, only the recovery modulus, which is analogous to a tangent modulus, is calculated. Figure 5.7 shows the relationships among tangent, secant, and recovery moduli. The average tangent, secant, and recovery modulus values of each test are calculated by averaging the respective modulus values over both loading cycles.

The tangent modulus is the best indicator of the rock's true modulus of deformation at higher stresses, particularly if small deformations are involved. The secant modulus is influenced by the effects of joint and microcrack closure during the initial part of the test and is more suitable for large stress changes. The recovery modulus includes effects due to the hysteresis of the rock mass. Because the latter most closely duplicates the behavior of the rock mass during overcore stress relief, the recovery modulus is used in solving for the stress tensor.



- $\frac{\sigma_1}{\epsilon_1}$ = SECANT MODULUS
- $\frac{\sigma_2}{\epsilon_2}$ = TANGENT MODULUS
- $\frac{\sigma_3}{\epsilon_3}$ = RECOVERY MODULUS

 ENGINEERS GEOLOGISTS	FOUNDATION SCIENCES, INC. PORTLAND, OREGON		
	LLNL SPENT FUEL TEST-CLIMAX DEFINITIONS OF DEFORMATION MODULI		
DATE NOV. 1983	JOB NO. 247-1	SCALE NONE	FIG. 5.7

5.3 CSIRO Cell Analysis

5.3.1 Stress Tensor Calculation -- CSIRO Cell

The CSIRO cell measures circumferential, axial, and 45 degree strains at three separate orientations, thus providing enough strain measurements to calculate the complete stress tensor from a single test. The equations relating the observed strains in the CSIRO cell to the change in stress in the rock mass at the cell location are (Worotnicki and Walton, 1976):

$$\epsilon_{\theta} = (\sigma_y + \sigma_z) \frac{K1}{E} + 2(1-\mu)^2 [(\sigma_z - \sigma_y) \cos 2\theta - 2\tau_{yz} \sin 2\theta] \frac{K2}{E} - \frac{\mu K4}{E} \sigma_x \quad (5.3.1)$$

$$\epsilon_x = \frac{\sigma_x - \mu(\sigma_y + \sigma_z)}{E} \quad (5.3.2)$$

$$\gamma_{\theta x} = 4(1+\mu)(\tau_{zx} \cos \theta - \tau_{xy} \sin \theta) \frac{K3}{E} \quad (5.3.3)$$

$$\epsilon_{+45^\circ} = 0.5(\epsilon_x + \epsilon_{\theta} + \gamma_{\theta x}) \quad (5.3.4)$$

where

ϵ_{θ} = circumferential strain at angle θ (see Figure 5.8)

ϵ_x = strain in x direction (see Figure 5.8)

$\gamma_{\theta x}$ = shear strain in θx plane

ϵ_{+45° = strain at $+45^\circ$ from x axis (see Figure 5.8)

$\left. \begin{array}{l} K1 \\ K2 \\ K3 \\ K4 \end{array} \right\} = \text{constants correcting for the mechanical properties and geometry of the CSIRO cell (see Worotnicki and Walton, 1976), equal to 1.12, 1.13, 1.08 and 0.91 respectively in this study}$

E = modulus of deformation of the rock

μ = Poisson's ratio of the rock

$\left. \begin{array}{l} \sigma_x \\ \sigma_y \\ \sigma_z \\ \tau_{xy} \\ \tau_{yz} \\ \tau_{zx} \end{array} \right\} = \text{Components of stress tensor, local coordinate system}$

The coordinate system used in the above equations is shown on Figure 5.8. The x axis is the long axis of the borehole and CSIRO cell. The angle θ is measured clockwise from the "left hand horizontal" when looking down the borehole, with the B rosette installed downward.

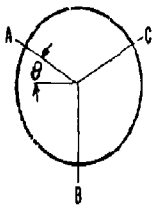
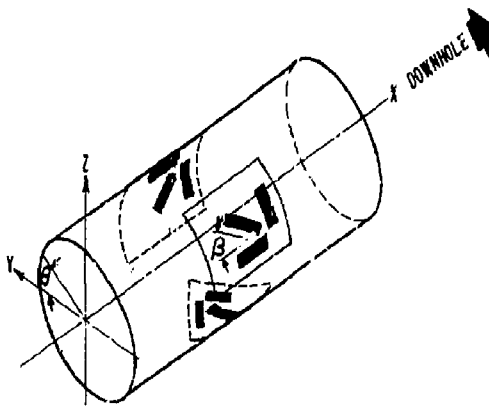
The CSIRO cell measures three circumferential, two axial, and four oblique ($\pm 45^\circ$) strains. Each of these 9 strains may be written in the form

$$U = J_1\sigma_x + J_2\sigma_y + J_3\sigma_z + J_4\tau_{xy} + J_5\tau_{yx} + J_6\tau_{zx} \quad (5.3.5)$$

where the J_i values depend on strain gage orientation and rock properties. Since there are nine equations and six unknowns for the CSIRO cell, multiple regression analysis (e.g. Panek, 1966) is used to solve for the stresses. This "best fit" tensor is then used to calculate expected strains using equations (5.3.1) through (5.3.4), and each computed strain is compared with the measured strain. Large deviations indicate anomalous data; if this happens, the tensor is recalculated, omitting the anomalous data. This process is repeated until all remaining calculated and measured strains are in good agreement. In instances where small bubbles were observed in the epoxy glue above or near a strain gage, the data from that gage was routinely deleted from the solution to determine if the deviations could be reduced for the remaining strain gages. In most instances, however, small bubbles (<1/8 in.) had little or no effect on strain gage errors, and the gages in question were ultimately included in the solution. Up to three gages could be discarded by this technique, but in this study, removal of one gage was generally sufficient to correct any large deviations (> 10 microstrain), though in a few cases, removal of two gages was required (see Table 7.3).


5.3.2 Secondary Principal Stress Calculations -- CSIRO Cell

In order to directly compare the results of the CSIRO cell and the USBM gage in a single borehole, it is useful to compare the secondary principal stresses determined by each instrument. For the



	A	B	C
θ	30°	270°	150°
β	$0^\circ 90^\circ 45^\circ$	$45^\circ 90^\circ 135^\circ$	$0^\circ 90^\circ 45^\circ$

FROM MOROTNICKI AND WALTON, 1970.



**ENGINEERS
GEOLOGISTS**

FOUNDATION SCIENCES, INC.
 PORTLAND, OREGON

LLNL SPENT FUEL TEST-CLIMAX

ORIENTATION OF STRAIN GAUGES
 IN THE CSIRO CELL

DATE MAY 1984 JOB NO. 247-1 SCALE NONE FIG. 5.8

CSIRO cell, these stresses are easily evaluated once the complete stress tensor is determined. As given by Obert and Duvall (1967), these stresses are:

$$P, Q = \frac{\sigma_z + \sigma_y}{2} \pm \frac{1}{2} [(\sigma_z - \sigma_y)^2 + 4\tau_{yz}^2]^{1/2} \quad (5.3.6)$$

$$\theta_{P,Q} = \frac{1}{2} \tan^{-1} \frac{2\tau_{yz}}{\sigma_z - \sigma_y} \quad (5.3.7)$$

where:

P, Q = principal stresses in plane perpendicular to borehole axis

$\theta_{P,Q}$ = angle in degrees to principal stress

$\left. \begin{array}{l} \sigma_z \\ \sigma_y \\ \tau_{yz} \end{array} \right\}$ stresses from complete stress tensor (notation is consistent with Figure 5.8)

5.3.3 Biaxial Modulus and Poisson's Ratio Calculation -- CSIRO Cell

The basis for calculating the modulus and Poisson's ratio from a biaxial compression test on a rock core with a CSIRO cell installed in the center hole is the theory of deformation of a thick walled cylinder (Obert and Duvall, 1967). Because of the symmetry of the problem, the equations reduce to the form:

$$E = \frac{2Pb^2}{\epsilon_{\theta}(b^2 - a^2)} \quad (5.3.8)$$

$$\mu = -\frac{\epsilon_x}{\epsilon_{\theta}} \quad (5.3.9)$$

where:

E = modulus of deformation

μ = Poisson's ratio

P = pressure on outside of rock core

b = outer radius of rock core

a = radius of inner hole

ϵ_x = average axial strain

ϵ_{θ} = average circumferential strain

In the CSIRO cell test, the strain gages are mounted slightly inward from the surface of the inner hole (because of the thickness of the cell wall and epoxy cement), rather than directly on the inner surface, as equations (5.3.8) and (5.3.9) assume. Because of this, the magnitude of ϵ_{θ} is slightly higher than it would be at the rock surface (see Figure 5, Worotnicki and Walton, 1976). The magnitude of the increase is given by the factor K_1 (defined following equation (5.3.4) and equal to 1.12 in this study). Thus,

$$E_t = K_1(E) \quad (5.3.10)$$

where:

$$E_t = \text{true rock modulus}$$

This same type of analysis would imply that the calculated Poisson's ratio should also be increased by the factor K_1 . However, Worotnicki and Walton (1976) showed by testing in an aluminum block (material properties similar to those of Climax quartz monzonite) that the uncorrected Poisson's ratio from the test was nearly equal to the material's actual Poisson's ratio. They hypothesized that the biaxial test itself induces axial tension in the rock core, thus increasing the magnitude of ϵ_x which compensates for the effect of strain gage location.

Therefore, all raw modulus values from CSIRO biaxial tests were increased as given by Equation (5.3.10), while Poisson's ratios were not changed.

Tangent, secant and recovery modulus values and Poisson's ratio are calculated for each pressure change. Average values are calculated by combining respective results over both loading cycles. As discussed in Section 5.2.3, the average recovery modulus is used in calculating the stress tensor.

6.0 BIAxIAL COMPRESSION TEST RESULTS

6.1 USBM Gage Tests

A total of 50 USBM gage biaxial compression tests were performed, using the procedure and equipment described in Section 4.3. The data were analyzed by the methods presented in Section 5.2.3. The raw data, reduced data, and pressure-deformation curves for each test are contained in Appendix C. The recovery modulus results are summarized in Table 6.1.

Modulus values of the Climax quartz monzonite, determined by analysis of USBM gage data, generally range from 9 to 11×10^6 psi, with a mean of about 10×10^6 psi. The pressure-deformation curves indicate that the rock is generally elastic.

One test, test 10 (refer to Table 6.1), was conducted in an inclusion of mafic rock. The modulus of this material, about 8×10^6 psi, is slightly lower than that of the quartz monzonite itself.

6.2 CSIRO Cell Tests

A total of 25 CSIRO biaxial compression tests were performed, using the procedures and equipment described in Section 4.3. The data were analyzed using the methods presented in Section 5.3.3. The raw data, reduced data, and pressure-deformation curves for each test are contained in Appendix C. The recovery modulus and Poisson's ratio results are summarized in Table 6.2. The recovery modulus values are corrected as described in Section 5.3.3.

A review of the pressure-deformation curves in Appendix C reveals apparent differences in measured behavior between Phase I and Phase II tests. Figure 5.6 shows typical behavior for Phase I tests, which exhibited relatively elastic stress-strain response. Figure 6.1 shows typical behavior for Phase II tests, which exhibited some negative hysteresis in circumferential gage response and an apparent permanent plastic strain, at least over the pressure range and time period of the test. Examination of the test records does not reveal any differences between Phase I and Phase II test conditions or procedures, except for a dif-

Table 6.1

USBM GAGE BIAxIAL COMPRESSION TEST RESULTS

Test No.	Test Depth, ft	Orientation, Degrees*	Recovery Modulus x 10 ⁶ psi		
			Channel 1	Channel 2	Channel 3
4-1-B	3.2	176	9.9	9.0	8.9
4-3-B	9.8	174	9.6	9.9	9.4
4-5-B	13.7	47	9.0	9.2	9.2
5-1-B	3.3	20	9.2	8.3	7.6
5-3-B	6.8	154	9.8	10.2	9.6
5-5-B	13.6	87	10.4	10.2	10.4
6-1-B	3.6	23	12.1	10.5	11.4
6-2-B	5.5	106	9.3	10.9	9.7
6-3-B	7.3	15	11.2	10.5	11.1
6-5-B	11.9	114	11.1	9.7	9.9
6-6-B	13.4	142	12.2	11.5	13.0
6-7-B	15.0	123	10.2	9.6	10.3
6-8-B	16.6	101	10.4	8.3	9.1
7-1-B	4.0	108	10.4	9.7	9.3
7-3-B	7.4	139	9.8	9.7	9.7
7-5-B	10.6	157	10.1	10.4	10.2
7-6-B	13.8	155	11.2	11.1	11.6
7-7-B	15.3	98	9.4	9.2	9.8
8-1-B	3.7	143	10.6	10.4	10.1
8-3-B	10.3	165	9.6	10.4	9.4
8-5-B	15.2	154	9.9	10.7	10.1
8-6-B	16.8	77	11.1	10.1	10.4
8-8-B	28.4	166	11.2	9.4	10.8
8-10-B	43.8	6	10.1	9.4	8.7
8-12-B	61.1	14	9.5	9.5	9.0
8-14-B	75.4	121	9.5	9.5	9.3
8-16-B	78.9	147	10.1	9.8	9.4
8-18-B	82.6	173	9.1	9.3	9.4
8-19-B	86.1	162	9.9	9.7	9.3
8-20-B	95.2	94	10.0	9.2	9.4
8-22-B	104.3	133	9.7	12.1	9.6
9-2-B	37.7	21	9.5	8.8	8.3
9-4-B	41.1	115	9.9	9.0	9.0
9-6-B	44.9	64	10.9	9.4	10.7
9-8-B	48.9	171	9.7	8.9	9.4
9-10-B	53.6	167	9.6	9.3	9.1
9-11-B	56.3	86	10.6	10.3	10.2
9-12-B	57.9	28	9.5	9.7	9.6

*Degrees clockwise to Channel 1 from vertical-up, looking down borehole.

**Mafic Inclusion

Table 6.1 Continued

USBM GAGE BIAxIAL COMPRESSION TEST RESULTS

Test No.	Test Depth, ft	Orientation, Degrees*	Recovery Modulus x 10 ⁶ psi		
			Channel 1	Channel 2	Channel 3
10-5-B	66.3	14	11.4	10.0	8.5
10-7-B	75.0	28	9.9	10.1	9.8
10-8-B	76.4	35	11.3	9.1	9.9
10**	77.1	0	8.6	7.9	7.4
11-1-B	61.7	5	9.0	8.7	9.0
11-2-B	63.6	8	8.4	7.9	7.7
11-3-B	66.9	30	10.3	9.5	9.4
11-5-B	73.4	10	9.0	9.7	9.4
11-7-B	78.0	167	11.1	10.7	10.6
11-8-B	82.4	3	11.2	11.3	9.8
11-10	87.4	105	11.1	10.4	9.6
11-12-B	91.4	5	10.5	11.1	10.5

*Degrees clockwise to Channel 1 from vertical, looking down borehole.

**Mafic Inclusion

Table 6.2

CSIRO CELL BIAxIAL COMPRESSION TEST RESULTS

Test No.	Test Depth, ft	Recovery Modulus $\times 10^6$ psi	Poisson's Ratio
5-2-C	5.3	9.6	0.33
5-6-C	14.8	10.4	0.26
7-2-C	5.5	11.6	0.29
8-2-C	7.5	9.2	0.27
8-4-C	12.7	9.6	0.28
8-7-C	21.3	9.9	0.34
8-9-C	41.3	10.0	0.27
8-13-C	67.8	10.8	0.31
8-17-C	81.0	10.2	0.31
8-21-C	96.7	10.6	0.30
8-25-C	109.4	10.4*	0.31*
9-3-C	39.1	9.5	0.27
9-5-C	42.6	10.0	0.28
9-7-C	46.9	10.2	0.30
9-9-C	50.5	10.4	0.27
9-13-C	59.2	10.4	0.29
10-2-C	64.4	10.8	0.26
10-4-C	67.8	10.2	0.27
10-6-C	73.1	10.3**	0.27**
10-9-C	80.4	10.3	0.27
11-4-C	70.6	9.5	0.29
11-6-C	75.5	11.0	0.31
11-9-C	84.3	9.5***	0.29***
11-11-C	89.4	10.1	0.26
11-13-C	94.5	10.1	0.29

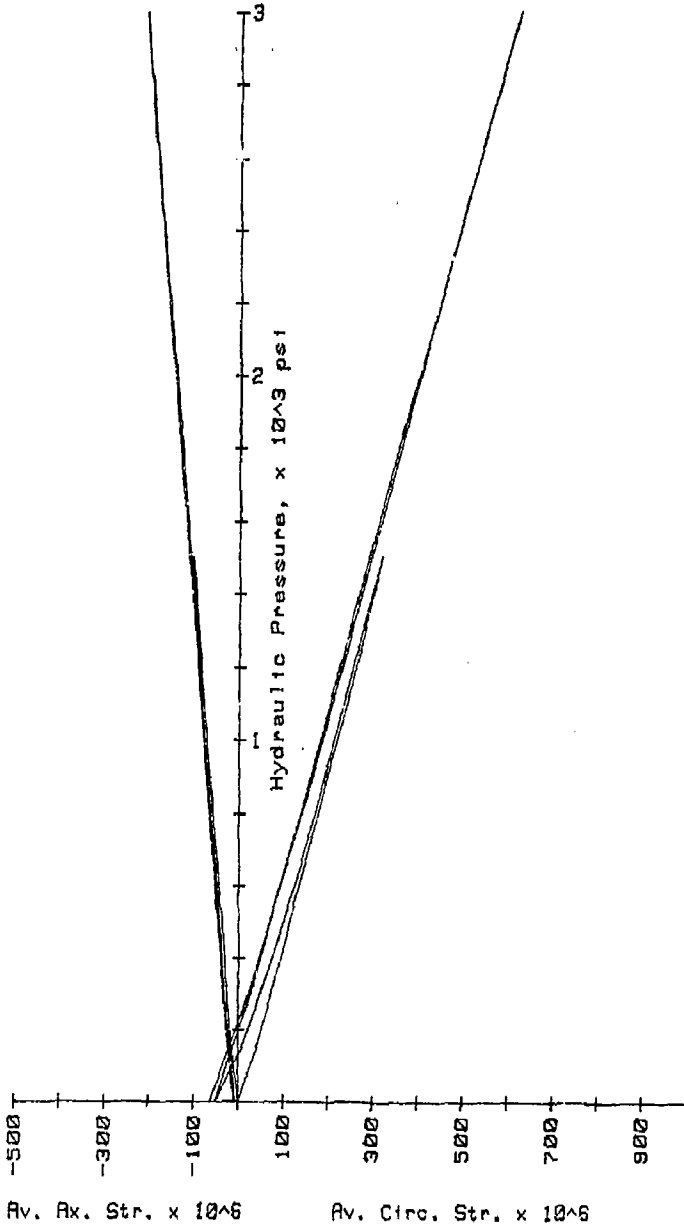
* Values obtained from averaging test results of 8-17-C and 8-21-C

** Values obtained from averaging test results of 10-4-C and 10-9-C

*** Axial gage Ch-1 not used in solutions

Figure 6.1
 Phase II
 CSIRO Biaxial Modulus Test
 Test No.: ISS-11-13-C
 Depth: 94.5 ft.
 Date: 04/06/84

Average Tangent Modulus: 9.9×10^6 psi
 Average Secant Modulus: 10.4×10^6 psi
 Average Recovery Modulus: 9.0×10^6 psi
 Average Poisson's Ratio: .294



ference in elapsed time between CSIRO installation in the borehole and performance of the biaxial compression test. Differences in borehole orientation are not considered to influence the biaxial results. In addition, USBM modulus tests in borehole ISS-11 did not show any significant non-elastic behavior, leading to the conclusion that the negative hysteresis is associated with the CSIRO cell, rather than reflecting an actual rock property. In general, Phase I biaxial tests were performed 2 to 7 days after CSIRO installation, while Phase II tests were performed within 1 day of installation. It is possible that the epoxy cement used to install CSIRO cells does not completely cure within 1 day of mixing and, therefore, exhibits some plastic behavior. The negative hysteresis may reflect a permanent extrusion of epoxy under biaxial loading, without breaking the bond between the CSIRO cell and the rock. In any case, this is a minor effect, because despite the observed differences in pressure deformation curves, average recovery modulus values for both Phase I and II are identical.

Recovery modulus values of the Climax quartz monzonite, determined from analysis of CSIRO cell data, generally range from 9 to 11 x 10⁶ psi, with a mean of about 10 x 10⁶ psi. Poisson's ratio ranges from 0.26 to 0.34, with a mean of 0.29.

6.3 Comparison of Results

A summary of deformation properties for each instrument type is presented in Table 6.3. No statistically significant difference exists between the average recovery modulus of the two instrument types.

Table 6.3

SUMMARY OF DEFORMATIONAL PROPERTIES

<u>Gage Type</u>	<u>Average Recovery Modulus x 10⁶ psi</u>	<u>Average Poisson's Ratio</u>
CSIRO	10.2 (0.5)*	0.29 (0.02)
USBM	9.9 (0.9)	NA

*Numbers in parentheses are standard deviations of the data sets x 10⁶ psi

7.0 IN SITU STRESS MEASUREMENT RESULTS

7.1 General

A total of 53 USBM gage and 37 CSIRO cell overcore tests were attempted during this study. Good test data were obtained for 43 USBM gage attempts (81% success ratio) and 25 CSIRO cell attempts (68% success ratio). Unusable USBM gage data resulted from loose or sticking contact buttons, poor contact of the buttons with the borehole wall, poor temperature stabilization after the overcore test, gage slippage during overcoring, core breakage during overcoring, and damaged signal cables. One CSIRO cell failure resulted from signal cable damage. The remainder of the unsuccessful CSIRO cells failed because of gluing problems during installation: five cells that were improperly glued were not overcored, and six overcored cells were later found to have large voids in the glue between the strain gages and the rock, which significantly affected the response of a large enough number of strain gages so that too few valid measurements were available to permit calculation of the stress tensor.

The data for each successful overcore test were analyzed by the methods presented in Section 5.0. Table 7.1 summarizes the selected initial and final USBM gage overcore test output readings and their differences (deltas). The delta values are multiplied by the appropriate USBM gage calibration factors, given in Table B3.2, Appendix B, to calculate the diametral deformation values given in Table 7.2, which are used in analyzing USBM overcore tests. The modulus values used are given in Table 6.1. The value of Poisson's ratio for USBM gage data analyses is 0.29, the average from all of the CSIRO biaxial compression tests. Initial and final CSIRO cell overcore test output readings and the strain changes used in analyzing CSIRO cell tests, are given in Table 7.3. Modulus and Poisson's ratio values are given in Table 6.2. All overcore and biaxial test data from which these tables are derived are presented in raw, reduced, and plotted form in Appendix C.

Axial strain values used in computing USBM gage secondary principal stresses in rib boreholes ISS-8, 9, 10, and 11 were derived from

Table 7.1
SUMMARY OF USBM GAGE OVERCORE OUTPUT READINGS

Test No.5	Output Reading, microstrain*								
	Channel 1			Channel 2			Channel 3		
	Initial	Final	Delta	Initial	Final	Delta	Initial	Final	Delta
4-3-B	14929	14489	440	14942	14634	308	15021	15062	-41
4-5-B	21915	21623	292	22117	22077	40	22078	21716	362
5-3-B	16956	16710	246	16954	16350	604	17010	16945	65
5-5-B	14920	15150	-230	14958	14628	330	15028	14576	452
6-1-B	15229	14938	-291	15028	15084	-56	13074	12394	680
6-2-B	14826	14673	153	14899	14357	542	15261	15261	-100
6-3-B	17975	17691	284	17960	18136	-176	18000	17576	424
6-4-B	21964	21588	376	21994	22044	-50	22044	21964	80
6-5-B	17992	18064	-72	17965	17651	314	18012	18049	-37
6-6-B	18004	**	**	17963	17665	298	17980	17829	151
6-7-B	24954	24849	105	24943	24694	249	25046	25092	-46
7-1-B	23063	22844	219	23063	22351	712	23046	22816	230
7-3-B	17995	17460	535	17995	17466	529	17995	18010	-15
7-5-B	18020	17455	565	18008	17705	303	17995	17921	74
7-6-B	18999	18575	424	19000	18783	217	18999	18870	129
7-7-B	21996	22067	-71	21993	21501	492	21998	21902	96
8-1-B	22989	22764	225	22991	22457	534	22990	22880	110
8-3-B	18036	17544	492	17987	17903	84	18063	17850	213
8-5-B	13956	13255	701	13998	13626	372	14056	13890	166
8-6-B	17835	17770	65	17941	17540	401	18024	17678	346
8-8-B	13920	13453	467	13712	13210	502	13981	13635	346
8-10-B	18001	17799	202	18001	17774	227	18000	17863	137
8-12-B	17007	16612	395	17004	16576	428	16679	16998	319
8-14-B	22997	22741	256	22987	22630	357	22997	22638	359
8-16-B	22997	22651	346	22996	22796	200	22999	22659	340
8-18-B	14854	14636	218	14831	14509	322	15206	15004	202
8-19-B	14998	14672	326	14998	14560	438	15001	14792	209
8-20-B	16997	16840	157	17004	16836	168	17002	16646	356

*Positive readings indicate increase in borehole diameter.
**Data invalid.

Table 7.2

SUMMARY OF USBM GAGE OVERCORE DATA

Test No.	Depth, ft	Orientation, Degrees*	Diametral Deformation, microinches**			Axial Strain, microstrain***
			CH-1	CH-2	CH-3	
4-3-B	9.8	174	417	301	- 40	8
4-5-B	13.7	47	305	40	371	8
5-3-B	6.8	154	254	596	66	8
5-5-R	13.6	87	-238	326	457	8
6-1-B	3.6	23	293	- 55	680	8
6-2-B	5.5	106	154	537	-100	8
6-3-B	7.3	15	286	-174	424	8
6-4-B	10.0	4	379	- 50	80	8
6-5-F	11.9	114	- 73	311	- 37	8
6-7-B	15.0	123	108	246	- 47	8
7-1-B	4.0	108	204	700	224	8
7-3-B	7.4	139	498	520	- 15	8
7-5-B	10.6	157	525	298	72	8
7-6-B	13.8	155	394	213	126	8
7-7-B	15.3	98	- 74	497	98	8
8-1-B	3.7	143	232	527	111	-64
8-3-B	10.3	165	508	83	216	-28
8-5-B	15.2	154	665	364	162	-12
8-6-B	16.8	77	68	405	355	- 7
8-8-B	28.4	166	488	507	355	12
8-10-B	43.8	6	216	236	142	30
8-12-B	61.1	14	413	432	327	43
8-14-B	75.4	121	268	361	368	51
8-16-B	78.9	147	362	202	349	53
8-18-B	82.6	173	228	325	207	55
8-19-B	86.1	162	341	442	214	56
8-20-B	95.2	94	164	170	365	60
9-2-B	37.7	21	30	335	417	50
9-4-B	41.1	115	237	199	234	51
9-6-B	44.9	64	113	226	281	51
9-8-B	48.9	171	610	211	514	52
9-10-B	53.6	167	213	354	218	52
9-12-B	57.9	28	252	118	346	53
10-3-B	66.3	14	59	524	326	60
10-5-B	69.6	86	836	19	327	71
10-7-B	75.0	28	354	560	170	86
10-8-B	76.4	35	438	620	232	89

*Orientation in degrees clockwise from vertical-up to Channel 1.

**Positive deformations are increases in Ex hole diameter during over-coring.

***Values used in computing secondary principal stresses.
Positive values are core extension during overcoring.

Table 7.2 Continued

SUMMARY OF USBM GAGE OVERCORE DATA

Test No.	Depth, ft	Orientation, Degrees*	Diametral Deformation, microinches**			Axial Strain, microstrain***
			CH-1	CH-2	CH-3	
11-2-B	63.6	8	741	609	153	52
11-3-B	66.9	30	209	78	365	50
11-5-B	73.4	10	632	309	248	47
11-8-B	82.4	3	523	830	338	43
11-10-B	87.4	105	328	599	817	41
11-12-B	91.4	5	952	394	- 57	39

* Orientation in degrees clockwise from vertical-up to Channel 1.

** Positive deformations are increases in Ex hole diameter during over-coring.

***Values used in computing secondary principal stresses.
Positive values are core extension during overcoring.

Table 7.3

SUMMARY OF CSIRO CELL OVERCORE DATA

Test No.	Depth ft	Orientation, Degrees*	Strain Readings and Change, Microstrain**									
			Ch-1 Axial	Ch-2 Circ.	Ch-3 45°	Ch-4 45°	Ch-5 135°	Ch-6 Circ.	Ch-7 Axial	Ch-8 Circ.	Ch-9 45°	
5-2-C	5.3	185	Final	-3463	-3266	-3505	-3568	-3412	-3478	-3407	-3248	-3071
			Initial	-3508	-3520	-3518	-3513	-3512	-3527	-3499	-3518	-3508
			Delta	45***	254	13	45	100	49	92	270	437
5-6-C	14.8	187	Final	-3486	-3311	-3473	-3473	-3425	-3352	-3572	-3340	-3380
			Initial	-3502	-3500	-3492	-3508	-3490	-3489	-3520	-3487	-3497
			Delta	16***	189	19	35	65	137	-52	147	117
7-2-C	5.5	186	Final	-3072	-2857	-2872	-3052	-3050	3073	-3073	-2740	-3060
			Initial	-3069	-3071	-3069	-0373	-3068	3229	-3069	-3069	-3069
			Delta	-3	214	197	21	18	-156***	-4	329	9
8-2-C	7.5	190	Final	490	914	525	524	494	552	233	712	653
			Initial	496	757	505	496	502	502	248	492	498
			Delta	-6	157	20	28	-8	50	-15	220	155
8-4-C	12.7	186	Final	1434	1688	1568	1534	1556	1669	1437	1837	1656
			Initial	1500	1502	1500	1500	1500	1500	1499	1502	1501
			Delta	-66	186	68	34	56	169	-62	335	155
8-7-C	21.3	186	Final	1530	1810	1570	1628	1706	1768	1497	1712	1732
			Initial	1499	1499	1499	1501	1503	1498	1501	1500	1500
			Delta	31	311	71***	127	203	270	-4***	212	232
8-9-C	41.3	182	Final	1014	1084	1030	1047	1060	1100	0025	1153	1068
			Initial	998	998	999	1001	998	998	0004	1000	948
			Delta	16	85	31	46	62	102	29	153	120

*Orientation in degrees clockwise from vertical-up to "B" rosette

**Positive change is extension during overcore test

***Data not used in stress calculations

Table 7.3 Continued

SUMMARY OF CSIRO CELL OVERCORE DATA

Test No.	Depth ft	Orientation, Degrees*	Strain Readings and Change, Microstrain**									
			Ch-1 Axial	Ch-2 Circ.	Ch-3 45°	Ch-4 45°	Ch-5 135°	Ch-6 Circ.	Ch-7 Axial	Ch-8 Circ.	Ch-9 45°	
8-13-C	67.8	2	Final	-3930	-3780	-3897	-3852	-3960	-3905	-3950	-3844	-3916
			Initial	-4000	-4001	-4001	-4001	-4001	-4001	-4001	-4000	-4001
			Delta	70***	221	104	149	41	96	51	156	85
8-17-C	81.0	181	Final	-2958	-2832	-2800	-2948	-2804	-2843	-2945	-2906	-2959
			Initial	-3000	-2999	-2999	-3000	-3000	-2843	-2945	-2906	-2959
			Delta	42***	167	199	52	196	157	54	95	40
8-21-C	96.7	180	Final	-3452	-3376	-3384	-3434	-3427	-3432	-3454	-3434	-3482
			Initial	-2502	-3501	-3503	-3502	-3502	-3502	-3501	-3503	-3503
			Delta	50	125	119	68	75	70	47	69	21
8-25-C	109.4	192	Final	-1902	-1793	-1754	-1846	-1787	-1720	-1883	-1992	-2004
			Initial	-2000	-2003	-2003	-2001	-2003	-2003	-2003	-2003	-2001
			Delta	98	210	249	155	216***	282	120***	11	3
9-3-C	39.1	180	Final	-3518	-3467	-3451	-3403	-3530	-3344	-3504	-3374	-3493
			Initial	-3586	-3536	-3536	-3543	-3582	-3558	-3564	-3582	-3548
			Delta	68	69	85	140	52***	214	60	208	55
9-5-C	42.6	175	Final	1039	1128	1062	1146	1020	1125	993	1108	1025
			Initial	1005	1012	1007	1000	1001	998	957	997	1001
			Delta	34	116	55	146	19	127	36	111	24
9-7-C	46.9	178	Final	-2474	-2421	-2415	-2399	-2535	-2176	-2464	-2367	-2532
			Initial	-2502	-2502	-2502	-2502	-2501	-2502	-2501	-2502	-2502
			Delta	28***	81	87	103	34	26	37	135	30

*Orientation in degrees clockwise from vertical-up to "B" rosette

**Positive change is extension during overcore test.

***Data not used in stress calculations

Table 7.3 Continued

SUMMARY OF CSIRO CELL OVERCORE DATA

Test No.	Depth ft	Orientation, Degrees*	Strain Readings and Change, Microstrain**									
			Ch-1 Axial	Ch-2 Circ.	Ch-3 45°	Ch-4 45°	Ch-5 135°	Ch-6 Circ.	Ch-7 Axial	Ch-8 Circ.	Ch-9 45°	
9-9-C	50.5	0	Final	935	994	942	925	963	1003	928	1080	1042
			Initial	870	869	870	872	866	873	868	869	868
			Delta	65	125	72	53	97	130	60	211	174
9-13-C	59.2	173	Final	776	842	889	839	748	851	753	903	702
			Initial	702	706	706	701	700	700	700	702	700
			Delta	74***	136	183***	138	48	151	53	201	2
10-2-C	64.4	296	Final	-3458	-3257	-3488	-3322	-3574	-3462	-3442	-3230	-3320
			Initial	-3504	-3504	-3503	-3503	-3505	-3505	-3503	-3502	-3504
			Delta	46	247	15	181	69	43	61	272	184
10-4-C	67.8	2	Final	- 514	- 448	- 486	- 396	- 174	- 79	- 498	- 503	- 290
			Initial	- 601	- 601	- 601	- 603	- 602	- 601	- 604	- 600	- 602
			Delta	87***	153	115	207	428	522	106***	97	312
10-6-C	73.1	180	Final	- 496	- 481	- 425	- 409	- 396	- 261	- 510	- 340	- 493
			Initial	- 581	- 583	- 580	- 592	- 584	- 588	- 581	- 583	- 581
			Delta	85	102	155	183	188	327	71***		243
10-9-C	80.4	264	Final	1098	1249	1112	1170	985	1083	1099	1235	1147
			Initial	997	1000	998	1001	1000	1000	1000	1000	1000
			Delta	101	249	114	169	15***	83	99	235	147

*Orientation in degrees clockwise from vertical-up to "B" rosette

**Positive change is extension during overcore test

***Data not used in stress calculations

Table 7.3 Continued

SUMMARY OF CSIRO CELL OVERCORE DATA

Test No.	Depth ft	Orientation, Degrees*	Strain Readings and Change, Microstrain**									
			Ch-1 Axial	Ch-2 Circ.	Ch-3 45°	Ch-4 45°	Ch-5 135°	Ch-6 Circ.	Ch-7 Axial	Ch-8 Circ.	Ch-9 45°	
11-4-C	70.6	190	Final	- 552	- 453	- 551	- 457	- 960	- 457	- 530	- 402	- 480
			Initial	- 600	- 602	- 599	- 599	- 993	- 594	- 595	- 597	- 597
			Delta	48	147	48	142	33	137	65***	195	117
11-6-C	75.5	174	Final	- 563	- 372	- 483	- 428	- 560	- 398	- 554	- 339	- 513
			Initial	- 609	- 611	- 611	- 611	- 607	- 607	- 599	- 610	- 605
			Delta	46	239	128	183	47	209	45	271	92
11-9-C	84.3	182	Final	- 574	- 143	- 403	- 314	- 467	- 305	- 556	- 300	- 398
			Initial	- 601	- 603	- 602	- 602	- 605	- 602	- 603	- 602	- 602
			Delta	27***	460***	199	288	138	297	47	302	204
11-11-C	89.4	168	Final	- 565	- 65	- 312	- 381	- 403	- 359	- 551	- 458	- 520
			Initial	- 598	- 601	- 601	- 601	- 605	- 600	- 604	- 601	- 601
			Delta	33	536	289	220	202	241	53	143	81
11-13-C	94.5	183	Final	- 670	- 16	- 213	- 608	- 510	- 586	- 691	- 532	- 699
			Initial	- 702	- 699	- 708	- 708	- 710	- 708	- 706	- 699	- 703
			Delta	32	683	495	100	200***	122	15***	167	4

*Orientation in degrees clockwise from vertical-up to "B" rosette.

**Positive change is extension during overcore test.

***Data not used in stress calculations.

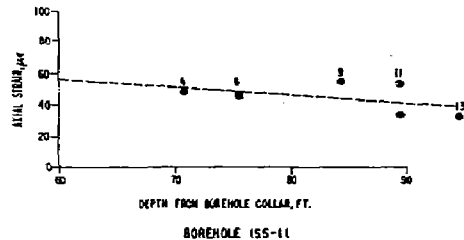
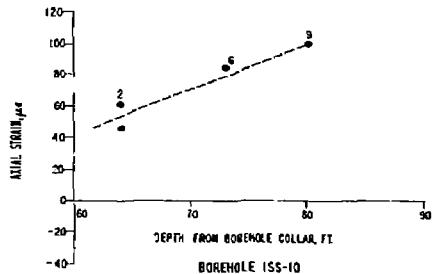
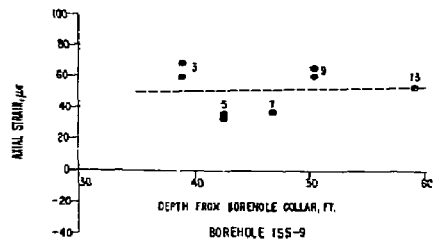
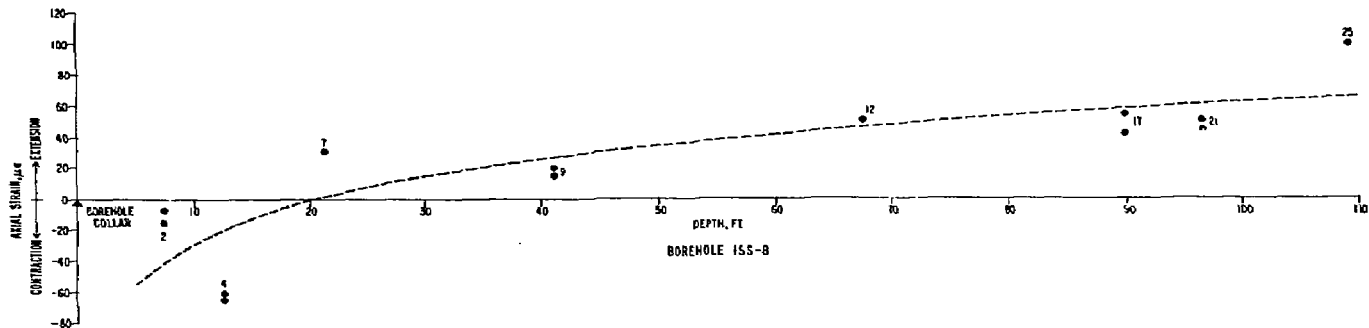
regression curves of all valid CSIRO cell axial strain measurements. These data and curves are shown on Figure 7.1. The curve for borehole ISS-8 is logarithmic, while the other three are linear. Only four valid CSIRO cell axial strain measurements were obtained in the pillar boreholes. These show a great deal of scatter, so the average value of 8 microstrain was used in analyzing USBM gage tests in the pillars. A sensitivity analysis of the chosen axial strain was performed, which indicated that, as a rule-of-thumb, a change of 1 microstrain produced a change of 2 psi in stress magnitude and did not affect the orientation of the stress. If the differences between the measured axial strain and the regression curves shown on Fig. 7.1 are representative of the real scatter of the data, then the errors introduced by using regression and average values are only a few percent of the total stress magnitude. The axial strain values used in calculating USBM gage secondary principal stresses are given on Table 7.2.

7.2 Rib Stress Measurements -- Boreholes ISS-8, 9, 10, and 11

7.2.1 Secondary Principal Stress Solutions -- Rib Boreholes

The results of all secondary principal stress calculations are presented in Table 7.4. The secondary principal stresses for the rib boreholes are presented graphically on Figures 7.2 through 7.6. The orientations on Figures 7.2 through 7.4 are shown as if an observer were looking into the borehole from the borehole collar. From inspection of the table and figures, it is apparent that the USBM gage and CSIRO cell results agree fairly well with respect to secondary principal stress orientation; however, the USBM gage stress magnitudes average about 30% higher than the CSIRO cell magnitudes.

In borehole ISS-8, the maximum secondary principal stress is predominantly vertical in the 20-ft zone closest to the test facility and ranges in magnitude from about 1,000 to 1,800 psi. The minimum secondary principal stress appears to increase gradually as the depth increases from about 5 to 20 ft.



● AXIAL DEFORMATIONS FROM STRAIN
 GAGES (AND TEST NO. SHOWN)
 --- AXIAL DEFORMATION USED IN USDM
 BASE SECONDARY PRINCIPAL STRESS
 CALCULATIONS



FOUNDATION SCIENCES, INC.
 PORTLAND, OREGON

LLNL SPENT FUEL TEST - CLIMAX
 AXIAL STRAINS FROM CSIRO
 CELL TESTS
 BOREHOLES 155-9, 10, & 11

DATE MAY 1984 JOB NO. 241-1 SCALE SHOWN FIG. 71

Table 7.4

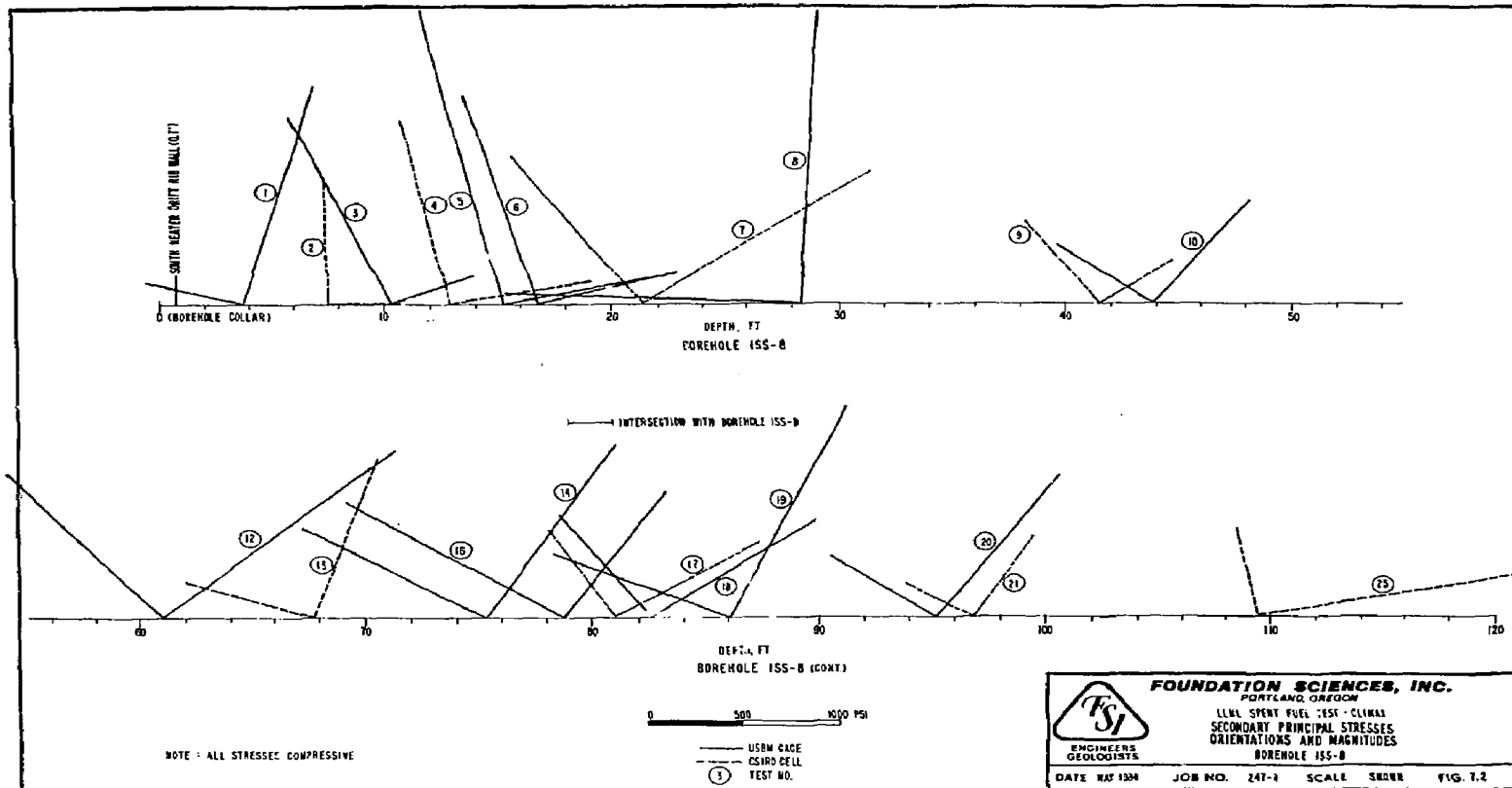
SUMMARY OF SECONDARY PRINCIPAL STRESSES

Test No.	Depth	Major Principal Stress, psi	Minor Principal Stress, psi	Orientation of Major Principal Stress, Counterclockwise from Right Horizontal
4-3-B	9.3	1296	333	72
4-5-B	13.7	1141	468	79
5-2-C	5.3	1362	674	87
5-3-B	6.8	1711	547	66
5-5-B	13.6	1498	-111	88
5-6-C	14.8	781	629	57
6-1-B	3.6	2191	439	112
6-2-B	5.5	1506	51	114
6-3-B	7.3	1471	32	111
6-4-B	10.0	1030	51	95
6-5-B	11.9	676	-202	93
6-7-B	15.0	674	76	104
7-1-B	4.0	1914	777	102
7-2-C	5.5	1531	662	97
7-3-B	7.4	1818	579	100
7-5-B	10.6	1602	641	97
7-6-B	13.8	1332	696	106
7-7-B	15.3	1165	33	103
8-1-B	3.7	1464	527	76
8-2-C	7.5	826	378	91
8-3-B	10.3	1334	464	113
8-4-C	12.7	1231	760	112
8-5-B	15.2	1969	929	102
8-6-B	16.8	1407	641	106
8-7-C	21.3	1477	1193	36
8-8-B	28.4	1900	1554	87
8-9-C	41.3	657	465	126
8-10-B	43.8	847	609	53
8-12-B	61.1	1528	1263	42
8-13-C	67.8	1099	722	72
8-14-B	75.4	1323	1109	59
8-16-B	78.9	1348	978	147
8-17-C	81.0	894	656	31
8-18-B	82.6	1059	812	40
8-19-B	86.1	1502	1013	66
8-20-B	95.2	1118	674	55
8-21-C	96.7	617	425	59
8-25-C	109.4	1399	574	11

Table 7.4 Continued

SUMMARY OF SECONDARY PRINCIPAL STRESSES

<u>Test No.</u>	<u>Depth</u>	<u>Major Principal Stress, psi</u>	<u>Minor Principal Stress, psi</u>	<u>Orientation of Major Principal Stress, Counterclockwise from Right Horizontal</u>
9-2-B	37.7	1238	527	155
9-3-C	39.1	1015	581	151
9-4-B	41.1	894	772	771
9-5-C	42.6	631	584	14
9-6-B	44.9	1042	670	107
9-7-C	46.9	610	307	107
9-8-B	48.9	2049	1168	121
9-9-C	50.5	967	678	121
9-10-B	53.6	1119	810	45
9-12-B	57.9	1142	683	105
9-13-C	59.2	979	782	133
10-2-C	64.4	1383	646	157
10-3-B	66.3	1625	672	3
10-4-C	67.8	2061	771	2
10-5-B	69.6	2413	681	15
10-6-C	73.1	1536	886	162
10-7-B	75.0	1868	1027	16
10-8-B	76.4	2075	1334	20
10-9-C	80.4	1293	771	4
11-2-B	63.6	2096	1000	60
11-3-B	66.9	1128	562	104
11-4-C	70.6	863	702	106
11-5-B	73.4	1778	1033	75
11-6-C	75.5	1440	1226	112
11-8-B	82.4	2966	1680	39
11-9-C	84.3	2110	1417	59
11-10-B	87.4	2659	1775	64
11-11-C	89.4	2080	947	65
11-12-B	91.4	2852	624	71
11-13-C	94.5	2491	734	59

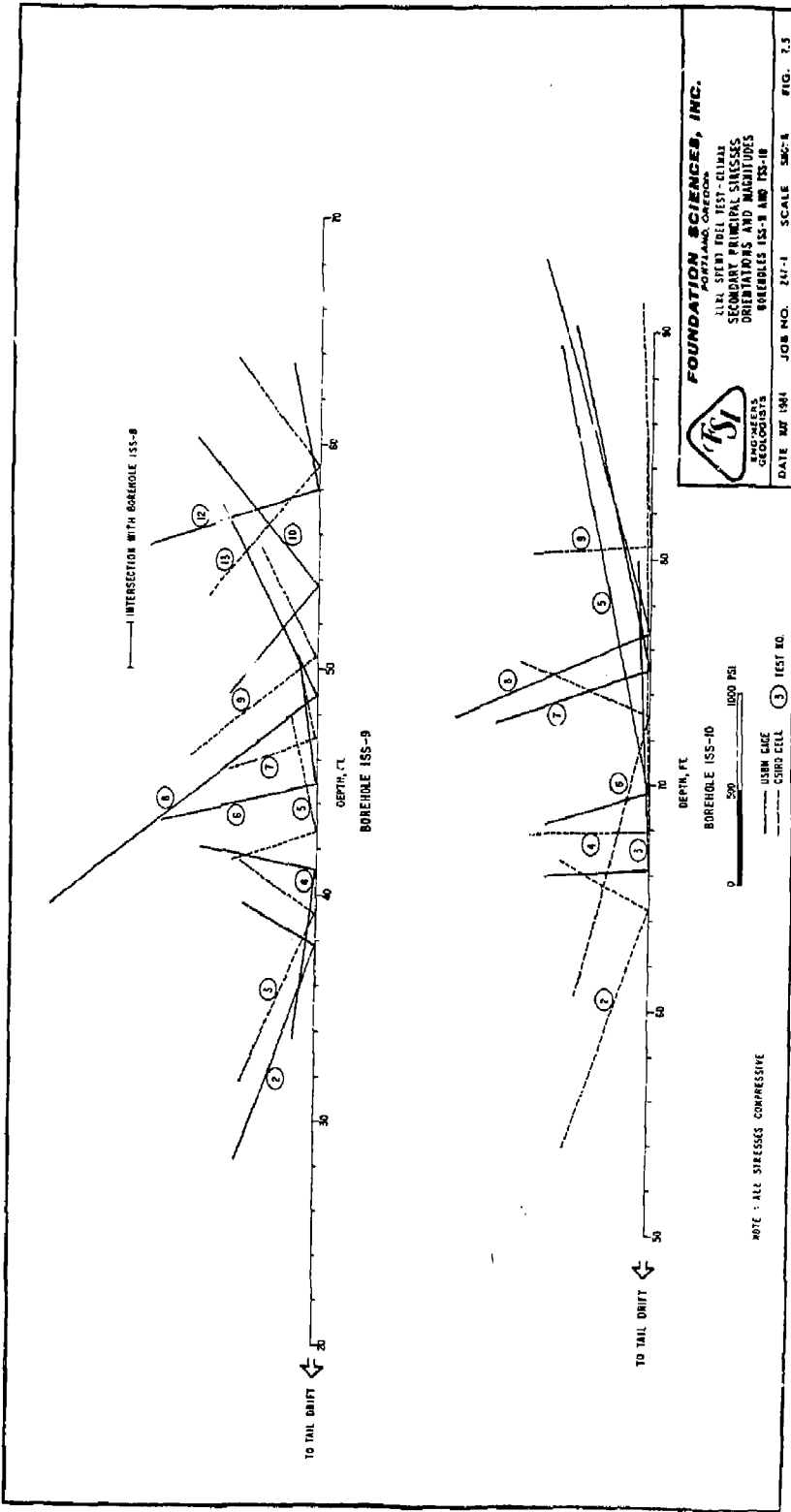


NOTE: ALL STRESSES COMPRESSIVE

0 500 1000 PSI

USM RAGE
CIRD CELL
TEST NO.

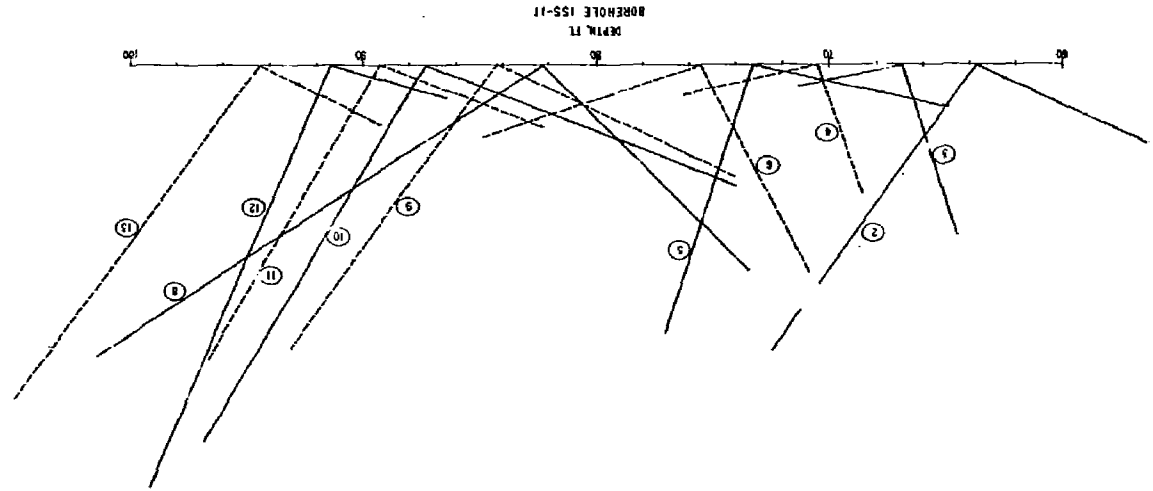
FOUNDATION SCIENCES, INC.
 PORTLAND, OREGON
 LLNL SPENT FUEL CASE - CLIMATE
 SECONDARY PRINCIPAL STRESSES
 ORIENTATIONS AND MAGNITUDES
 BOREHOLE ISS-B
 ENGINEERS
 GEOLOGISTS
 DATE MAR 1984 JOB NO. 247-1 SCALE 8000R FIG. 7.2

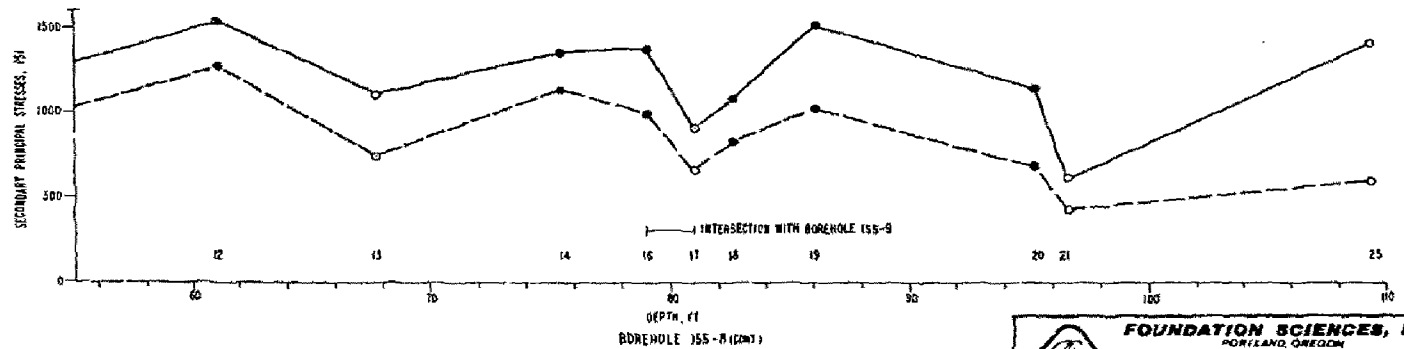
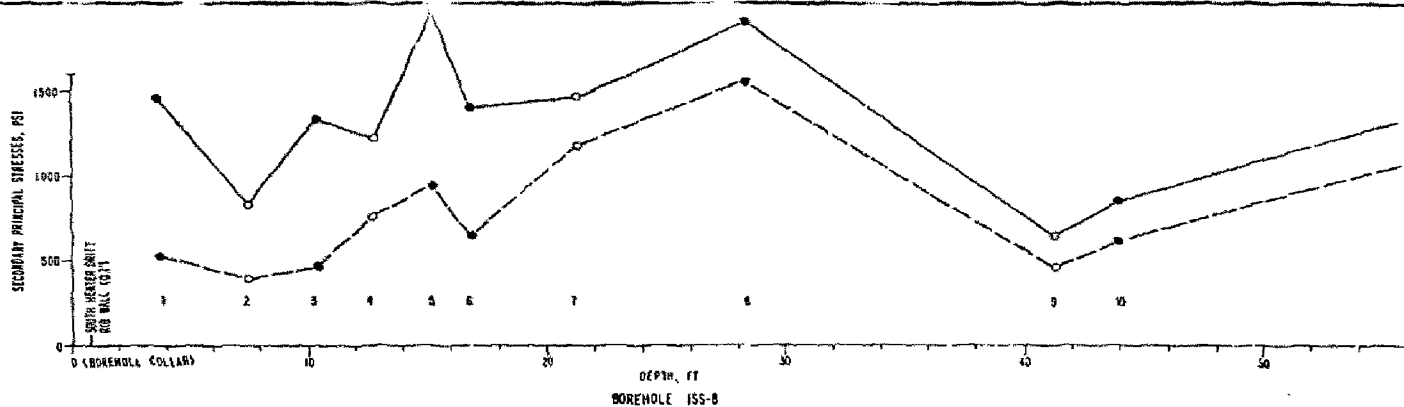


DATE MAY 1988
 JOB NO. 241-1
 SCALE SHOWN
 FIG. 14
 FOUNDATION SCIENCES, INC.
 PORTLAND, OREGON
 LIMIT SPREAD PILE TEST - CLIMAX
 SECONDARY PRINCIPAL STRESSES
 ORIENTATIONS AND MAGNITUDES
 BOREHOLE ISS-11
 ENGINEERS
 GEOLOGISTS



NOTE: ALL STRESSES COMPRESSIVE





NOTE - COMPRESSIVE STRESS IS POSITIVE.

- USBM GAGE
- CSIRO CELL
- MAJOR PRINCIPAL STRESSES
- - - MINOR PRINCIPAL STRESSES
- 15 TEST NUMBER



FOUNDATION SCIENCES, INC.

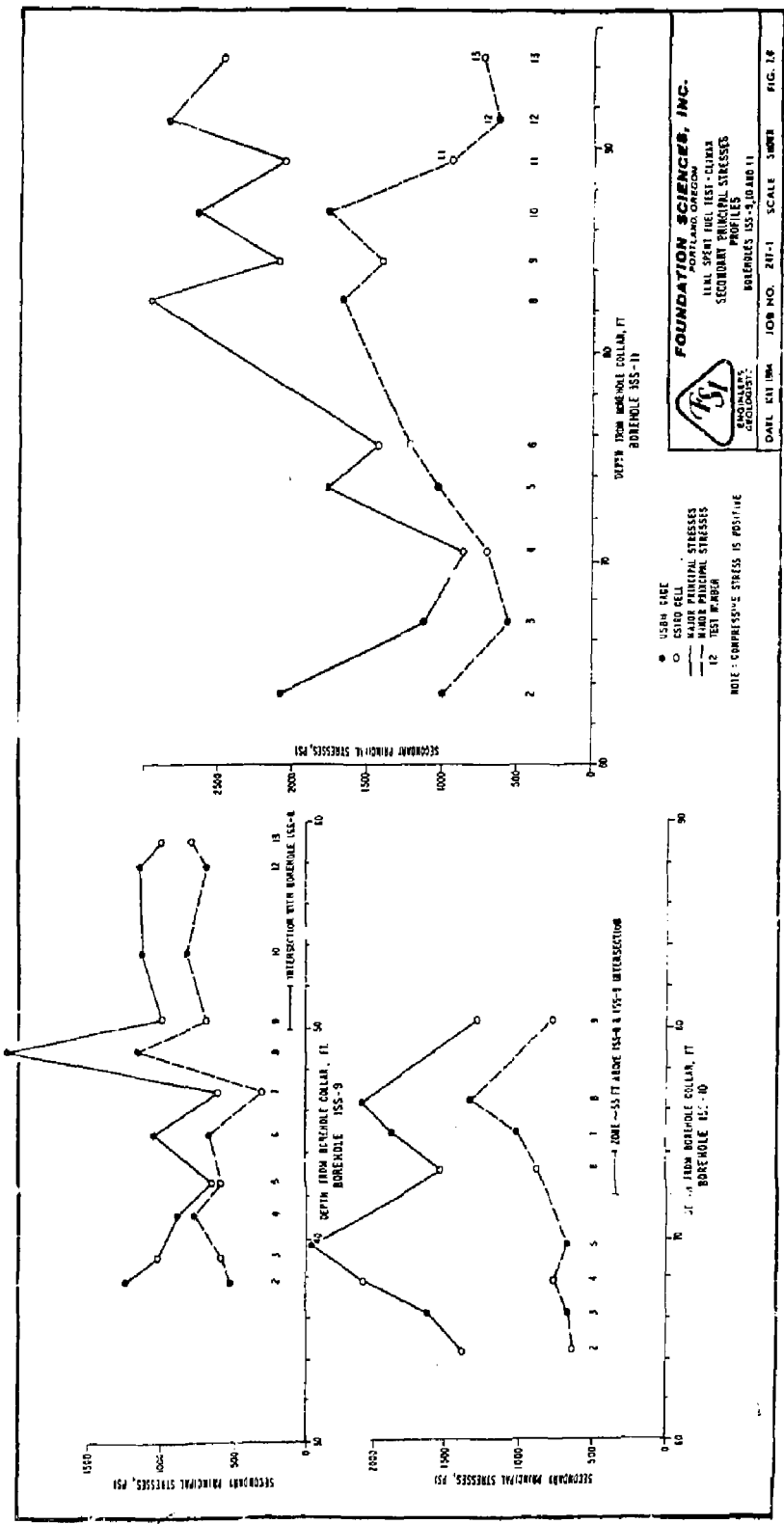
PORTLAND, OREGON

LLNL SPENT FUEL TEST - DYNAMIX
SECONDARY PRINCIPAL STRESSES
PROFILE

BOREHOLE 155-B

ENGINEERS
GEOLOGISTS

DATE MAY 1984 JOB NO. 247-1 SCALE SWORN FIG. T.5



A low stress zone of about 850 psi maximum was observed from about 40 to 45 ft depth in borehole ISS-8. The secondary principal stresses at depths greater than 60 ft in borehole ISS-8 appear fairly constant, though significant local variations do occur. Beyond a depth of 60 ft, the magnitude of the maximum secondary principal stress has an average value of about 1200 psi.

In borehole ISS-9, the magnitude of the maximum secondary principal stress is fairly uniform, with an average value of about 1,000 psi. This stress is oriented about 60° counter-clockwise from vertical (as observed by someone looking down the borehole) from a depth of about 37 to 42 ft, then changes orientation to about 30° counter-clockwise from vertical out to 60 ft.

In borehole ISS-10, the secondary principal stress orientations and magnitudes show no trend with depth. The maximum secondary principal stress is predominantly near-horizontal (referenced to the local borehole coordinates) with an average magnitude of about 1,800 psi.

In borehole ISS-11, the secondary principal stress results are somewhat variable up to a depth of about 80 ft. Beyond 80 ft, the principal stresses are generally consistent, having a maximum secondary principal stress orientation of about 30° counter-clockwise from vertical (referenced to local borehole coordinates) and an average magnitude of about 2,500 psi. Overall, the maximum secondary principal stress in this borehole averages about 2,000 psi.

7.2.2 Principal Stress Solutions -- Rib Boreholes

7.2.2.1 CSIRO Cell Solutions

The principal stress orientations and magnitudes from individual CSIRO cell overcore tests in boreholes ISS-8, 9, 10, and 11 are presented in Table 7.5. These results are presented graphically on Figures 7.7 through 7.11 on polar equal-area stereonet (upper hemisphere projection).

TABLE 7.5 SUMMARY OF CSIRO CELL
PRINCIPAL STRESS SOLUTIONS

<u>Test No.</u>	<u>Test Depth, ft</u>	<u>Stress, psi</u>	<u>Azimuth, Degrees cw from North</u>	<u>Inclination, Degrees up from horizontal</u>
5-2-C	5.3	2290	37	40
		836	273	34
		433	158	32
5-6-C	14.8	822	338	68
		674	108	16
		-294	202	17
7-2-C	5.5	1838	13	64
		668	126	11
		254	221	24
8-2-C	7.5	882	27	71
		385	128	4
		147	219	19
8-4-C	12.7	1233	105	68
		762	297	22
		-20	206	4
8-7-C	21.3	1589	44	41
		1471	291	25
		823	178	40
8-9-C	41.3	734	69	44
		478	326	13
		433	224	44
8-13-C	67.8	1263	236	22
		1058	20	63
		649	140	14
8-17-C	81.0	1304	238	28
		724	141	12
		589	30	60
8-21-C	96.7	903	210	27
		577	327	41
		397	98	36

Note: Positive stresses compressive

TABLE 7.5 SUMMARY OF CSIRO CELL (continued)
PRINCIPAL STRESS SOLUTION

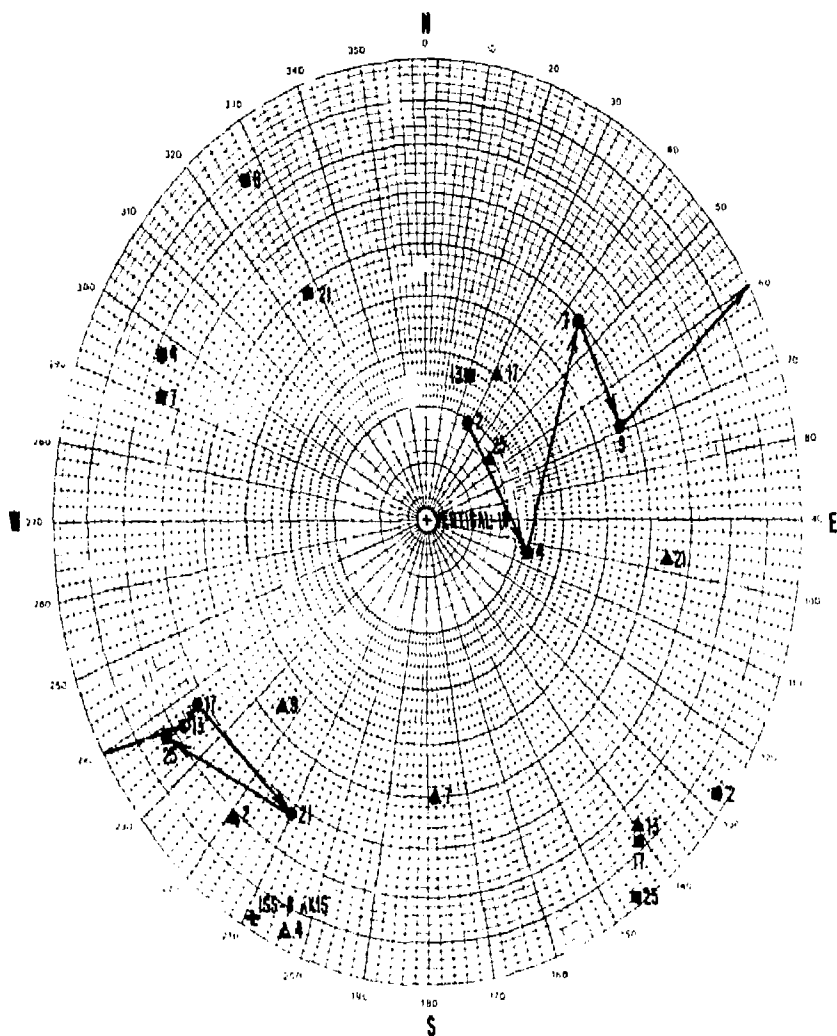
<u>Test No.</u>	<u>Test Depth, ft</u>	<u>Stress, psi</u>	<u>Azimuth, Degrees cw from North</u>	<u>Inclination, Degrees up from horizontal</u>
8-25-C	109.4	1828	237	17
		1271	146	1
		515	52	73
Borehole ISS-8 combined solution All tests beyond 60 ft		1216	229	29
		828	325	10
		589	72	59
9-3-C	39.1	1275	259	28
		781	167	2
		555	73	62
9-5-C	42.6	925	257	6
		591	27	81
		394	166	7
9-7-C	46.9	1083	268	34
		432	69	55
		99	172	9
9-9-C	50.5	1178	272	33
		841	143	44
		673	22	28
9-13-C	59.2	1494	265	32
		782	33	45
		549	155	29
Borehole ISS-9 combined solution all tests		1153	262	28
		617	58	60
		472	166	10
10-2-C	64.4	1670	215	55
		1105	15	33
		348	111	10
10-4-C	67.8	2773	244	44
		1697	20	37
		585	129	24

Note: Positive stresses compressive

TABLE 7.5 SUMMARY OF CSIRO CELL (continued)
 PRINCIPAL STRESS SOLUTION

Test No.	Test Depth, ft	Stress, psi	Azimuth, Degrees cw from North	Inclination, Degrees up from horizontal
10-6-C	73.1	1772	240	58
		1433	6	20
		799	106	24
10-9-C	80.4	1658	272	58
		1273	29	16
		693	127	27
Borehole ISS-10 combined solution all tests		1907	238	49
		1384	15	33
		686	120	22
11-4-C	70.6	1020	77	45
		863	277	43
		586	177	10
11-6-C	75.5	1651	82	8
		1357	337	60
		956	177	29
11-9-C	84.3	2228	3	55
		1448	261	8
		1320	165	34
11-11-C	89.4	2080	335	42
		1234	109	38
		939	221	25
11-13-C	94.5	2668	331	22
		1118	86	48
		708	225	35
Borehole ISS-11 combined solution all tests		1713	333	41
		1364	88	27
		919	201	38
Borehole ISS-11 combined solution tests ISS-11-9, 11 and 13		2298	359	40
		1272	99	31
		991	214	35

Note: Positive stresses compressive



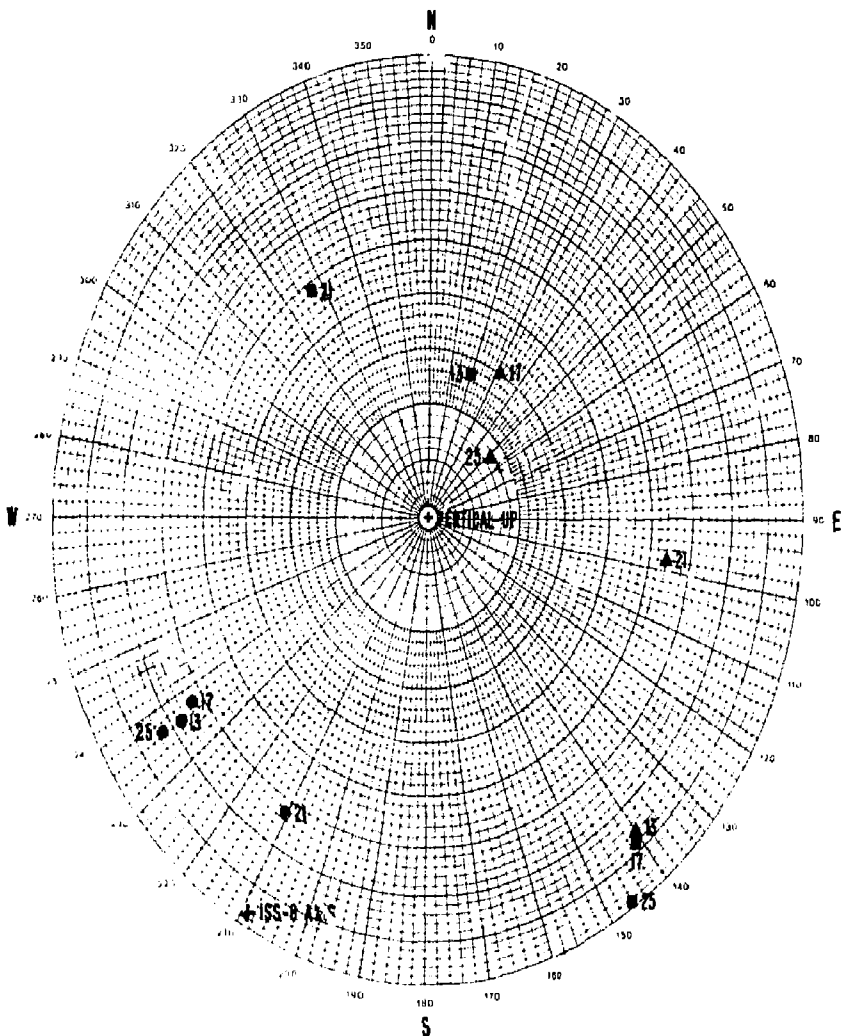
Principal Stresses, psi

ISS-8 Test No.	Depth, ft	σ_1	σ_2	σ_3
2	7.5	882	385	147
4	12.7	1,233	762	-20
7	21.3	1,589	1,471	823
9	41.3	734	478	433
13	67.8	1,263	1,058	649
17	81.0	1,304	724	589
21	96.7	903	577	397
25	109.4	1,828	1,271	515

LLNL Spent Fuel Test-Climax
CSIRO Cell Principal Stresses
Borehole ISS-8
All Tests

Figure 7.7

NOTE: Compressive stresses positive



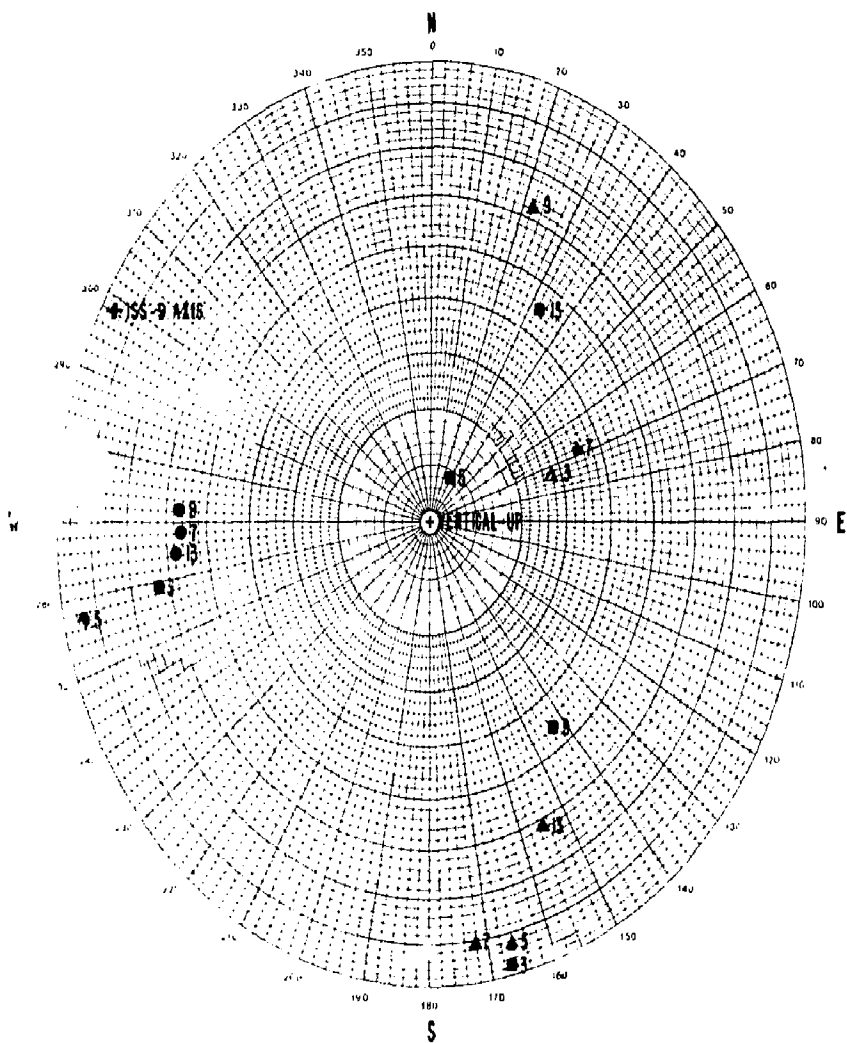
Principal Stresses, psi

ISS-B Test No.	Depth, ft	●	■	▲
		σ_1	σ_2	σ_3
13	67.8	1,263	1,058	649
17	81.0	1,304	724	589
21	96.7	903	577	397
25	109.4	1,828	1,271	515

LLNL Spent Fuel Test-Climax
 CSIRO Cell Principal Stresses
 Borehole ISS-8
 Tests from 67 to 110 ft

Figure 7.8

NOTE: All stresses compressive



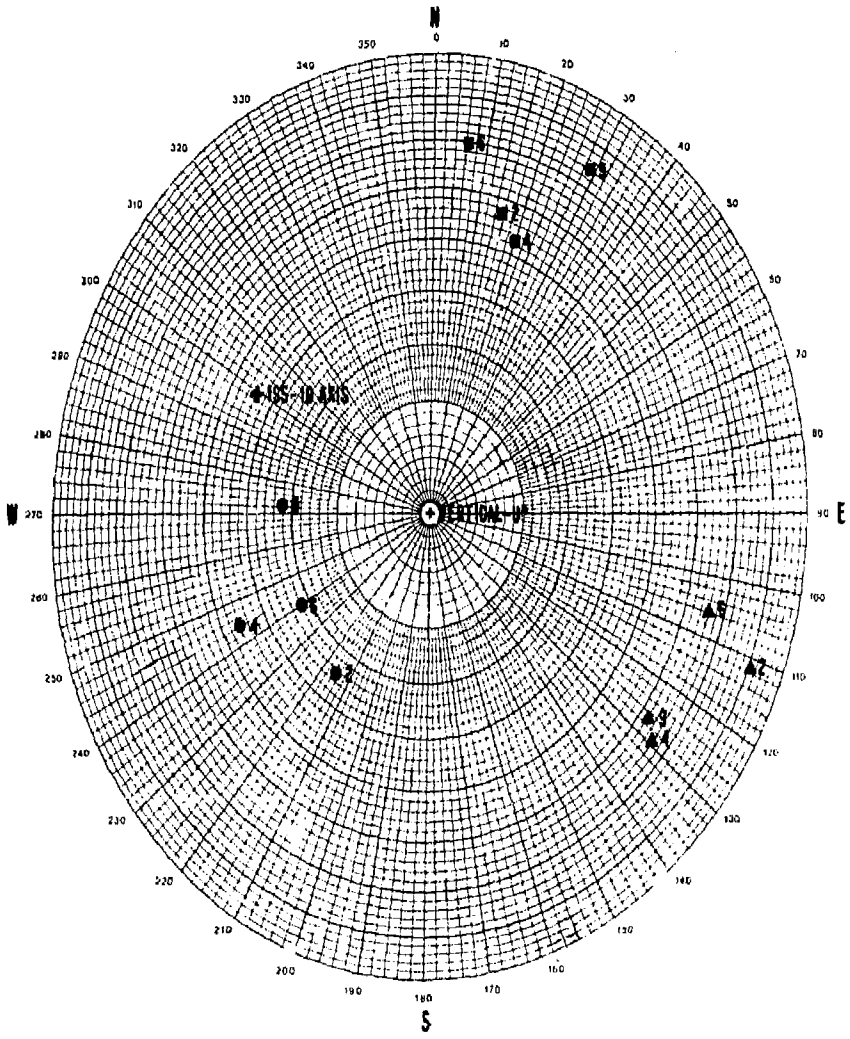
Principal Stresses, psi

ISS-9 Test No.	Depth, ft	● σ_1	■ σ_2	▲ σ_3
3	39.1	1,275	781	555
5	42.6	925	591	394
7	46.9	1,083	432	99
9	50.5	1,178	841	673
13	59.2	1,494	782	549

LLNL Spent Fuel Test-Climax
CSIRO Cell Principal Stresses
Borehole ISS-9

Figure 7.9

NOTE: All stresses compressive



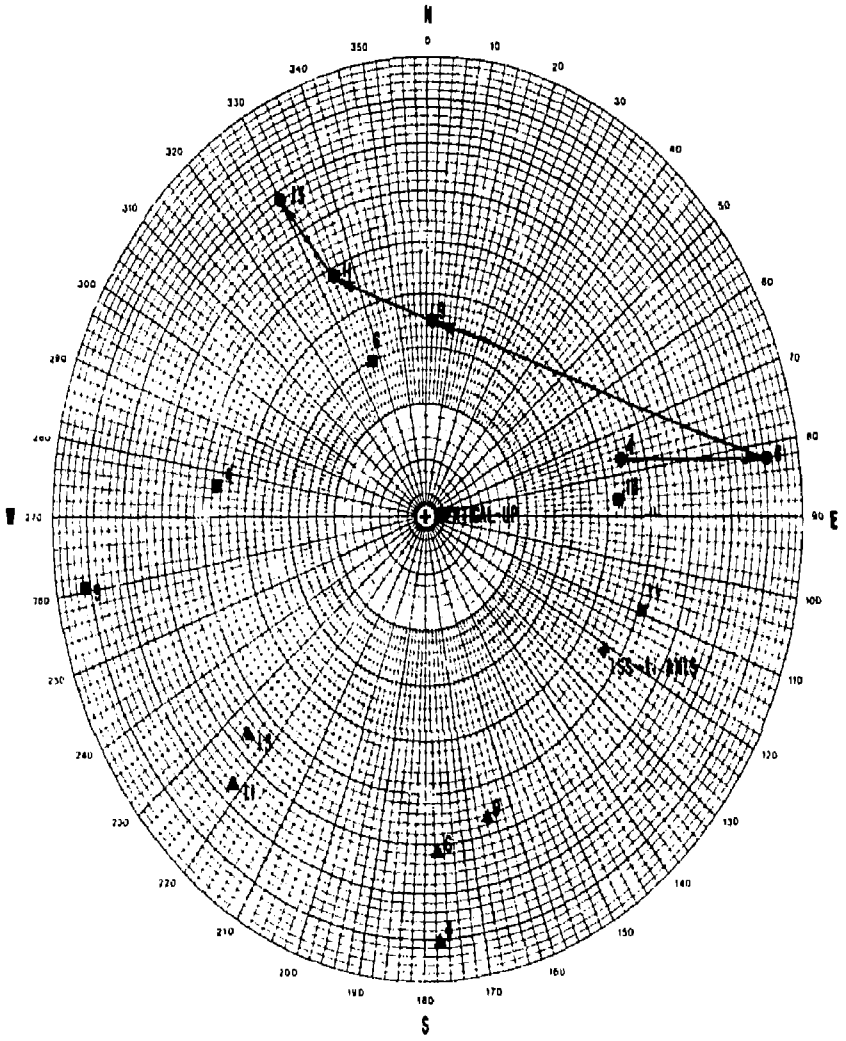
Principal Stresses, psi

ISS-10 Test No.	Depth, ft	● σ_1	■ σ_2	▲ σ_3
2	64.4	1,670	1,105	348
4	67.8	2,773	1,697	585
6	73.1	1,772	1,433	799
9	80.4	1,658	1,273	693

LLNL Spent Fuel Test-Climax
CSIRO Cell Principal Stresses
Borehole ISS-10

Figure 7.10

NOTE: All stresses compressive



Principal Stresses, psi

ISS-11 Test No.	Depth, ft	● σ_1	■ σ_2	▲ σ_3
4	70.6	1,020	863	586
6	75.5	1,651	1,357	956
9	84.3	2,228	1,448	1,320
11	89.4	2,080	1,234	939
13	94.5	2,668	1,118	708

LLNL Spent Fuel Test-Climax
CSIRO Cell Principal Stresses
Borehole ISS-11

Figure 7.11

Note: All stresses compressive

Figure 7.7 presents solutions for all CSIRO cell tests in borehole ISS-8. The arrow on the figure illustrates the change in orientation of the maximum principal stress as the test depth increases beyond the zone of influence on the test facility. The major principal stress orientations in tests 2 and 4 are nearly vertical. Tests 7 and 9 show a more inclined principal stress, which becomes nearly horizontal in tests 13, 17, 21, and 25. Tests 2 and 4 exhibit minor principal stresses which are near zero and are oriented along the axis of the borehole. All three principal stress magnitudes in test 9 are relatively low, though similar in orientation to other CSIRO tests, confirming the observation of a low stress zone at about 40 to 45 ft.

Figures 7.8, 7.9, and 7.10 present individual CSIRO cell principal stress solutions for borehole ISS-8 tests beyond a depth of 60 ft, all borehole ISS-9 tests, and all borehole ISS-10 tests, respectively. Differences in principal stress orientations are observed between the different plots, but within an individual borehole, the principal stresses are generally similar. Beyond 60 ft in borehole ISS-8 and in borehole ISS-9, the orientations of the intermediate and minor principal stresses display wide variations within a plane. However, since the difference in magnitudes between these stresses is usually small, their orientation within the plane is not well defined and for practical purposes may not be significant. Plots of tests in borehole ISS-10 exhibit good agreement of all principal stress orientations, primarily because of the larger differences in magnitude between the major, intermediate and minor principal stresses.

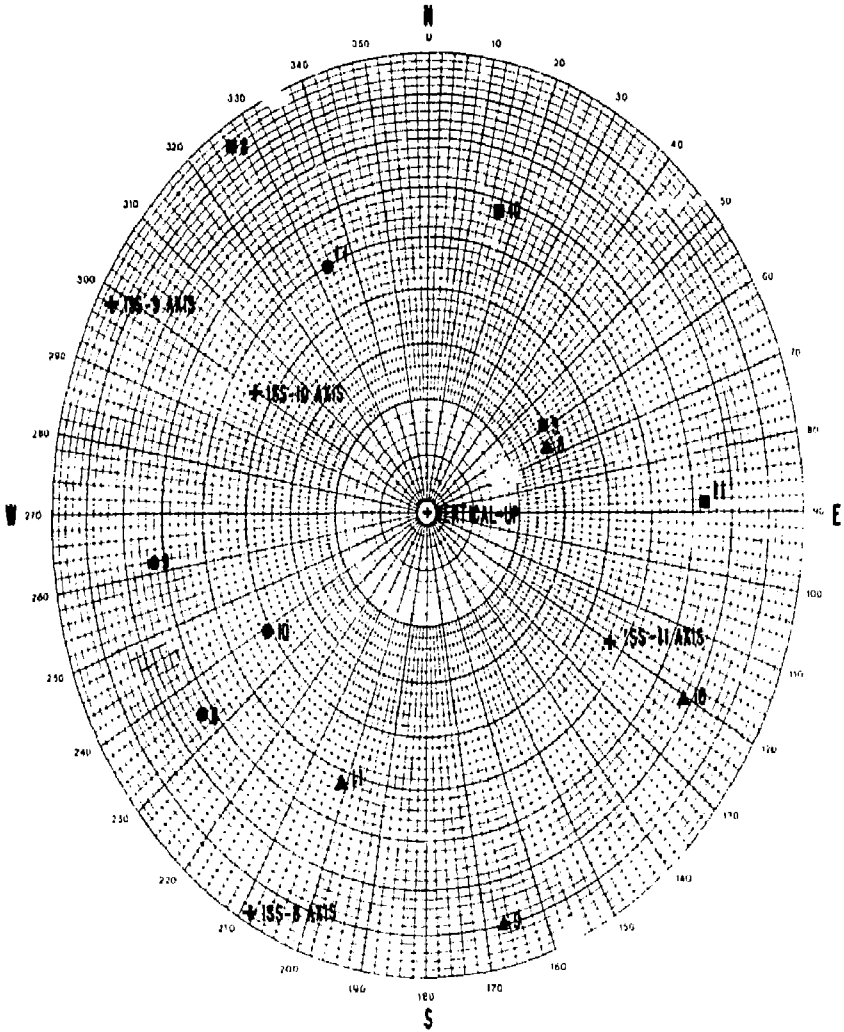
Figure 7.11 presents individual CSIRO cell principal stress solutions for all tests in borehole ISS-11. The plot appears to show a rotation, with increasing depth, of the major and intermediate principal stresses about an axis defined by the average minor principal stress. The arrows on Figure 7.11 show the change of direction of the major principal stress. The orientations of the minor principal stresses for all tests plot relatively close together.

Table 7.5 and Figure 7.12 present combined CSIRO cell principal stress solutions for each borehole. The solutions from boreholes ISS-8 and 9 are very similar in both orientation and magnitude. The principal stress orientations from borehole ISS-10 are somewhat similar to those from boreholes ISS-8 and 9, but the magnitudes are significantly higher. The magnitudes from borehole ISS-11 are similar to those from borehole ISS-10, but the respective orientations in borehole ISS-11 are significantly different from any of the other boreholes.

7.2.2.2 USBM Gage Solutions

Since only three non-parallel boreholes (not in the same plane) are required for a complete USBM gage principal stress solution, several combinations of data from the four rib boreholes are possible. The potentially available data includes: six tests from borehole ISS-8 within ± 20 ft of the intersection with borehole ISS-9; six tests from borehole ISS-9 within ± 15 ft of the intersection with borehole ISS-8; four tests from borehole ISS-10 within ± 5 ft of a point about 55 ft above the intersection of boreholes ISS-8 and ISS-9; and six tests from borehole ISS-11 within ± 20 ft of a point about 55 ft below the intersection of boreholes ISS-8 and 9, for a total of 66 individual deformation measurements (three per test).

The results of USBM gage principal stress solutions for several borehole combinations are listed in Table 7.6 and shown graphically on Figure 7.13. Because of the close proximity of tests made in boreholes ISS-8 and 9, and the similarity of the CSIRO cell solutions from these boreholes, it is likely that these tests are measuring the same stress field. Based on the CSIRO cell results, it appears that tests in boreholes ISS-10 and 11 are measuring different stress fields. Therefore, to maximize the validity of assuming the same stress field in each of the combined boreholes, boreholes ISS-8 and 9 were both included in each USBM gage solution.



Principal Stress, psi

Borehole No.	● σ_1	○ σ_2	▲ σ_3
ISS-8*	1,216	828	589
ISS-9**	1,153	617	472
ISS-10**	1,907	1,384	686
ISS-11**	1,713	1,364	919

LLNL Spent Fuel Test-Climax
 Combined CSIRO Cell Principal Stresses
 Boreholes ISS-8, 9, 10 and 11

Figure 7.12

- * Solution from all CSIRO cell tests beyond depth 60 ft
- ** Solution from all CSIRO cell tests in borehole.

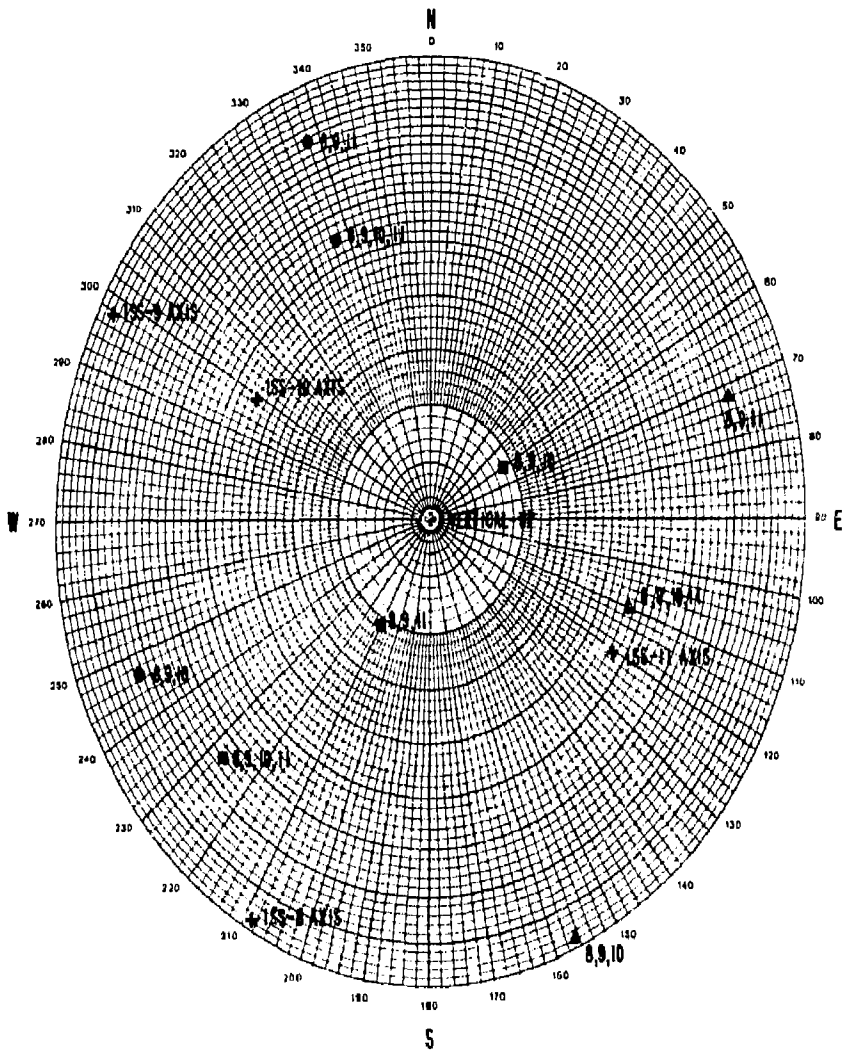
Table 7.6

USBM GAGE PRINCIPAL STRESS SOLUTIONS

<u>Borehole Combinations</u>	<u>Stress, psi (+ 95% conf. limits)</u>	<u>Azimuth Degrees cw from North</u>	<u>Inclination Degrees up from Horizontal</u>
ISS-8, 9, 10	1795 (343)	248	18
	1081 (314)	59	72
	714 (202)	157	3
ISS-8, 9, 11	1844 (363)	338	13
	1287 (245)	211	69
	557 (386)	72	16
ISS-8, 9, 10, 11	1654 (316)	338	35
	1195 (261)	227	26
	992 (302)	109	43

Note: All stresses compressive

Borehole ISS-8, includes all USBM gage tests
beyond depth 60 ft.



Principal Stresses, psi

Borehole Combinations	●	■	▲
	σ_1	σ_2	σ_3
ISS-8,9,10	1,795	1,081	714
ISS-8,9,11	1,844	1,287	557
ISS-8,9,10,11	1,654	1,195	992

LLNL Spent Fuel Test-Climax,
 USBM Gage Principal Stresses
 Boreholes ISS-8, 9, 10 and 11

Note: All stresses compressive

Figure 7.13

Borehole ISS-8 includes all US™ gage tests beyond depth 50 ft.

The various borehole combinations all result in similar USBM gage principal stress magnitudes (and similar magnitudes for the uncertainties); however, the orientations vary significantly between the different solutions.

7.3 Pillar Stress Measurements -- Boreholes ISS-4, 5, 6, and 7

7.3.1 Secondary Principal Stress Solutions -- Pillar Boreholes

The secondary principal stress magnitudes and orientations for the pillar boreholes are presented on Table 7.4 and Figures 7.14 and 7.15. The maximum secondary principal stress appears to be predominantly vertical and has a magnitude of about 2,000 psi near the heater drift wall, which decreases progressively toward the canister drift wall to values in the range of 700 to 1,000 psi. Minimum secondary principal stresses are nearly horizontal and are generally less than 700 psi.

7.3.2 Principal Stress Solutions -- Pillar Boreholes

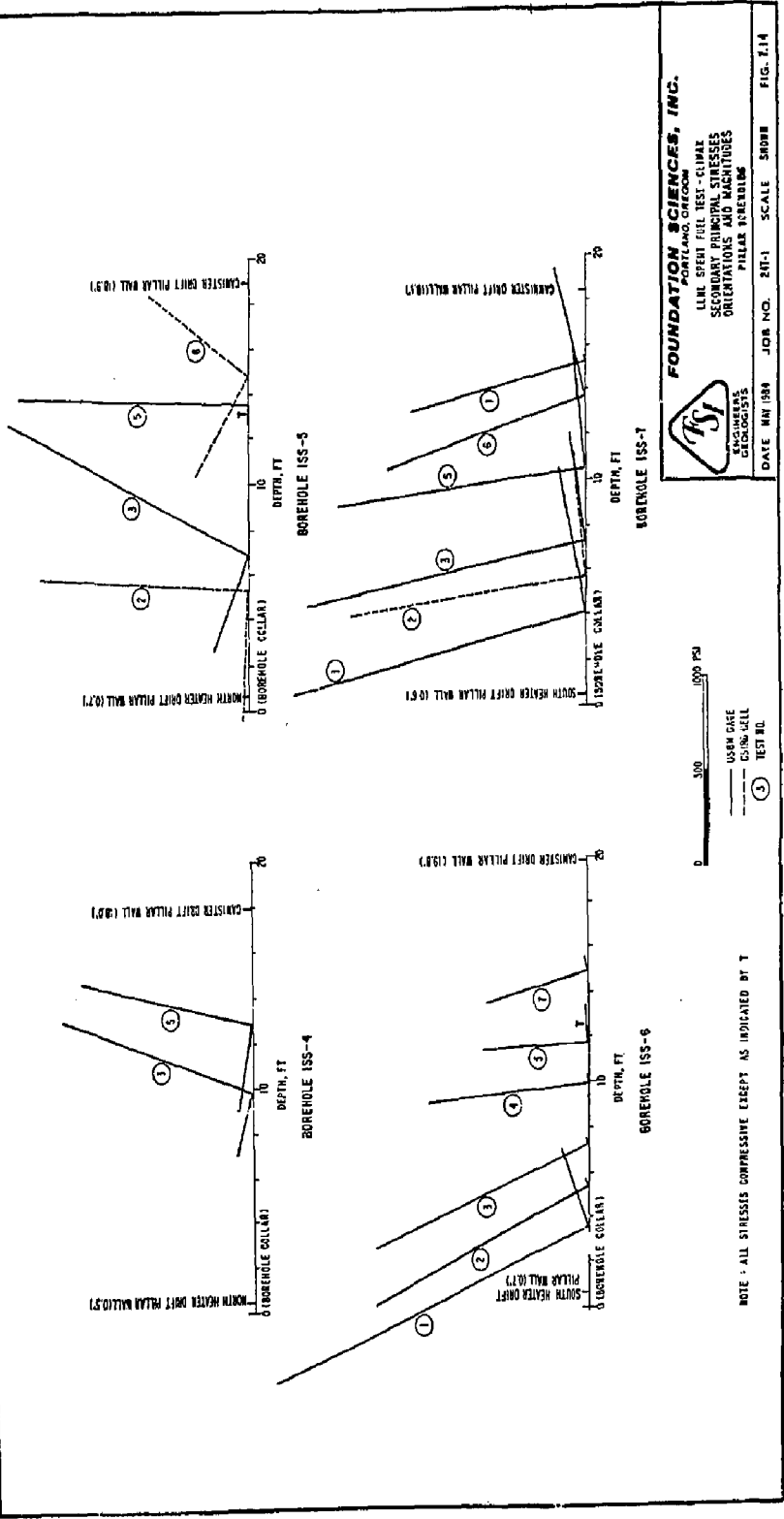
Figure 7.16 presents the principal stresses calculated from three CSIRO cell tests conducted in boreholes ISS-5 and 7. These results indicate that the major principal stresses in the pillars are on the order of 1,800 to 2,300 psi, and are oriented at an angle of 20 to 50° from vertical. As would be expected, the minor principal stresses are low and are oriented across the short dimension of the pillar. The intermediate principal stresses are nearly horizontal, oriented along the long axis of the pillars, and are on the order of about 700 psi.

7.4 Stress Measurements - Discussion and Conclusions

7.4.1 Quality of Test Results

7.4.1.1 General

The results of stress measurements made in the four rib boreholes, ISS-8 through 11, indicate significant variations in stress conditions in that region. Since no physical mechanisms that would cause these variations have been identified or are readily apparent, these results appear to contradict the assumption of uniform stress conditions which would otherwise be expected to exist. The major question raised by these results is whether the differences in measured stresses are caused

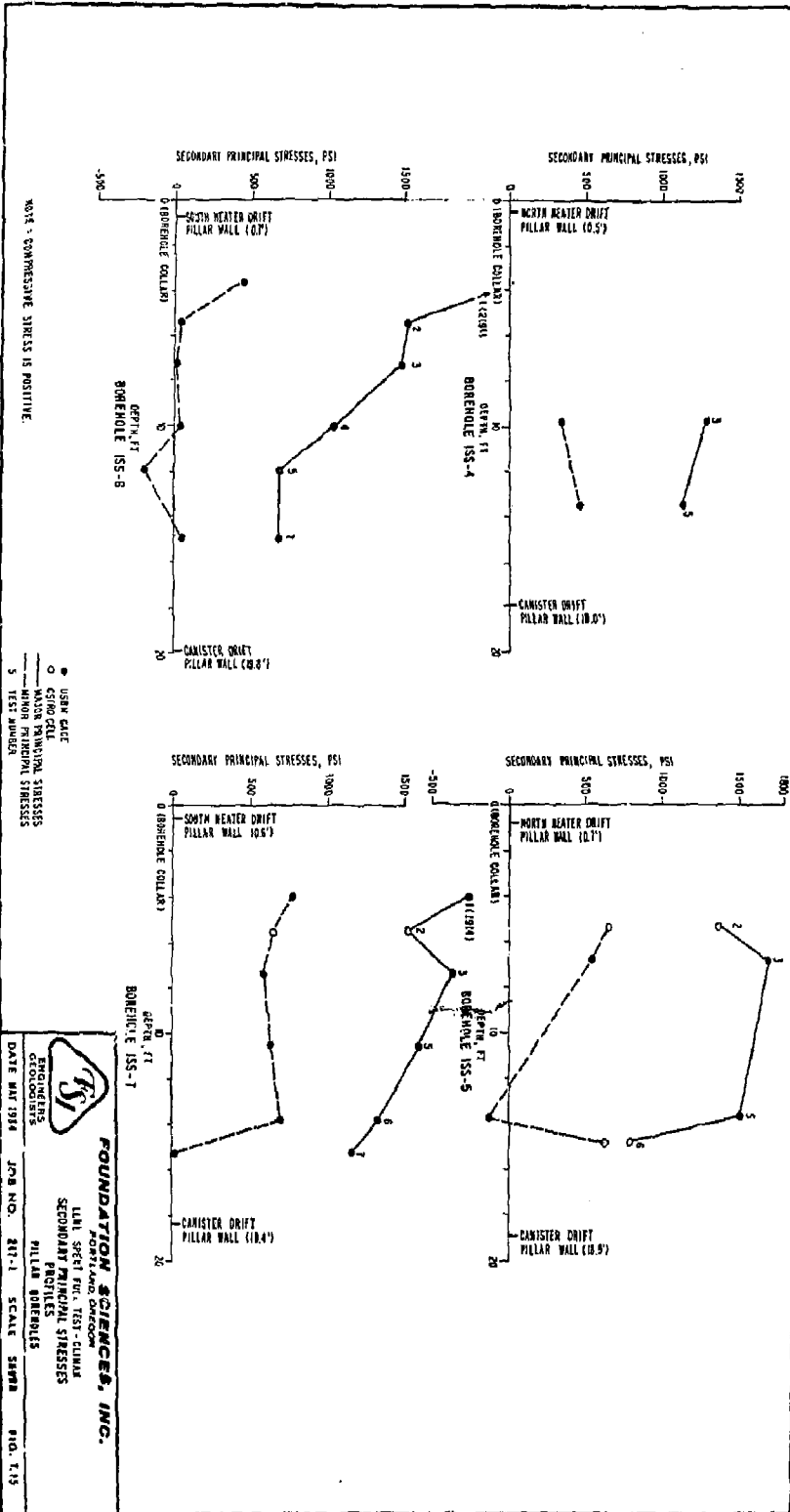


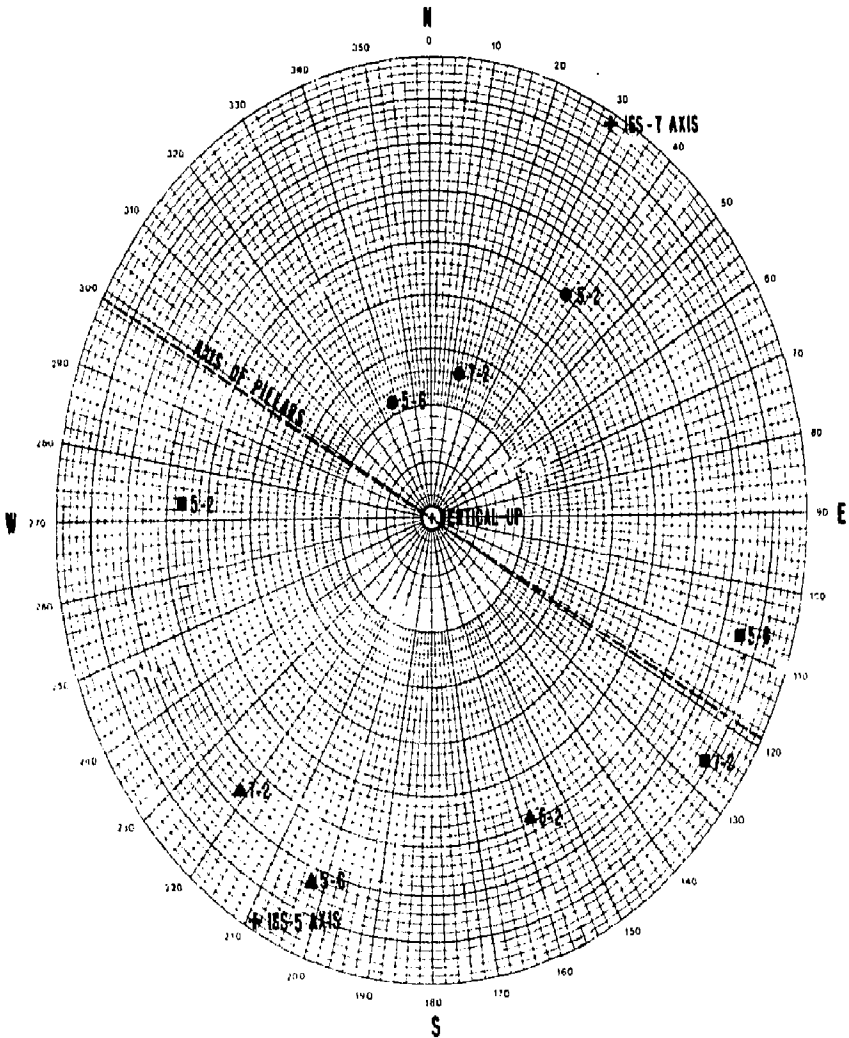
FOUNDATION SCIENCES, INC.
 1111 SWENHILL TEST DRIVE
 SUITE 1000
 ORIENTATIONS AND MACHININGS
 PILLAR STRENGTHING

**ENGINEERS
 GEOLOGISTS**

DATE: MAY 1989 JOB NO. 211-1 SCALE: SHOWN FIG. 7.14

NOTE: ALL STRESSES COMPRESSIVE EXCEPT AS INDICATED BY T





Principal Stresses, psi

<u>Test No.</u>	<u>Depth, ft</u>	<u>●</u> σ_1	<u>■</u> σ_2	<u>▲</u> σ_3
ISS-5-2	5.3	2,290	836	433
ISS-5-6	14.8	822	674	-294
ISS-7-2	5.5	1,838	668	254

LLNL Spent Fuel Test-Climax
CSIRO Cell Principal Stresses
Pillar Boreholes ISS-5 and 7

Figure 7.16

Note: Compressive stress positive

by uncertainties and limitations of the test methods, or whether they reflect real variations in the state of stress in the rock mass.

During this program, great care was taken to standardize test procedures, perform tests according to these procedures, and to reduce and analyze the test data. Special techniques were developed to minimize test-related uncertainties associated with the relatively great depths of testing in the boreholes and the thermal effects associated with testing in artificially heated rock. In general, the approach taken resulted in a state-of-the-art program with strong quality control.

Secondary principal stress solutions from USBM gage data are about 30% higher in magnitude than those from CSIRO cell data. However, the ratio of the maximum and minimum secondary stress magnitudes in a given test and orientations of the stresses are similar for both gage types. In addition, variations of stress within a borehole, e.g. high or low stress zones, were measured by both types of instruments. Therefore, except for a "scaling factor" the USBM gage and CSIRO cell results present essentially the same picture of in situ stress conditions.

Comparisons of CSIRO cell principal stress solutions in different boreholes indicate that the variations in measured stress between the various boreholes is much greater than the variation within an individual borehole. Also, USBM gage principal stress solutions for various borehole combinations are not consistent, Figure 7.13, with weighted averages of the CSIRO cell combined borehole principal stresses, Figure 7.12.

Based on these considerations, we believe that the data produced by this study are of sufficiently high quality and quantity to conclude that the indicated test results are generally correct and that the in situ stress field around the Spent Fuel Test Facility is not simple or uniform. Additional evidence for this conclusion is in Section 7.4.3.

7.4.1.2 Quality of USBM Gage Data

The USBM gage has a relatively long history of successful use in other stress measurement programs, and the results have generally been accepted as reasonably accurate. The USBM gage measures borehole deformations through direct physical contact between the sensing buttons and the rock. Also, the theoretical derivation of the data reduction equations is relatively straightforward with a minimum of uncertainties involved in the solutions, provided the fundamental assumptions of isotropic, homogeneous, elastic rock, and, for the three dimensional solution, a uniform stress field are met. For these reasons, we believe that the stress magnitudes and orientations of the USBM gage secondary principal stresses are generally accurate. However, based on a comparison of results from the various rib boreholes, the assumption of a uniform stress field does not appear to be valid. For this reason, the accuracy of in situ principal stresses calculated from the combination of USBM gage tests in different boreholes should be considered low. Since the USBM gage principal stress solution is a linear least-squares-regression method, combining test data from different stress states results in a solution that is an average of these different states, weighted in proportion to the relative number of tests included from each stress condition. This is apparent in the results.

7.4.1.3 Quality of CSIRO Cell Data

The record of use and validity of results for the CSIRO cell are not as well established as for the USBM gage. In addition, the in situ mechanical properties of the CSIRO cell, the epoxy cement, and the rock significantly affect the responses of the nine individual strain gages. Factors accounting for these properties and the geometry of the CSIRO have been derived, but their precision is not known. Therefore, the mechanics of the CSIRO cell and the theoretical derivation of the CSIRO cell principal stress solution are more complex than for the USBM Gage. For these reasons, the CSIRO cell results have been carefully assessed in light of the total body of data from this study.

As discussed in Section 7.4.1.1, USBM gage secondary principal stresses average about 30% higher than CSIRO cell stresses. Also, the same 30% difference exists between the two instruments when three-dimensional principal stress solutions are compared.

Some uncertainty in the orientations given by CSIRO cell solutions is suggested by comparing the principal stresses in boreholes ISS-8 and ISS-9 on Figures 7.8, 7.9, and 7.12. Since the tests represented by these stresses were performed in close proximity to each other, near the intersection of the two boreholes, it is reasonable to assume that the average stress field should be uniform for the two sets of stress measurements. Figure 7.12 shows that the major principal stresses agree well with respect to magnitude, but the orientations of each are displaced toward their respective borehole axes from an "average" direction midway between the two. This displacement, or apparent bias, is on the order of 10° . As discussed in Section 7.2.2.1, the intermediate and minor principal stresses for boreholes ISS-8 and 9 are similar in magnitude and can be defined within a plane. These two planes on Figure 7.12 are also rotated away from an "average" orientation by about 10° .

The other problem observed with the CSIRO cell is the negative hysteresis exhibited by the Phase II biaxial tests, as discussed in Section 6.2.

The reasons for the low CSIRO cell stress magnitudes, the directional bias, and the negative hysteresis during Phase II biaxial tests are not clear. It is possible that the complex relationships between gage response and material properties of the cell, the epoxy cement, and the rock may not be accurately modeled by the K factors (equations 5.3.1 and 5.3.3). Also, the differences between Phase I and Phase II biaxial test results suggest that the epoxy cement may not be completely cured by the time the gage is overcored. If this is true, then it is possible that deformations in the rock core during overcoring are under-

estimated because the epoxy creeps as the rock strains and complete deformation is not measured. This could also affect the values of the K factors used in data reduction. Finally, geometric factors, such as the relative balance in the directional sensitivity of the individual strain gages to the different components of the in situ stress tensor could systematically induce a directional bias in the calculated principal stress orientations, which is dependent on borehole orientation. Additional work will be required to more fully define and explore the variables affecting the results of CSIRO cell stress measurements.

The most positive aspect of the CSIRO cell is the ability to calculate a complete stress tensor from one overcore test with a redundancy in strain measurements. When the nine strain gage deltas from a single overcore test are combined in a least squares regression to calculate an average stress tensor, and the tensor in turn is used to predict each of the nine delta values, the measured deltas agree quite well with the predicted deltas. The deviation between the two sets is generally within 1 to 4 microstrain. This indicates that all nine strain gages are responding in a uniform manner consistent with the actual deformations in the rock core. A sensitivity analysis performed by entering known "bad" data into the regression confirms that deviations between measured and calculated deltas are in fact highly reflective of the quality of the original data.

Visual inspection of Figures 7.8 through 7.12 reveals that the scatter of CSIRO cell principal stress magnitudes and orientations within a given borehole is smaller than the difference in average stress magnitudes and orientations between the boreholes. In other words, corresponding principal stresses form distinct populations in the different boreholes. Furthermore, the differences between principal stresses in boreholes ISS-8 and 9, which logically would be expected to exist in a uniform stress field, is small, and is probably related more to a directional bias in the CSIRO cell results than to a real variation in stress field. However, variations between these two boreholes and the other rib boreholes are more significant.

Based on these observations, we conclude that CSIRO cell probably underestimates stress magnitudes. It also appears that the orientations of the CSIRO cell solutions are biased to a minor degree by the borehole orientations. In spite of these deficiencies, we believe that for this study, the errors associated with the CSIRO cell are minor and that the ability to completely determine the state of stress with one test significantly improves our understanding of the in situ stresses in the different zones of stress encountered. In our opinion, the CSIRO principal stress orientations given on Figures 7.7 through 7.12 are reasonably accurate within normal data scatter and probably do not exhibit more than about 20° of systematic directional bias. Also, the apparent error in stress magnitude is less than the indicated differences between stress zones. For these reasons, we believe that the results of the CSIRO cell solutions present a reasonably accurate representation of in situ stresses at discrete locations. We recommend, however, that the stress magnitudes presented on the figures and tables in this section be increased by 30% to account for the probable underestimation of stress magnitude.

7.4.2 Stress Gradient into Rib from South Heater Drift

In Borehole ISS-8, the major principal stress within 20 ft of the south heater drift is predominately vertical and is on the order of about 1,500 psi. The minor principal stress is small (near zero) and is oriented in a nearly horizontal direction perpendicular to the axis of the south heater drift, as would be expected. These results indicate that there is no large concentration of vertical stress caused by the test facility. Beyond depth 20 ft, the minor principal stresses increase and the major principal stresses rotate away from vertical. A low stress zone of about 900 psi maximum stress was observed from about 40 to 45 ft depth in borehole ISS-8. Both USBM and CSIRO tests show the same low stress, so it is probably real. The cause of the low stress zone is not clear, but it may be related to two open, weathered joints, that were seen in the core to intersect at a depth of about 40 ft. Beyond a depth of 60 ft, the principal stresses are relatively consistent in orientation and magnitude.

7.4.3 In Situ State of Stress -- Rib Boreholes

As previously discussed, we conclude that the differences in measured stresses between borehole ISS-10, borehole ISS-11, and boreholes ISS-8 and 9 reflect real stress variation in the rock mass surrounding the test facility. This conclusion is based on comparisons of CSIRO cell principal stresses in Figures 7.8 through 7.12, comparisons of CSIRO cell and USBM Gage principal stress solutions in Figures 7.12 and 7.13, and analyses of secondary principal stresses from both gage types. Comparisons of principal stress solutions have been discussed in preceding sections. Analysis of secondary principal stresses and the vertical components of CSIRO principal stresses are presented below.

Secondary principal stresses suggest a variation in stress field, with both types of stress-measuring devices giving similar results. Since boreholes ISS-9, 10, and 11 lie in the same vertical plane, the average horizontal stress component of each borehole should be about the same, assuming a uniform stress field. Summing the horizontal components of the secondary principal stresses in each borehole (CSIRO cell results are increased 30%) results in the following average values:

<u>Borehole</u>	<u>Horizontal Stress, psi</u>
ISS-9	1250
ISS-10	2200
ISS-11	2050

Clearly, the horizontal stresses measured in boreholes ISS-10 and 11 are significantly greater than in borehole ISS-9.

A comparison of the average vertical stresses measured in the rib boreholes can be made using the vertical components of the CSIRO principal stresses given on Figure 7.12 (increased 30%):

<u>Borehole</u>	<u>Vertical Stress, psi</u>
ISS-8	1000
ISS-9	900
ISS-10	2050
ISS-11	1700

Only the average vertical stress measured in borehole ISS-11 agrees with the expected overburden value of 1600 psi (Heuze, et al., 1981). Average vertical stresses for boreholes ISS-8 and 9 together, and borehole ISS-10, are about 60% and 120% of the expected value, respectively.

The results presented in this section indicate that three zones of significantly different in situ stress were encountered in the four rib boreholes. Only tests in boreholes ISS-8 and 9 appear to be measuring the same state of stress. In addition to the large variations in stress between zones, smaller but significant variations in stress were measured within individual zones. Some of these variations probably result from normal measurement error and are not significant, but other variations were measured by more than one test and likely indicate actual stress differences. In particular, tests in borehole ISS-11 indicate significant changes in stress magnitude and a regular rotation of stress orientation about the minor principal stress axis with increasing test depth.

We believe that the stress conditions in the rib are best represented by the averages of the stresses measured in each of the three stress zones encountered during this study. Therefore, we recommend that the combined CSIRO cell principal stresses for individual boreholes, given on Figure 7.12, be used to determine the average state of stress in each of these zones. We also recommend that magnitudes on that figure be increased 30% to account for the probable underestimation of stress by the CSIRO cell. In the case of boreholes ISS-8 and 9, where two sets of principal stresses are given for the same stress zone, an average of the orientations and magnitudes (increased 30%) is probably a good estimate of the stress state at that location. The summary principal stresses presented on Figure 2.1 incorporate these recommendations.

The reasons are not obvious for the apparent changes in the average stress field over the relatively short distances between boreholes, the

indicated regular rotation of stresses in borehole ISS-11, or the other smaller but significant variations in stress within a general stress zone. Possible hypotheses include the effects of joints and shear zones in the rock mass, thermally induced stresses from the Spent Fuel Test, cooling history of the quartz monzonite, unrecognized effects of the test facility itself, influences from nearby nuclear detonations, and other geologic/tectonic mechanisms that may be recognized in the future as work at the test facility progresses.

7.4.4 Pillar Stresses

Stress measurements made in the four pillar boreholes present a relatively consistent profile of secondary principal stresses, as presented in Section 7.3. Maximum secondary principal stresses are near vertical and are highest near the heater drifts, decreasing toward the canister drift. CSIRO cell tests also indicate predominately vertical major principal stresses. The intermediate and minor principal stresses are oriented parallel and transverse to the pillar axis, respectively. Conclusions concerning stress concentration effects are difficult to make, due to the variability of the surrounding in situ stress state.

8.0 REFERENCES

Ballou, L.B., Patrick, W.C., Montan, D.N., and Butkovich, T.R., 1982, Test Completion Plan for Spent Fuel Test-Climax, Nevada Test Site, Lawrence Livermore National Laboratory, UCRL-53367.

Duncan Fama, M.E. and Pender, M.J., 1980, "Analysis of the Hollow Inclusion Technique for Measuring In Situ Rock Stress", Int. J. Rock Mech. Min. Sci. and Geomech. Abstr., Vol. 17.

Ellis, W.L. and Magner, J.E., 1982, Determination of In Situ Stress in Spent Fuel Test Facility, Climax Stock, Nevada Test Site, Nevada, U.S. Geological Survey Open File Report 82-458.

Gray, W.M. and Toews, N.A., 1967, "Analysis of Accuracy in the Determination of Ground-Stress Tensor by Means of Borehole Devices", Status of Practical Rock Mechanics, Proceedings of the Ninth Symposium on Rock Mechanics, Golden, Colorado.

Heuze, F.E., Patrick, W.C., De la Cruz, R.V., and Voss, C.F., 1981, In Situ Geomechanics, Climax Granite, Nevada Test Site, Lawrence Livermore National Laboratory, UCRL-33076.

Hooker, V.E., Aggson, J.R. and Bickel, D.L., 1974, Improvements in the Three-Component Borehole Deformation Gage and Overcoring Techniques, Report of Investigations 7894, U.S. Bureau of Mines, Washington, D.C.

Hooker, V.E. and Bickel, D.L., 1974, Overcoring Equipment and Techniques Used in Rock Stress Determination, Information Circular 8618, U.S. Bureau of Mines, Washington, D.C.

Obert, L. and Duvall, W.I., 1967, Rock Mechanics and the Design of Structures in Rock, John Wiley and Sons, New York.

Panek, L.A., 1966, Calculation of the Average Ground Stress Components from Measurements of the Diametral Deformation of a Drill Hole, RI 6732, U.S. Bureau of Mines, Washington, D.C.

Wilder, D.G. and Yow, J.L., 1981, Fracture Mapping at the Spent Fuel Test-Climax, Lawrence Livermore National Laboratory, UCRL-53201.

Worotnicki, G. and Walton, R.J., 1976, "Triaxial 'Hollow Inclusion' Gauges for Determination of Rock Stresses In Situ", Proceedings ISRM Symposium Investigation of Stress in Rock and Advances in Shear Measurement, Sydney Supplement.

The Spent Fuel Test-Climax (SFT-C) is being conducted under the technical direction of the Lawrence Livermore National Laboratory for the U.S. Department of Energy. As part of the Nevada Nuclear Waste Storage Investigations, it is managed by the Nevada Operations Office of the DOE.